Mechanisms of local and global motion detection in *Drosophila*

Dissertation

for the award of the degree

"Doctor rerum naturalium" (Dr.rer.nat.)

of the Georg-August-Universität Göttingen

within the doctoral program Sensory and Motor Neuroscience

of the Georg-August University School of Science (GAUSS)

submitted by

Miriam Henning

Born in Rheine, Germany

Mainz, 2021

Thesis Committee

Prof. Dr. Marion Silies

Institute of Developmental Biology and Neurobiology, Johannes Gutenberg-Universität Mainz, Mainz

Prof. Dr. Andreas Stumpner

Department of Cellular Neurobiology, Schwann-Schleiden Research Centre, Georg-August-Universität, Göttingen.

Prof. Dr. Hansjörg Scherberger

Neurobiology Laboratory, German Primate Center, Göttingen

Members of the Examination Board

Referee:	Prof. Dr. Marion Silies
	Institute of Developmental Biology and Neurobiology, Johannes Gutenberg-Universität Mainz, Mainz
2nd Referee:	Prof. Dr. Andreas Stumpner
	Department of Cellular Neurobiology, Schwann-Schleiden Research Centre, Georg-August-Universität, Göttingen.

Further members of the Examination Board

Prof. Dr. Tim Gollisch

Sensory Processing in the Retina, University Medical Center Göttingen

Dr. Jan Clemens

Neural Computation and Behavior, European Neuroscience Institute Göttingen

Prof. Dr. Siegrid Löwel

Department Systems of Neuroscience, Institute for Zoology and Anthropology, University of Göttingen

Date of oral examination: June 29th, 2021

Affidavit

Herewith I declare that I prepared the PhD Thesis "Mechanisms of local and global motion detection in *Drosophila*" on my own and with no other sources and aids than quoted.

Miriam Henning

Mainz, 30.04.2021

ABSTRACT

Visual motion is an essential cue for many sighted animals. This can either be caused by the movement of an object, or the relative movement of the entire world caused by self-motion of the animal. Accordingly, the brain must compute both local motion cues, corresponding to spatiotemporal changes in luminance, and global motion patterns composed of many local motion vectors. In the fly eye, which is composed of hexagonally arranged visual units, the first-direction selective cells, the T4 and T5 neurons, are known as local motion detectors. Global motion was thought to be computed downstream, in large wide-field cells that sample information from many local motion detectors. Despite many years of research, the detailed mechanisms underlying local motion tuning in T4 and T5 cells, as well as the transformation of local into global motion information is not fully understood.

In this thesis, I first studied the mechanisms of local motion detection and how local motion information is transferred into a global information about self-motion. First, blocking GABAergic signaling in the whole brain leads to a loss of direction-selectivity in T4 and T5 cells, arguing for a significant role of GABAergic circuits for local motion computation (Fisher et al., 2015a). However, GABAergic cell types and their potential interactions with the neuronal circuit responsible for motion detection had not yet been identified. Based on a behavioral genetic screen, *in vivo* calcium imaging and genetic analyses, we propose a GABAergic feedback mechanism, implemented by the two columnar C2 and C3 cells, to be required for directional tuning of T4 and T5 cells. Both neurons mainly interact with neurons upstream of T4 and T5 cells, indirectly affecting motion processing. While our data suggest a specific role of C2 for suppressing responses into the neuron's non-preferred direction in T4 cells, C3 silencing affected the temporal properties of T4 and T5.

T4 and T5 cells have been classified anatomically into four subtypes, ostensibly responding to the four cardinal directions of visual motion (Fisher et al., 2015a; Maisak et al., 2013). How these four motion axes arise, given the hexagonal arrangement of visual units in the fly eye, was not clear. Furthermore, it was not known how local cardinal motion from T4/T5 inputs can be transformed into complex optic flow fields encoded downstream. To understand how global motion is represented by the population of T4 and T5 cells, I used *in vivo* two-photon calcium imaging to characterize the direction tuning of T4 and T5 cells across visual space and the extent of the lobula plate. In contrast to the four anatomically subtypes described previously, we found six functional subtypes of local motion detectors at the population level / across the lobula plate. On average, tuning of these six subtypes matches the hexagonal structure of the eye. Tuning of neighboring motion detectors gradually changes, such that all T4/T5 cells of one subtype encode global motion patterns induced by translational and rotational self-movements of the fly. Together, the T4/T5 population represents six types of self-motion encountered during flight. Thus, downstream LPTCs can simply pool information from the local motion detectors, T4 and T5, to compute diverse complex flow fields. This population code for optic flow is reminiscent of coding of retinal ganglion cells in the vertebrate retina where only four directions of self-motion faced during walking are represented (Sabbah et al., 2017). While the number of motion dimensions encoded by the local motion detectors differ, this suggests a general coding strategy of visual

systems to extract self-motion of the animal, adapted to the complexity of maneuvers encountered during locomotion.

Taken together, the data presented in this thesis provide new insights about local as well as global mechanisms of visual motion processing in the fly and suggest striking parallels but also highlight differences between the vertebrate and invertebrate visual system. This is critical not only for understanding computational principles of visual systems but also for understanding how evolution adapts neuronal coding strategies to the animal's behavioral constraints.

Table of Contents

1 INTRODUCTION

Any living organism needs to extract relevant information from its environment to behave appropriately in different situations. Understanding how the brain computes such relevant information and how this depends on the ethological constraints of an animal is a merging goal of neuroscience and evolution. Therefore, it is essential to understand how specific physiological properties and the organization of single neurons within a network lead to distinct behaviors of the animal and how different or similar mechanisms may have evolved during evolution between different species. The computation of visual motion information is probably one of the most comprehensively understood mechanisms studied in many species ranging from primates, mice, turtles, and birds to flies. Visual motion patterns elicited on the eye during self-motion are essential cues for many sighted animals used for navigation and course control. These motion patterns, also named optic flow patterns, strongly depend on the animal's locomotion behavior, such that the neuronal computation behind motion vision may not only be specialized to environmental constraints but also the distinct behaviors of the animal. Such global motion patterns are composed of many local motion vectors, that first need to be computed by small local processing units of the eye.

In this thesis, I aim to provide further insight on the mechanisms of local as well as global motion detection in the visual system of *Drosophila melanogaster*. Here neuronal anatomy, as well as neuronal connectivity in the visual system, are known with exquisite detail (Fischbach and Dittrich, 1989; Meinertzhagen and O'Neil, 1991; Rivera-Alba et al., 2011; Takemura et al., 2013, 2015; Zheng et al., 2018). Genetic access to almost any cell type and a rich pool of genetic tools for neuronal labeling, activity measurements (e.g. calcium or voltage measurements, Chen et al., 2013; Dana et al., 2019; Yang et al., 2016), and manipulations (Klapoetke et al., 2014; Mattis et al., 2012; Simpson, 2009) allows to precisely affect the circuit and make predictions about the functional importance of neurons that can be ultimately linked to behavior.

1.1. Visual processing in *Drosophila melanogaster*

The compound eye of the fruit fly *Drosophila melanogaster* is in relation to the body size one of the biggest eyes among most insects, which is thought to relate to the fast-flying behavior of these animals (Leuckart, 1876). Additionally, the visual systems cover almost two-thirds of the brain volume, indicating the importance of vision for the fly to guide many behaviors. Especially the information of visual motion cues has been shown to be relevant for fly navigation. Visual motion is elicited on the eye when objects move in front of the observer, but also when the observer itself moves through the world. It thus contains information about potential threats but also about the type of self-motion of the animal. Motion computation requires a comparison of local luminance changes over space and time, such that motion information is first computed for local points in space. To compute global motion patterns which are generated on the eye during self-movements, this local motion

information needs to be pooled across space. In the following paragraphs I will explain, how the visual system of *D. melanogaster* is constructed and how visual information is processed to extract local motion information.

1.1.1 Anatomy of the *Drosophila* visual system

The *Drosophila* compound eye contains approximately 750 visual units, also known as ommatidia that are arranged in a hexagonal fashion. Each ommatidium consists of eight light-sensitive photoceptors (R1 to R8), supporting cells, and a dense sheet of pigment cells that optimally isolate individual units from each other (Hardie, 1985; Kirschfeld, 1967). Whereas the six outer achromatic photoreceptors R1-R6 primarily inform the motion detection pathways (Heisenberg and Buchner, 1977; Yamaguchi et al., 2008), the two inner photoreceptors R7 and R8 sense light of a particular wavelengths and feed into the color vision channel (Chou et al., 1996; Heisenberg and Buchner, 1977; Salcedo et al., 1999). A group of six photoreceptors of the same type that are located in different adjacent ommatidia sample light from the same ~ 5° - wide "point" in visual space and project their axons into one common cartridge of the optic lobe (**Figure 1A, B**). Thus, photoreceptors within one ommatidium utilize the same optical apparatus but have different optical axes and hence belong to different visual units (Katz and Minke, 2009; Kirschfeld, 1967; Liang et al., 1989). This specific case of visual mapping is known as neural superposition and is also found in other insect species (Braitenberg, 1967; Kirschfeld, 1967, 1973). In this arrangement, retinotopy is established in neurons downstream of photoreceptors.

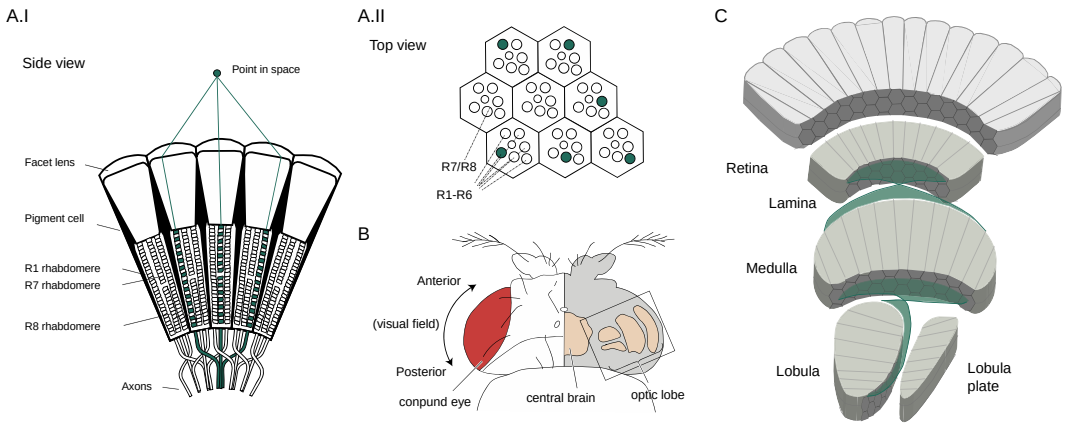

Figure 1. Anatomy of the compound eye of Drosophila melanogaster. (**A**) Side view (**A.I**) and top view (**A.II**) of neighboring ommatidia in the retina of the Drosophila eye. Light from one point in space (green) hits the lenses of six ommatidia and is captured by a different photoreceptor type (R1 to R6) in each ommatidium, whose axons converge to the same cartridge of the lamina, illustrating the neural superposition phenomenon. (**B**) Dorsal view of a fly's head. The right side illustrates the central brain and the optic lobe that is situated below the retina. (**C**) Illustration of the visual system showing the retina and the four neuropiles of the optic lobe: lamina, medulla and the lobula complex composed of the lobula and the lobula plate. The chiasm from lamina and medulla and lobula to lobula plate are indicated in green. Illustrations were modified after (Nilsson D. E., 1989; Shinomiya et al., 2019a).

Together the layer of photoreceptors constitutes the **retina** of the eye. Below the retina, the optic lobe consists of four neuropils: lamina, medulla, lobula, and lobula plate (**Figure 1C**). Each of them is again tiled into ~750 retinotopically-arranged cartridges or columns such that visual signals from different points in space are processed in parallel (Bausenwein et al., 1992). However, two chiasms, the outer chiasm from lamina to medulla and the inner chiasm from medulla to lobula complex invert this retinotopic map (**Figure 1C**, Fischbach and Dittrich, 1989; Shinomiya et al., 2019a).

Within the *Drosophila* visual system, almost 100 cell types have been described and can be uniquely identified based on their specific anatomical characteristics (Fischbach and Dittrich, 1989; Nern et al., 2015). Of these, the first neuropile, the **lamina**, houses 12 neuronal cell types in each cartridge or column (**Figure 2**). These include the five lamina monopolar neurons L1-L5, two putative feedback neurons C2 and C3, and the tangential neuron T1, as well as the multicolumnar wide-field neurons Lai, Lawf1, Lawf2, and Lat (Fischbach and Dittrich, 1989). Direct input from photoreceptors R1 to R6, which extend their axons into the lamina, is given to L1, L2, an amacrine cell and L3 or a glia cell, forming tetrade synapses. All other lamina neurons are informed by either one of them (Fröhlich and Meinertzhagen, 1982; Meinertzhagen and O'Neil, 1991). Most lamina cells further extend their axons into the second neuropile, the **medulla** (Fischbach and Dittrich, 1989; Takemura et al., 2008). In the medulla, most lamina neurons form synaptic contacts with medulla intrinsic (Mi), transmedullary (Tm, TmY), or distal and proximal medulla (Dm, Pm) neurons, some of which are illustrated in **Figure 2**.

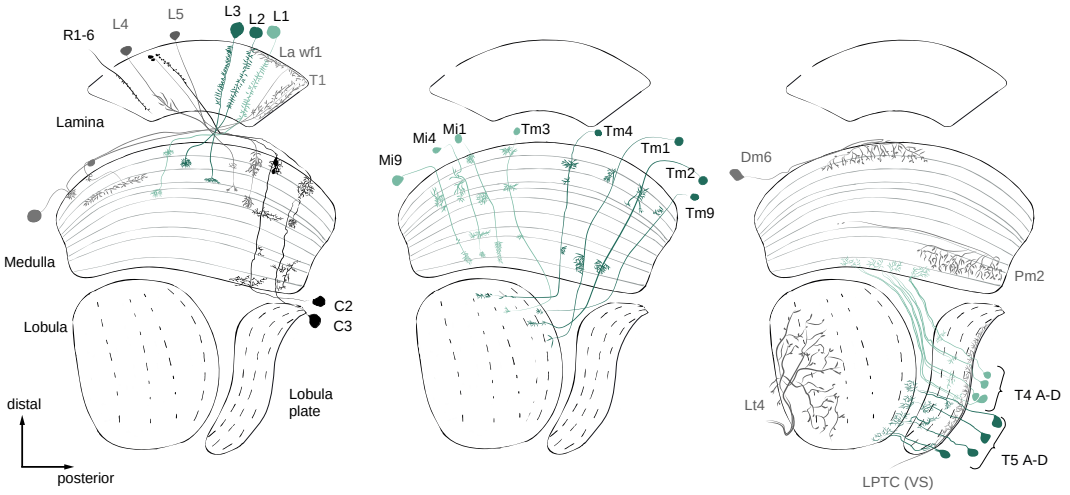

Figure 2. The visual system of the fruit fly. Shown are different types of neurons that process visual information from the lamina to the medulla and the lobula and lobula plate. These include the photoreceptors (R), lamina neurons (L), a tangential neuron (T), two columnar neurons (C2 and C3), medulla intrinsic (Mi) and transmedulla (Tm) neurons, dorsal and proximal medulla neurons (Dm and Pm), a lobula tangential neuron (Lt) as well as the local motion detection neurons T4 and T5. Neurons involved into motion detection are shown in color. Darker color depicts neurons assigned to the OFF pathway while ON pathway neurons are colored in light green. Note that only a few of more than 100 cell types are shown for simplicity. Furthermore, most cell types shown here exist once per cartridge or column.

The columnar architecture of the lamina and medulla is maintained in downstream neuropiles, by different T neurons in the **lobula** and the **lobula plate**. Of these, the T4 and T5

neurons will be important here, because they are the first direction-selective cells of the visual system. While both, T4 and T5, extend their axon terminals into the lobula plate, T4 houses its dendrites exclusively in the proximal medulla layer M10, whereas T5 extends its dendrites into the first layer of the lobula (**Figure 2**). T4 and T5 cells each come in four anatomical subtypes that can be distinguished based on the projections of their axon terminals into four distinct layers of the lobula plate (Fischbach and Dittrich, 1989). Downstream of T4 and T5 cells visual projection neurons (VPN) in the lobula plate, the lobula plate tangential cells (LPTCs) project their axons into the central brain. Within the lobula plate, LPTCs extend their dendrites along one or two particular layers of the lobula plate where they receive input from T4 and T5 cells as well as lobula plate intrinsic neurons (LPi) (Mauss et al., 2015) and thus signal global motion information (Joesch et al., 2008; Schnell et al., 2010). On the other hand, the VPNs located in the lobula of the visual system are mainly involved into other visual pathways for example object detection (Aptekar et al., 2012; Bahl et al., 2013, 2015; Keleş et al., 2019; Poggio and Reichardt, 1976). These include for example the most numerous lobula columnar (LC) neurons that project to multiple optic glomeruli in the central brain (Mu et al., 2012; Wu et al., 2016) as well as the large tangential (LT) neurons. Together with another set of giant cells that project into several neuropils at once e.g. the amacrine cell (CT1), Y cells, tangential neurons (Mt), translobula neurons (Tl), and lobula complex columnar neurons (Lccn), there is a large variety of different cell types in the visual system (Fischbach and Dittrich, 1989). Of these, only a few cell types have been shown to be important for the computation of visual motion information.

1.1.2 Motion vision pathway

The first instances of visual processing are the photoreceptors R1 to R6 that express the broad-band rhodopsin Rh1 to absorb photons and transform the energy into an electrical potential by phototransduction. In contrast to vertebrate cones and rods, photoreceptors in the fly retina respond with a depolarization to an increase of light (Laughlin, 1989; Zheng et al., 2006). Photoreceptors R1 to R6 transmit signals to the lamina via release of histamine, where postsynaptic lamina neurons express a histamine-gated chloride channel leading to a reversal of the response polarity (Hardie, 1987, 1989; Meinertzhagen and O'Neil, 1991; Rivera-Alba et al., 2011). Thus most lamina neurons respond with a depolarization to the offset of light and a hyperpolarization to the onset of light (Laughlin and Hardie, 1978).

From the level of the lamina down to the level of the lobula and lobula plate, neurons involved into motion processing are typically classified into two major pathways, namely the ON and the OFF pathway, which are selective for processing movement of brightness increments (ON) and decrements (OFF), respectively (Maisak et al., 2013). Based on behavioral and physiological studies, L1 has been shown to predominantly contribute to the computation of ON motion, while L2 and L3 have been shown to provide input to the OFF motion pathway (**Figure 3A**, Clark et al., 2011; Joesch et al., 2010; Rister et al., 2007; Silies et al., 2013; Tuthill et al., 2013). While L1 and L2 show a transient response to the offset of light, signaling contrast (Clark et al., 2011; Laughlin and Hardie, 1978; Zheng et al., 2006), L3 has been shown to report information about luminance. This is required to correct the estimation

of contrast in rapidly changing environments where adaptation could not yet take place (Ketkar et al., 2020). A sign inversion from L1 to medulla neurons of the ON pathway mediated through a multisynaptic process involving both GABAergic and glutamatergic inhibition leads to depolarizations to the onset of light and thus ON selective responses of neurons downstream of L1 in the ON pathway (Behnia et al., 2014; Molina-Obando et al., 2019; Yang et al., 2016). In contrast, neurons downstream of L2 or L3 are OFF selective (Arenz et al., 2017; Behnia et al., 2014; Serbe et al., 2016).

Besides anatomical evidence (Takemura et al., 2013, 2015), the contribution of L4 and L5 for visual processing remains unknown (Bahl et al., 2015; Meier et al., 2014; Silies et al., 2013; Tuthill et al., 2013). The four feedback neurons C2, C3, Lawf1 and Lawf2 have been suggested to broadly shape visual processing given their reciprocal connections to many lamina but also medulla neurons (Takemura et al., 2015; Tuthill et al., 2013; Yang and Clandinin, 2018). C2 and C3 have been shown to also have an effect on motion processing and motion-parallax for distance evaluation (Triphan et al., 2016; Tuthill et al., 2013).

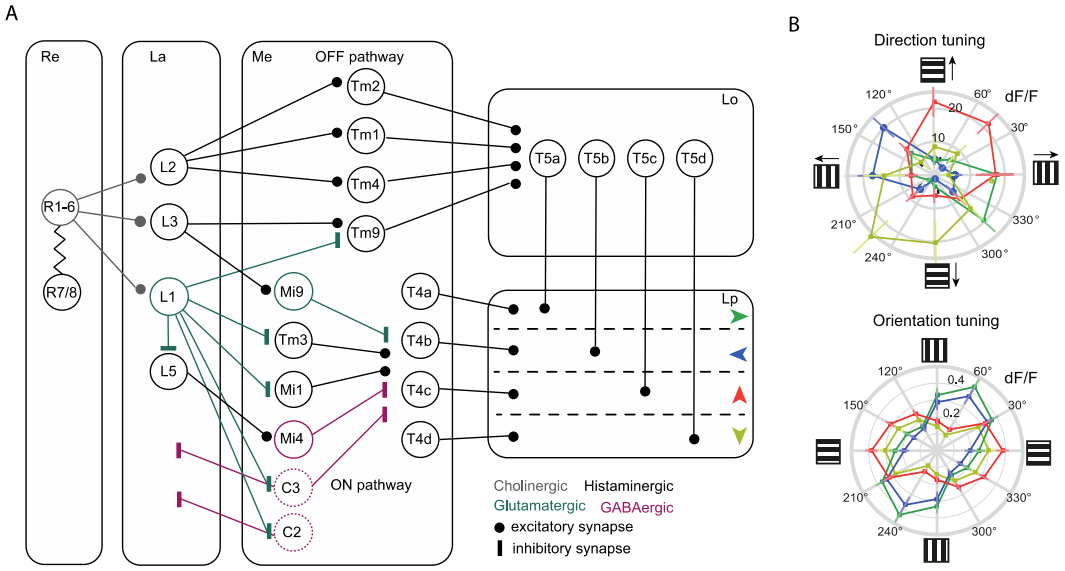

Figure 3. Motion detection circuit in D.melanogaster. (**A**) Schematic of neurons involved into motion processing of the ON and OFF pathway. Different compartments illustrate the retina (Re) and the four neuropiles, the lamina (La), medulla (Me), lobula (Lo) and lobula plate (Lp) of the visual system. Colors indicate validated neurotransmitter phenotype: Histaminergic (grey), cholinergic (black), glutamatergic (green), GABAergic (magenta). Neuron connections that are so far only based on connectomic data are depicted in dotted lines. All other neurons shown have been functionally and anatomically validated to be important for motion detection. Modified from Yang and Clandinin (2018). (**B**) Direction and orientation tuning of the local motion detectors T4 and T5. Polar plots show maximum calcium responses to gratings moving into eight different directions (top) or static gratings with different orientations. (Data from Fisher et al., 2015b)

In the medulla, few of the many neuronal cell types have so far been identified to be part of core motion detection circuits based on functional studies and connectomes. In the **ON pathway**, these are mainly the four medulla neurons Mi1, Tm3, Mi4 and Mi9 (**Figure 3A**). Of these only Mi1, Tm3 and Tm4 are ON selective (Arenz et al., 2017; Behnia et al., 2014; Strother et al., 2017). Mi9 on the other hand receives inputs from L3 and depolarizes to OFF (Arenz et al., 2017; Strother et al., 2017; Takemura et al., 2017). This shows that at the level of the local motion detector T4, inputs from both ON selective and OFF selective neurons are

utilized to extract ON motion responses. How this is important for the computation of motion will be discussed later. Besides the above described neurons, C3, CT1 and TmY15 have been show to provide synaptic contacts to T4 (Shinomiya et al., 2019b; Takemura et al., 2017).

On the other hand, the four medulla neurons Tm1, Tm2, Tm4 and Tm9 have been assigned to the **OFF pathway** (**Figure 3A**). All these Tm neurons project their axon terminals to the lobula where they directly synapse onto the OFF motion-selective T5 neuron (Shinomiya et al., 2014, 2019b) and have also been shown to functionally contribute to the OFF motion processing pathway (Fisher et al., 2015b; Serbe et al., 2016). While Tm1, Tm2 and Tm4 receive their main inputs from L2 and are thus OFF selective (Behnia et al., 2014), Tm9 integrates L3 and L1 inputs (Fisher et al., 2015b; Takemura et al., 2013). Measurements of the receptive field structure of Tm9 and Tm2 show that they are comprised of an OFF center and a wider inhibitory ON component (Ramos-Traslosheros and Silies, 2021). Therefore, also at the level of T5, ON and OFF inputs are integrated for OFF motion processing. Interestingly, the GABAergic amacrine cell CT1 does not only synapse onto T4 but also onto T5 and has recently been described to be compartmentalized, in a way that it could provide local ON selective information to T4 and local OFF-selective signals to T5. It has therefore been suggested to be important for local motion processing in T4 and T5, which remains to be tested functionally (Meier and Borst, 2019; Shinomiya et al., 2019b; Takemura et al., 2017).

As described previously, the local motion detectors T4 and T5 both extend their axons into four anatomical distinct layers of the lobula plate (**Figure 2**, **Figure 3A**). Based on the layer they project to (layer A-D), these neurons have been categorized into four anatomical subtypes each (Fischbach and Dittrich, 1989). First recordings using activity labeling with 2-deoxyglucose have shown that each of these four layers in the lobula plate displays directional tuning into one of four cardinal directions of motion (Bausenwein and Fischbach, 1992). Calcium imaging experiments in *Drosophila* confirmed that it is the axon terminals of the local T4 and T5 cells that display this direction tuning into ostensibly four directions of motion (**Figure 3B**, Fisher et al., 2015b; Maisak et al., 2013). Additionally, orientation tuning orthogonal to the axis of their preferred motion axis sharpens the directional tuning of the motion detectors T4 and T5 (**Figure 3B**, Fisher et al., 2015b). Further characterizations have shown that the direction tuning already arises at the dendrites of T4 and T5 cells in the lobula and medulla (Fisher et al., 2015a), whereas all input neurons to T4 and T5 are not directional. This suggests that directional tuning and thus motion information is computed at the level of T4 and T5 dendrites. Downstream of the local motion detectors, LPTCs pool information from many T4/T5 cells (Mauss et al., 2014; Schnell et al., 2012) and thus signal motion across a large part of the visual field.

1.2. Computations underlying local motion detection

1.2.1 Algorithms of local motion detection

To compute motion information, T4 and T5 cells need to compare local luminance changes over space and time. Already 60 years ago, long before the neurons in the visual system of flies or the vertebrate retina have been mapped, algorithmic models were proposed to describe how direction selectivity, a hallmark of motion detection could be extracted by a neuronal network. These include the Hassenstein-Reichardt Correlator (HRC), the Barlow-Levick model (BLM) and the Motion Energy Model proposed by Adelson and Bergen (Adelson and Bergen, 1985; Barlow and Levick, 1965; Von Hassenstein and Reichardt, 1956a). All three models describe motion detectors that correlate inputs of neighboring points in visual space across time leading to either enhanced responses into the detector's preferred direction (PD) or suppressed responses into the non-preferred or so-called null direction (ND). For many years the HRC has been the major model for motion detection in flies as many behavioral responses to a wide range of different stimuli, quantitatively matched predictions of the HRC (Werner, 2013). However, recordings of the local direction selective T4 and T5 cells have shown that they integrate both excitatory and inhibitory signals to become direction-selective, suggesting that a combination of an HRC and BLM – type mechanism is implemented in the *Drosophila* brain (as comprehensively discussed in our review: Ramos-Traslosheros, **Henning**, Silies, 2018). Both models require non-linear filtering to become direction selective. Additionally, recent voltage recordings suggest that direction selectivity in T4 and T5 cells is established by a linear summation of excitatory and inhibitory signals and that a nonlinear voltage-to-calcium transformation accounts for the previously measured non-linearities (Gruntman et al., 2018, 2019; Wienecke et al., 2018). Taken together, T4 and T5 cells integrate excitatory inputs with inhibitory signals that suppress signals to non-preferred directions of motion.

1.2.2 Inhibitory signaling for motion computation

Inhibitory signaling in the brain of *D. melanogaster* can be mediated by gamma-Aminobutyric acid (GABA) and glutamate (Enell et al., 2007; Kolodziejczyk et al., 2008; Küppers et al., 2003; Liu and Wilson, 2013). **Glutamate** is an amino acid that is one of the major excitatory neurotransmitters in vertebrates and can be both excitatory and inhibitory in invertebrates. It mediates its diverse effects by binding to different types of receptors including metabotropic glutamate receptors (mGluRs) or ionotropic glutamate receptors like the N-methyl-D-aspartate (NMDA) receptor or the glutamate gated chloride channel (GluClα). While NMDA and mGluRs have been shown to be important for activity dependent postsynaptic plasticity (Bogdanik et al., 2004; Tabone and Ramaswami, 2012; Xia and Chiang, 2008), GluClα mediates an inhibitory chloride influx upon glutamate binding and thus leads to a hyperpolarization of the post synaptic cell (Liu and Wilson, 2013). GluClα was also shown to be highly expressed in the visual system of *D. melanogaster* (Davis et al., 2020; Fendl et al., 2020; Molina-Obando et al., 2019).

GABA is synthesized from glutamate by glutamate decarboxylate (*Gad1*) (Featherstone et al., 2000), transported into synaptic vesicles by the vesicular GABA transporter (vGAT) and removed from the synaptic cleft by the plasma membrane GABA transporter GATs1-3 (Fei et al., 2010; Schousboe, 2000). On the post synapse GABA binds to two classes of GABA

receptors, the metabotropic $GABA_B$ receptors and the ionotropic $GABA_A$ receptors. In the olfactory system $GABA_B$ was shown to mediate slow inhibition while $GABA_A$ receptors mediate fast inhibitory transmission (Wilson and Laurent 2005). Both $GABA_B$ and $GABA_A$ receptors are also highly expressed in many different neuron types in the visual system shown by immunostainings (Enell et al., 2007; Kolodziejczyk et al., 2008), genetically labelling the endogenous proteins (Fendl et al., 2020) and RNA sequencing data (Davis et al., 2020). The $GABA_A$ receptor is composed of different types of subunits (Hosie et al., 1997; Buckingham et al., 2005). Different types of $GABA_A$ subunit compositions were shown to form either GABA-gated chloride channels (*Rdl*/*Lcch3*) or GABA-gated cation channels (*Lcch3*/*Grd*) (Gisselmann et al., 2004; Zhang et al., 1995). The latter was recently shown to be expressed in the lamina neurons L1, L2 and L3 (Davis et al., 2020). But, the *in vivo* function of the different subunit composition is not known so far.

Both GABA and glutamate signaling have been shown to be functionally important for the processing visual information. For example, a full loss-of-function of the GluClα subunit abolished ON motion responses in T4 neurons, because its function is critical for the sign inversion from L1 to ON selective medulla neurons (Molina-Obando et al., 2019). Additionally, the same study has shown that GABAergic signaling is also important for the computation of ON selectivity. Furthermore, GABAergic signaling has been shown to affect early visual processing in the OFF pathway, where it shapes the center surround organization of L2 (Freifeld et al., 2013). Most importantly, a pharmacological block of $GABA_A$ receptors results in a loss of orientation and direction-selectivity of T4 and T5 neurons, such that both neurons respond to any direction of motion (Fisher et al., 2015a). This shows that GABAergic signaling is not only important for peripheral processing of visual information but also required for the computation of direction-selective signals in T4 and T5 neurons. However, little is known about the role and the implementation of GABAergic circuitry in the *Drosophila* visual system.

1.2.3 Neurotransmitter identity of motion detection neurons

Diverse studies were set out to identify the neurotransmitter identity of the neurons involved in motion detection. These include immunostainings (Brotz et al., 2001; Datum et al., 1986; Kolodziejczyk et al., 2008; Meyer et al., 1986; Sinakevitch et al., 2003), expression of reporter transgenes (Raghu and Borst, 2011; Raghu et al., 2011, 2013) or tagging neurotransmitter transporters with fluorophores (Pankova and Borst, 2017). Additionally, cell type-specific and single cell RNA sequencing predicted a neuron's neurotransmitter phenotype using the enzymes and transporters expressed by a single neuron (Davis et al., 2020; Konstantinides et al., 2018). Together they revealed several GABAergic cell types in the visual system including the GABAergic neurons C2, C3, Mi4, Dm10, Pm3, Pm4 and CT1. Notably the two columnar neurons C2 and C3 were suggested to be GABAergic already within the first attempts of classifying neurotransmitter identity (Buchner et al., 1988; Datum et al., 1986; Kolodziejczyk et al., 2008; Meyer et al., 1986). Additionally, several glutamatergic cell types were identified, including L1, Mi9 and several Dm and Tm neurons (Davis et al., 2020). Taken together, two cell types of the ON pathway that directly synapse with dendrites of T4

cells, are inhibitory, the glutamatergic Mi9 neuron and the GABAergic Mi4 neuron. In addition, two GABAergic neurons, CT1 and C3, form synapses with T4 dendrites. The other two main inputs, Mi1 and Tm3 are cholinergic (**Figure 3A**). On the other hand, all main inputs to T5 are cholinergic. The only direct inhibitory input to T5 could be mediated by CT1.

1.2.4 Implementation of PD enhancement and ND suppression

In the last decade, a range of connectomic, physiological, behavioral and genetic approaches were taken to identify the molecular and circuit mechanisms behind motion computation (as extensively reviewed by: Borst et al., 2020; Ramos-Traslosheros et al., 2018; Silies et al., 2014; Yang and Clandinin, 2018). Based on the anatomic arrangement of the major presynaptic inputs onto the dendrites of T4/T5 direction selectivity, the proposed neurotransmitter identity of these inputs, and their temporal filter properties, new models were proposed to explain how PD enhancement and ND suppression are implemented in T4 and T5 cells. For T4 this model is comprised of a slow inhibitory OFF input on the leading side, a fast ON component in the center and a slow inhibitory ON component on the trailing side (**Figure 4A**). Connectomics revealed that the medulla neurons Mi1 and Tm3 both synapse at the center of the T4 dendritic tree while the slow Mi4, C3 and CT1 neurons mainly synapse with the trailing side of the T4 dendrite and were thus suggested to implement ND suppression (**Figure 4B**, Shinomiya et al., 2019b; Takemura et al., 2017). Furthermore the OFF-selective Mi9 neuron provides synapses on the leading side of the T4 dendrite, which was proposed to enhance PD responses to ON edges by release of inhibition (Borst, 2018; Shinomiya et al., 2019b). This model has been shown to capture direction selectivity in T4 cells (Arenz et al., 2017; Badwan et al., 2019; Zavatone-Veth et al., 2020). However, genetic silencing experiments so far only demonstrated a critical role of Mi1 and Tm3 for motion computation, whereas blocking Mi4 or Mi9 had no effect on T4 responses (Ammer et al., 2015; Strother et al., 2017). Furthermore, there is so far no evidence for a requirement of CT1 and C3 function for T4 responses. Together, this could either imply that PD enhancement alone is strong enough to compensate for the absent ND suppression, when blocking Mi4 or Mi9, or ND inhibition is not implemented by any of the direct inputs but by a so far unknown inhibitory circuitry. For DS responses in the OFF pathway, a similar model has been proposed, with Tm9 synapsing on the leading side, Tm1, Tm2 and Tm4 located in the center of the T5 dendrites, and CT1 providing trailing side inhibition (**Figure 4B**, Shinomiya et al., 2019b). Tm9 has been shown to transmit both ON and OFF information to T5 and could thus have a similar function for PD enhancement as Mi9 for T4 (Ramos-Traslosheros and Silies, 2021; Serbe et al., 2016). Besides CT1, all inputs to T5 are excitatory, however if CT1 is functionally important for DS in T5 is not known so far.

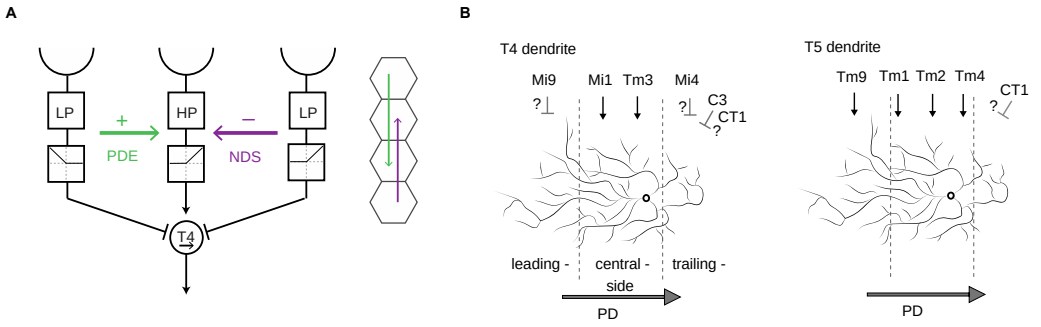

Figure 4. Core mechanism for direction-selectivity of T4 and T5 neurons. (**A**) Three-arm motion detector for ON motion computation in T4. This model is comprised of a slow inhibitory OFF input on the preferred side, a fast ON component in the center and a slow inhibitory ON component on the null side. T4/T5 neurons sample from three to four neighboring columns. (**B**) Dendrites of an example T4 or T5 neuron. Synaptic sides of input neurons are organized across the dendrite such that they mainly target either the preferred- the central- or the null-side of the dendrite.

Taken together, both T4 and T5 cells implement ND suppression, however the circuitry to implement this remains unknown. Furthermore, GABAergic signaling is required for direction selectivity in T4 and T5 neurons, but the GABAergic neurons, that are required for T4 and T5 responses have not been revealed so far.

1.3. From local to global motion detection

All computations described above focused on the extraction of local motion information. However, for many visual animals, including the fly, the processing of global motion information is highly relevant for various types of behavior as for example navigation. As a fly moves through its environment, a particular type of self-motion will elicit specific global motion patterns also named optic flow patterns on the eye. To detect these optic flow patterns it is crucial to for example counteract deviations of the intended flight path (Krapp, 2008).

1.3.1. Wide field motion detectors

In mice, optic flow is already represented in the population level of local direction selective ganglion cells (DSGCs, Sabbah et al., 2017). In contrast, in flies and many other insects, including moth, locusts and dragonflies, optic flow patterns are thought to be first time detected by the wide field motion-sensitive LPTCs in the lobula plate of the visual system (Evans et al., 2019; Hengstenberg et al., 1982; Kern, 1998; Kien, 1974; Rind, 1990; Rowell, 1988; Stöckl et al., 2016; Theobald et al., 2010). In total 60 different types of these LPTCs located in the lobula plate have been described in blowflies (*Calliphora*) (Borst and Haag, 2002; Egelhaaf, 2013; Hausen, 1982; Hengstenberg et al., 1982; Krapp, 2000, 2008; Krapp

and Hengstenberg, 1996; Krapp et al., 1998, 2001), and several LPTC types have been described in the fruit fly (Boergens et al., 2018; Schnell et al., 2010; Scott et al., 2002; Wei et al., 2020). These include three horizontal system (HS) cells and six vertical system (VS) as well as the dorsal and ventral centrifugal horizontal (dCH, vCH) cells, H1, H2 and V1 neurons and figure detection neurons (FD1, FD3). Of these, the three horizontal cells, HSN (north), HSE (equatorial) and HSS (south) and the six VS cells (VS1-VS6) have been characterized most extensively (**Figure 5**).

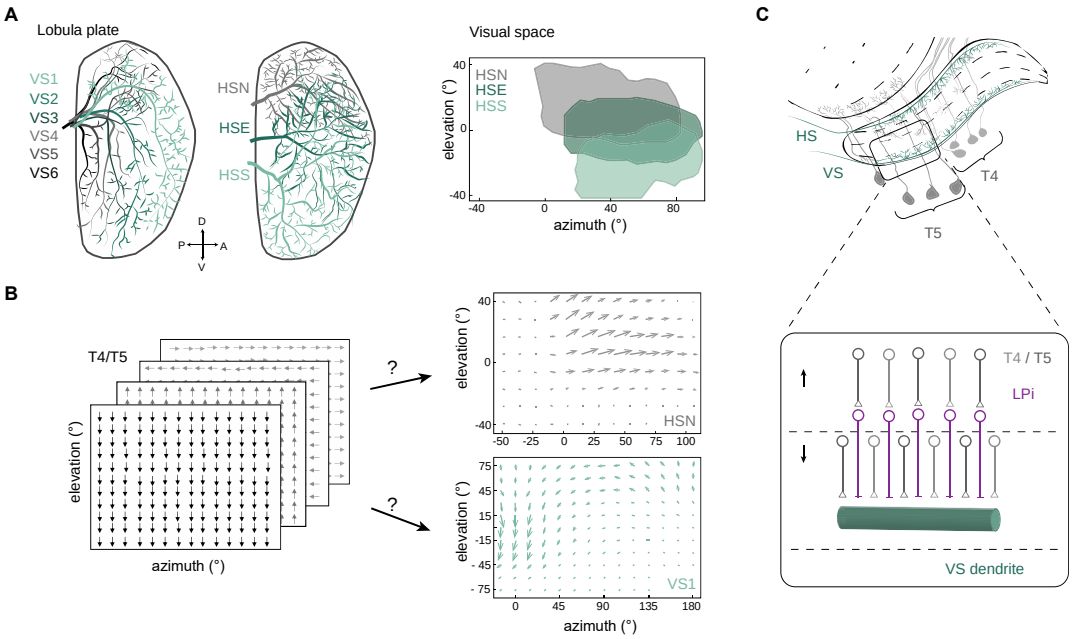

Figure 5. Self-motion induced optic flow is encoded by LPTCs. (**A**) Dendritic arborizations of VS and HS cells in the lobula plate and an outline of the estimated receptive fields of the three HS cells (modified from Schnell et al., 2010 and Scott et al., 2002). (**B**) Illustration of the apparent uniform vector field representation by the four populations of T4 and T5 cells (left). Measured vector fields of a Drosophila HSN cell and a Calliphora VS1 cell (right). (modified from Krapp and Hengstenberg, 1996 and Schnell et al., 2010). (**C**) Illustration of a VS cell dendrite pooling from T4 and T5 cells in layer D of the lobula plate. LPi cells mediate inhibitory input from T4 and T5 cells with opposite directional preference.

While the six VS cell dendrites project mainly into layer D of the lobula plate and tile it sequentially along the posterior-anterior axis, the three HS cells extend their dendrites to either dorsal, equatorial or ventral parts of layer A in the lobula plate (**Figure 5A**, Boergens et al., 2018a; Fischbach and Dittrich, 1989; Schnell et al., 2010; Scott et al., 2002). Electrophysiological recordings confirmed that each VS cell is sensitive to vertical motion, whereas HS cells are sensitive to horizontal motion in a restricted region of the visual field (**Figure 5A**, Joesch et al., 2008; Schnell et al., 2010; Suver et al., 2016). Measuring local preferred tuning and sensitivities of these cells to small local motion stimuli at different positions of the visual field, revealed their receptive field organization (**Figure 5B**, Krapp and Hengstenberg, 1996; Schnell et al., 2010). Local preferred tuning systematically varied across the visual field, such that VS cells were described to be tuned to different types of rotatory optic flow along the horizontal plane of the fly, including nose up pitch (VS1) or roll rotations

(VS6) (Hengstenberg et al., 1982; Krapp and Hengstenberg, 1996; Krapp et al., 1998; Scott et al., 2002). HS cells on the other hand are predominantly tuned to forward translation (**Figure 5B**, Hausen, 1982; Krapp, 2000, 2008; Krapp et al., 2001; Schnell et al., 2010).

1.3.2. Computation of global motion

The complex receptive field structures of LPTCs, where local motion preferences vary with the receptive field location, are surprising given that HS dendrites project exclusively into one layer of the lobula plate, where they pool from T4/T5 cells that were suggested to have a uniform tuning from front-to-back (**Figure 5B, C**, Maisak et al., 2013; Mauss et al., 2014; Schnell et al., 2012). The same is true for VS cells that mainly reside in layer D of the lobula plate, with the exception of small branches extending into layer C (Boergens et al., 2018). Therefore, several studies tried to understand the computation of complex optic flow tuning from local T4/T5 inputs and revealed several circuit mechanisms but also dendritic processes within LPTCs that may help to specialize their tuning. First of all, LPTCs do not only receive inputs from T4/T5 cells but additionally receive feed-forward inhibition from lobula plate intrinsic (LPi) neurons that pool responses from T4/T5 cells with opponent motion sensitivity (**Figure 5C**). This leads to hyperpolarizing responses of LPTCs to non-preferred directions of global motion, establishing motion opponency in these cells (Mauss et al., 2015). Additionally, LPTC dendrites are oriented to match the sequence of PD stimuli hitting the eye and selectively amplify inputs if the spatiotemporal sequence matches the neurons global tuning preference (Barnhart et al., 2018). Some evidence additionally suggests that, HS and VS cells are electrically coupled to each other (Cuntz et al., 2007; Farrow et al., 2005; Haag and Borst, 2004; Joesch et al., 2008; Schnell et al., 2010). Other cell types as for example H1 cells, that preferentially respond to backward translational optic flow in *Calliphora*, receive inputs from layer B on the ipsilateral side and additionally innervate the lobula plate on the contralateral side of the brain in layer A and B where H1 is likely presynaptic to other LPTCs. This way H1 receives binocular motion information which may be useful to disambiguate rotational and translational motion (Egelhaaf et al., 2002; Wei et al., 2020).

Taken together, several mechanisms may mediate the computation of complex receptive field structures tuned to optic flow of self-motion, however it is unclear if these computations are sufficient for the complex transformation of cardinal information to flow fields. Neither has it been shown whether the described directional selectivity of the local motion detectors extends across the whole extend of the visual field. Given the arrangement of ommatidia along the curvature of the eye suggest that local tuning preference which depends on the structure of neighboring ommatidia, may be more distributed than previously suggested (Heisenberg, M. & Wolf, 1984; Petrowitz et al., 2000).

1.4. Aims of the dissertation

The aim of this thesis is to further elucidate the mechanisms and neuronal circuits underlying motion computation. This includes the local computation of direction-selective responses in T4 and T5 neurons, as well as the tuning distribution of the population of T4 and T5 cells for global motion computation.

First of all, GABAergic inhibitory signaling is crucial for the local computation of direction-selective signals in the direction-selective T4 and T5 cells (Fisher et al., 2015). Based on direct measures of inhibitory signals in T4 and T5 cells (CITE) this inhibitory signal was suggested to be a direct connection onto T4 and T5 cells. However, none of the inhibitory cell types that synapse onto T4 and T5 cells has been shown to be required for the computation of direction selectivity (CITE). This argues that the inhibitory GABAergic signaling required for DS in T4/T5 might be implemented in upstream circuitry. Therefore, the first aim of this thesis is to **elucidate the GABAergic circuitry that shapes direction-selectivity in T4 and T5 neurons**. Revealing the expressing pattern of genetic driver lines that showed deficits in motion guided behaviors upon genetically blocking output of the targeted cell types, I aimed to identify GABAergic neurons that are likely relevant for motion vision. Using *in vivo* two photon calcium imaging I further aimed to characterize response properties of the identified GABAergic neuron candidates to visual stimuli. Blocking neuronal activity of these neurons I aimed to identify their functional role for downstream neurons of the motion vision circuitry including the direction-selective T4 and T5 cells.

For the second part of my thesis, I aimed to understand how local motion information computed by the T4/T5 cells is transformed into a global information of optic flow that is generated during self-motion in downstream lobula plate tangential cells (LPTCs). In mice, optic flow is already represented in the population level of local direction selective ganglion cells (DSGCs, Sabbah et al., 2017). In flies the local T4/T5 cells are thought to be uniformly tuned to the four cardinal directions of motion across visual space (Maisak et al., 2013). This suggests that to become tuned to optic flow, downstream LPTCs cannot simply pool from T4/T5 cells across visual space but must transform cardinal motion information into complex flow fields, which raises the question why flies would have evolved such a complex system compared to mice. Furthermore, the computation of local cardinal motion seems challenging given the hexagonal arrangement of ommatidia in the fly's eye which is further shaped by the curvature of the eye. To determine if the apparent cardinal tuning of T4/T5 cells generalized across the whole visual field, I aimed to **characterize the directional tuning distribution across the population of T4/T5 cells** using *in vivo* two photon calcium imaging.

2 REVIEW

The following review ‘Motion detection: cells, circuits and algorithms’ (https://doi.org/10.1515/nf-2017-A028) was originally published in Neuroforum in March 2018.

I wrote the first draft of part ‘Classical descriptions of motion detection algorithms’ and parts of ‘Novel insights into motion detection algorithms’ of this review (~ one third). The text was then jointly edited and finalized by all three authors.

DE GRUYTER Neuroforum 2018; 24(2): A61–A72

Giordano Ramos-Traslosheros, Miriam Henning and Marion Silies*

Motion detection: cells, circuits and algorithms

https://doi.org/10.1515/nf-2017-A028

Abstract: Many animals use visual motion cues to inform different behaviors. The basis for motion detection is the comparison of light signals over space and time. How a nervous system performs such spatiotemporal correlations has long been considered a paradigmatic neural computation. Here, we will first describe classical models of motion detection and introduce core motion detecting circuits in *Drosophila*. Direct measurements of the response properties of the first direction-selective cells in the *Drosophila* visual system have revealed new insights about the implementation of motion detection algorithms. Recent data suggest a combination of two mechanisms, a nonlinear enhancement of signals moving into the preferred direction, as well as a suppression of signals moving into the opposite direction. These findings as well as a functional analysis of the circuit components have shown that the microcircuits that process elementary motion are more complex than anticipated. Building on this, we have the opportunity to understand detailed properties of elementary, yet intricate microcircuits.

Keywords: Drosophila; motion detection; neurogenetics; neuronal circuits; visual system

Introduction

The environment we live in is ever changing, things are in constant motion. Visual motion originates from moving objects, but also when an entire visual scene moves past our eyes during self-motion. The perception of visual motion is an important sensory function for many animals. Motion could indicate an approaching threat or predator, a wandering pray, or a potential mating partner. In a still surrounding, the motion that emerges as a consequence of self-motion allows animals to safely navigate the environment. These examples also illustrate how motion can be local, when an insect flies past the eye; or global, when the full visual space is moving during navigation. Global and local motion are related in the sense that global motion can be decomposed into the motion of the local features of the visual scene. Thus, visual systems detect local motion in order to perceive both local and global motion. The smallest perceivable motion would be between two points in space at the limit of the resolution of a visual system. The unit that detects these smallest movements is called an elementary motion detector (EMD). At this scale, the visual system has to extract luminance changes over both space and time to produce a direction-selective (DS) signal, which is a hallmark of elementary motion detection. Consequently, each EMD has a direction of motion that it is most sensitive to, its so-called preferred direction (PD).

How are visual systems able to detect movement at such a fine scale? Somewhere in the nervous system, an EMD must be implemented in a way that the output neurons are direction-selective and therefore able to detect local motion. Identifying the biological substrate of the EMDs and the algorithm behind computing the direction of motion has therefore been considered an interesting topic that can shed light onto an important function of nervous systems. Since motion vision is behaviorally salient for many visual animals, it has been studied in species as diverse as monkeys, cats, mice, but also in various fly species including the fruit fly *Drosophila*, which we will mostly focus on in this review.

Classical descriptions of motion detection algorithms

How biological systems extract motion signals has received extensive attention since the 1950s (reviewed in Borst and Euler, 2011). The first popular algorithmic model that could explain direction-selective responses emerged from analyzing behavioral responses to moving stimuli, the so-called optomotor behavior of the *Chlorophanus* beetle (Hassenstein and Reichardt, 1956). This model laid the foundation for subsequent studies of motion detection

*Corresponding author: **Marion Silies,** European Neuroscience Institute Göttingen (ENI), University Medical Center Göttingen, Grisebachstr. 5, 37077 Göttingen, Germany, Mail: m.silies@eni-g.de, Web: www.silieslab.com
Giordano Ramos-Traslosheros, European Neuroscience Institute Göttingen (ENI), University Medical Center Göttingen, Grisebachstr. 5, 37077 Göttingen, Germany; International Max Planck Research School Neuroscience, University of Göttingen, Göttingen, Germany, Mail: l.ramos@eni-g.de
Miriam Henning, European Neuroscience Institute Göttingen (ENI), University Medical Center Göttingen, Grisebachstr. 5, 37077 Göttingen, Germany, Mail: m.henning@eni-g.de

in other species that refined properties of the model and came to be known as the Hassenstein-Reichardt Correlator (HRC). This model proposes the comparison of two signals coming from two locally restricted points in visual space, accounting for the offset in space inherent to motion signals. And, to account for the offset in time, one signal is temporally delayed with respect to the other. Then, the two (delayed and non-delayed) signals are combined, or correlated, in a nonlinear fashion at the output stage of the model (Figure 1A).

For an EMD selective for left-to-right motion, the signal arising from the left point in space will be processed with a delay relative to the signal at the right point (Figure 1A). The delay ensures that, for an object moving in the preferred direction (PD, left-to-right), both signals will temporally overlap at the output stage of the EMD. There, a nonlinear amplification of the overlapping signals generates a strong motion signal. Conversely, when the movement is in the non-preferred or null direction (ND, right-to-left), the delay will cause the signals to arrive at different times to the correlation stage so there is no signal integration, i.e., no motion signaling (Figure 1A). In other words, the HRC model predicts how a direction-selective signal can be generated from two input signals (reviewed in Borst and Euler, 2011; Silies et al., 2014).

The HRC relies on a nonlinear amplification of input signals, using feedforward excitation. Another model explaining direction-selectivity that emerged in the 1960s instead relied on signal suppression, implying inhibitory neuronal processes, in total contrast to the HRC. The Barlow-Levick model (BLM) was developed to explain the responses of direction-selective neurons in the vertebrate retina (Barlow and Levick, 1965). Like the HRC, the BLM also relies on a comparison of signals from two points in space temporally delayed with respect to each other, and nonlinearly combined. However, here they are combined via an AND-NOT operation at the output stage, such that there is only an output signal when there is no signal coming from the delayed input, which would cancel the previous signal (Figure 1A). Taking our previous example of an EMD with a left-to-right motion preference, the corresponding BLM will respond to motion as follows: for movement in the null direction, a signal will emerge first from the delayed component and then temporally overlap with the second signal at the output stage. There, the AND-NOT logical operation will result in a cancellation of the second signal, indicating nulling inhibition. In the EMD's preferred direction, the non-delayed signal will arrive first at the output stage, thus escaping the nulling inhibition from the slow signal, which will arrive later. The outcome of this operation is again a direction-selective signal.

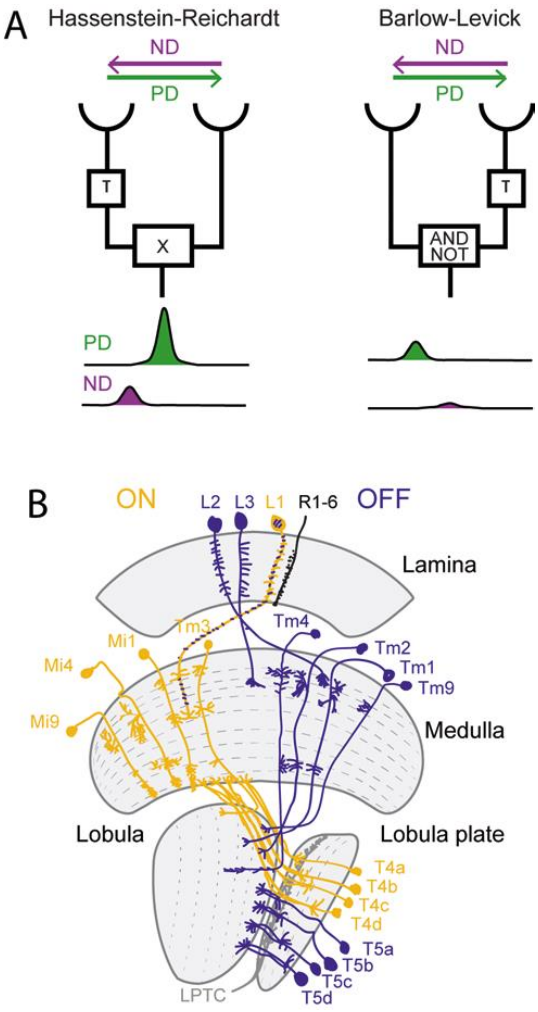

Fig. 1: A. Two models of motion detection. On the left, the Hassenstein Reichardt Correlator (HRC) correlated inputs from two adjacent points in space after one signal has been temporally delayed (τ). The outcome is a direction selective signal, in which signals moving in the preferred direction (PD) are nonlinearly amplified. On the right, the Barlow Levick Model (BLM) compares two signals in space through a logical AND NOT operation, after delaying one signal. The outcome is a direction selective signal, in which signals moving in the null direction (ND) are suppressed. **B.** Schematic of the fly visual system and core motion detecting circuits. Shown are neurons of the ON (yellow) and OFF (blue) pathways for which either behavioral roles have been shown, or a functional requirement for direction-selective responses in T4/T5 neurons. For details, see text.

In insects, the HRC originally gained widespread acceptance by successful predictions of behavioral and neural responses. One example is that the HRC response to a

moving grating is not tuned to the speed of the pattern but to the temporal frequency, which is the rate of contrast change at a particular location. In different fly species, responses were shown to be similar for gratings of different spacing as long as the temporal frequency was maintained (Buchner, 1976; Eckert, 1973; Götz, 1964; Reichardt, 1987). The HRC thus has an optimal speed that depends on the spatial wavelength in a linear way. This hypothesis was further supported by electrophysiological recordings in the lobula plate tangential cells (LPTCs), wide field neurons that integrate inputs from many individual EMDs along their dendritic arbors, in blow flies (Egelhaaf and Reichardt, 1987; Hausen, 1982; Hengstenberg et al., 1982) and the fruit fly (Joesch et al., 2008; Schnell et al., 2010).

The above described features of motion detection (among others) were experimentally confirmed in diverse species including flies, cats, and humans, which led to a wide popularity of the HRC to explain motion responses (Borst and Egelhaaf, 1989). In humans, another model – the motion energy model – is generally favored (Adelson and Bergen, 1985), but this models can be made algorithmically equivalent to the HRC to describe motion perception (van Santen and Sperling, 1985). Extensions of the HRC model to account for visual behaviors of *Anolis* lizards is another recent application in yet another species (Fleishman and Pallus, 2010).

In contrast, the model that has long been favored to describe motion responses in the vertebrate retina was the BLM. Barlow and Levick (1965) originally attributed direction-selective responses of retinal ganglion cells to null direction inhibition. This was strongly supported by the loss of direction-selective responses in retinal ganglion cells upon pharmacological block of GABAergic, inhibitory signaling (Caldwell and Daw, 1978; Wyatt and Day, 1976). Further experiments localized the source of GABAergic inhibition to starburst amacrine cells (Amthor et al., 2002; Yoshida et al., 2001).

A vast amount of literature led to the dominance of the HRC to explain motion detection in insects, and the BLM to explain motion responses in the vertebrate retina. Interestingly, recent work showed that a combination of the two algorithms is in fact used in both systems to establish direction-selectivity (Fisher et al., 2015b; Haag et al., 2016; Leong et al., 2016). In the following, we are first going to describe the identification of motion detection circuits in the fruit fly *Drosophila*. With the knowledge of these circuit elements, we will discuss an experimental handle to directly test the implementation of distinct algorithms at the output stage of the EMD. Finally, the results of such experiments, and their implications for the mechanistic implementation of the EMD will be highlighted in the last chapter of this review.

Mapping motion detecting circuits

Although algorithmic models of motion detection have existed for decades, the circuit implementation of motion computation remained elusive. This changed dramatically with the development of genetic tools to study circuit function in *Drosophila*. These could be applied well in a context where the anatomy of many neurons of the visual system was described with exquisite detail (Fischbach and Dittrich, 1989), and down to individual synapses (Meinertzhagen and O'Neil, 1991; Takemura et al., 2008; 2017).

The visual system of Drosophila melanogaster. The visual system of the fly is organized into the retina and three optic ganglia: the lamina, medulla and lobula complex, the latter being divided into lobula and lobula plate (Figure 1B). The retina is organized in an array of 800 parallel units, the ommatidia. Each ommatidium houses eight photoreceptors out of which the six outer photoreceptors (R1-R6) express the broadband-spectrum rhodopsin Rh1 that is required for motion detection (Heisenberg and Buchner, 1977). All R1-R6 cells that see the same point in space project onto the same targets in the lamina, most notably the L1-L3 neurons. Neighboring points in visual space are encoded by neighboring columns in the lamina, thus creating a retinotopic image of the visual input. This parallel columnar arrangement is maintained in the next ganglion, the medulla, were more than 60 different cell types pass on information to the lobula and the lobula plate.

Genetic strategies to map visual circuits. Major advances in visual circuit analysis came with the possibility to mark or manipulate neurons in the fly brain with great specificity. This included the development of genetic tools to manipulate or measure the activity of neurons on the one hand, and the ability to express these tools very specifically in the brain on the other hand. In *Drosophila*, so-called driver lines exist that control expression in different subsets of neurons. Over the last years, several thousands of these driver lines were developed that can be used to express different genetic tools in any pattern of interest (Gohl et al., 2011; Jenett et al., 2012). The optimal level of specificity would be expression in a single cell type or even in an individual neuron, but expression patterns of individual genes, enhancers, or promotors are often broader than

that. Therefore, intersectional strategies were developed that refine expression patterns to the above-mentioned level of specificity (Gohl et al., 2011; Luan et al., 2006; Pfeiffer et al., 2010). It is now in principle possible to obtain specific genetic access to every single neuron or cell type in the fly brain, including the ~100 cell types of the fly visual system.

The genetic tools that can be expressed with this level of specificity include reporter and effector genes. Reporter genes, such as green fluorescent protein (GFP), are for example commonly used to label all cells within a driver line to describe its expression pattern, or in an individual cell to describe the arborization pattern of a neuron's dendritic tree. Other reporter genes are fluorescent molecules that change their fluorescence with the state of neuronal activity. Such molecules include genetically encoded calcium indicators (e.g. GCaMP6, Chen et al., 2014), synaptopHluorins (Miesenböck et al., 1998), or genetically encoded voltage sensors (e.g. ASAP2, Yang et al., 2016), and allow different measures of neuronal activity, including intracellular calcium signals, vesicle release, or membrane voltage, respectively. In addition to labeling neurons with reporter genes, one can manipulate their activity using effector genes. These are genes that can inactivate or ectopically activate neurons. Among the most popular ones are genetic tools to block neuronal activity by hyperpolarizing a neuron, or by preventing vesicle recycling (Simpson, 2009), or tools to ectopically activate neurons using optogenetics, including Channelrhodopsin or Chrimson (Klapoetke et al., 2014; Mattis et al., 2011). In analogy to molecular genetic studies, this allows performing loss and gain of function experiments at the neuronal or circuit level, and ask which neurons are necessary or sufficient for a specific task.

Elementary motion detecting circuits. With increasingly specific genetic tools at hand, core motion detecting circuits could be identified. In particular, experiments in which behavioral responses to motion cues were measured while the outputs of individual cell types were genetically blocked, led to the identification of neurons that are required for motion detection. It was thus shown that there are two distinct pathways for motion detection, the ON and the OFF pathways, that guide responses to moving dark (OFF) or bright (ON) edges, respectively. These pathways split downstream of R1-R6 photoreceptors, where the first order lamina interneuron L1 is the major input to the ON pathway, whereas its L2 and L3 counterparts provide inputs to the OFF pathway (Clark et al., 2011; Joesch et al., 2010; Silies et al., 2013) (Figure 1B). Blocking the synaptic outputs of either L1 and L2, or L1 and L3 abolished all behavioral responses to motion cues in flies, arguing that these neurons are all required for motion detection (Clark et al., 2011; Rister et al., 2007; Silies et al., 2013). Two synapses further down in the lobula complex, the first direction-selective neurons can be found: T4 neurons respond to moving ON signals, and T5 neurons respond to moving OFF signals (Figure 1B). Both T4 and T5 neurons come in four different subtypes, of which each prefers motion in one of the four cardinal directions: upward, downward, front-to-back and back-to-front (Maisak et al., 2013). Again, genetically blocking the outputs of T4 and T5 neurons abolished behavioral responses to visual motion stimuli, placing these neurons at the output stage of the EMDs of both ON and OFF pathways (Maisak et al., 2013; Strother et al., 2017). Such data argued that a more or less simple one-to-one relationship existed between a visual system cell type and its computational role. If for example L1 neurons provide input to an ON edge detector, and T4 neurons are the direction-selective output neurons of such a detector, all that is in principle needed are two types of interneurons with different temporal filtering properties that connect inputs from two neighboring L1 neurons to the dendrites of the direction-selective T4 cells. This configuration could implement the computation as outlined above in the description of EMD models. Such interneuron candidates were suggested based on reconstructions of electron microscopic data, by identifying the neurons that most strongly connect L1 to T4 neurons as judged by synapse counts (Takemura et al., 2017) (Figure 1B). The two neurons that most strongly connect the L1 inputs to direction-selective T4 outputs were for example the neurons Mi1 and Tm3. Electrophysiological recordings identified differences in their temporal filtering properties, especially in the time to peak of the linear filter, which is shorter in Tm3 (Behnia et al., 2014).

Distributed coding in visual circuits. Both in the ON and the OFF pathways, medulla interneurons that connect lamina inputs to direction-selective T4 and T5 outputs have been described (Figure 1B). While core motion detecting circuits have thus been proposed (Ammer et al., 2015; Behnia et al., 2014; Fisher et al., 2015a; Serbe et al., 2016; Strother et al., 2017), behavioral phenotypes associated with the loss of, e.g., ON pathway interneuron function were surprisingly subtle (Ammer et al., 2015; Strother et al., 2017). Whereas genetic silencing of neural activity in T4 neurons lead to a loss of optomotor responses to ON edge motion, silencing either of the candidate medulla neurons of the ON pathway only reduced behavioral responses (e.g. for both Mi1 and Tm3). Still, blocking the outputs of these

neurons biased the behavioral responses to OFF edges and thus isolated a deficit in ON edge detection, when competing ON and OFF edges were used to probe behavioral function. Isolated behavioral deficits for specific temporal frequencies were found in other ON pathway interneuron candidates. The same story holds for the OFF pathway interneuron counterparts (Fisher et al., 2015a; Serbe et al., 2016). For example, blocking activity in OFF pathway interneuron Tm9 provides a strong preference for ON edges, when the two edge types are competing. At the same time, flies are able to respond to individual OFF edge motion (Fisher et al., 2015a). Phenotypes for other OFF pathway interneurons are even subtler, but can be enhanced by combinatorial silencing of more than one cell type (Serbe et al., 2016).

Together, these data suggest that, at least at this level of peripheral visual processing, a single cell type is not solely required for a specific task. Otherwise, taking out such a cell type would break the system. Instead, coding seems to be more distributed. There are different scenarios that could account for this lack of a phenotype. One possibility is that there are redundant circuit elements, and silencing one cell type alone can be covered up by the presence of other neurons. This would make the behaviorally very relevant motion computation robust to perturbations. Alternatively, we may have not identified all essential neurons so far. In addition to the interneurons that connect lamina neuron inputs (e.g. L1) to direction-selective outputs (e.g. T4) with the most number of synapses, many other neurons also receive inputs from the lamina inputs, or provide output synapses on the T4 or T5 dendrites. Moreover, the function of most of the more than 60 medulla neuron cell types is unknown. While synapse number is considered a strong indicator of functional relevance, there are examples that argue against this: the lamina input L3 receives much fewer synapses from photoreceptors than the L1 and L2 neurons (Rivera-Alba et al. 2011). One synapse further down, L3 synapses onto Tm9, with almost an order of magnitude fewer synapses than have been counted between L1 or L2 and its major downstream neurons (Takemura et al. 2013). Still, silencing Tm9 shows the most striking behavioral phenotype of all OFF pathway neurons tested (Fisher et al., 2015a; Serbe et al., 2016). Finally, interneurons with different temporal filtering properties have been identified in the ON and OFF pathways (Arenz et al., 2017; Behnia et al., 2014; Fisher et al., 2015a; Serbe et al., 2016; Strother et al., 2017; Yang et al., 2016) and might be important for motion vision at different speeds. Likely, a combination of these possibilities will be true.

In summary, core motion detection circuits have been proposed. While the identified cells and their physiological properties are sufficient to predict direction-selective responses in downstream neurons, the definite computational or behavioral roles that they actually implement are still subject to future studies.

Novel insights into motion detection algorithms

At the beginning of this review we described how work in insects led to a preference of the HRC model to describe motion detection, and identifying the underlying neurons was considered the “holy grail” of motion detection (Borst, 2014). In contrast, the BLM was long considered the predominant model to describe motion responses in the vertebrate retina. The identification of neurons of motion detecting circuits in general, and in particular of the T4 and T5 neurons as the first cells that exhibit direction-selectivity, has opened up the opportunity to study the mechanisms of motion detection directly at the output stages of the EMD. Recent work on the T4 and T5 cells has revealed surprising new insights on how motion information might actually be encoded in the fly visual system.

The axon terminals of both T4 and T5 arborize in the lobula plate and provide retinotopic input to the LPTCs. In the lobula plate, the axon terminals are organized in a layered fashion, in which T4 and T5 cells of a given directional preference (e.g. front-to-back motion) project into one layer (Figure 1B). The directional preferences of the four layers together cover the four cardinal directions of motion, making it easy to record from direction-selective cells of one subtype, using *in* vivo two photon calcium imaging (Maisak et al., 2013). At the level of the dendrites, measuring DS responses is not as straightforward. All four T4 subtypes project into the most proximal layer of the medulla, and all T5 subtypes project into the first layer of the lobula (Figure 1B). Nevertheless, elegant genetic experiments allowed to record from individual dendrites, and showed that direction-selectivity already emerges in the dendrites, arguing that this is where core computations are happening (Fisher et al., 2015b). T4 and T5 neurons were also found to be orientation tuned to static objects (Fisher et al., 2015b; Maisak et al., 2013) with an axis that is perpendicular to their preferred motion axis (Fisher et al., 2015b). So what are the algorithms implemented at the dendrites of T4 and T5?

Interestingly, a pharmacological block of GABAergic signaling in the fly visual system caused a loss of direction

as well as orientation selective signals in T4 and T5 cells (Fisher et al., 2015b). This is strikingly similar to results from the vertebrate retina and showed that GABAergic inhibition is crucial for DS responses in T4 and T5 cells of the fly as well.

Subsequent experiments directly mapped the spatiotemporal receptive fields of T4 and T5 cells using spatiotemporal ternary noise stimuli (Leong et al., 2016; Salazar-Gatzimas et al., 2016). These stimuli contained bars of randomly changing contrast that were just wide enough to cover the extent of the receptive field of an input neuron. Thus, they covered one point in space at the fly eye's resolution. The neuron's temporal response to each point in space was obtained using reverse correlation of a cell's change in calcium signal with the change of the contrast of each bar. These receptive fields of T4 and T5 contained an inhibitory and an excitatory subfield, which were tilted along a space-time axis (Figure 2A). The linear receptive field obtained by reverse correlation was qualitatively similar to the receptive field of a full model adding nonlinearities describing neuronal or calcium indicator properties (Leong et al., 2016). The tilt in space and time is consistent with an enhancement of signals moving into the preferred direction of the neuron, as predicted by the HRC. Interestingly, the spatiotemporal offset between the excitatory and inhibitory subfields predicts a suppression of motion in the null-direction by mutually canceling interactions (Figure 2A). Thus, these data suggest a combination of excitatory mechanisms as proposed by the HRC, and inhibitory mechanisms as proposed by the BLM (Leong et al., 2016).

The hypothesis that both HRC and BLM type models together account for motion responses in flies can be directly tested using so-called apparent motion stimuli. These stimuli utilize the fact that the perception of movement can be achieved by showing a temporal sequence of static images that are offset in space (as done in any television) (Figure 2B). If they are presented in fast succession, they are perceived as continuous motion due to the spatiotemporal limitations of visual processing. According to this logic, motion for the fly was mimicked by sequentially activating neighboring points in the visual field (Figure 2B) while recording T4 and T5 responses. To produce a motion response in such an apparent motion stimulus, two stimulation points should ideally hit two neighboring points in visual space in sequence, and with a time delay that matches the temporal delay of the EMD. If the time delay is too long, no motion response will be elicited upon stimulation of two adjacent points. Instead, one can use these isolated responses to build a linear (summed) prediction of the single stimulations to the apparent motion response (Figure 2C). If the two inputs were combined linearly for a fast sequence of stimulation, the predicted sum should fit the actual motion response of the neuron. Conveniently, the HRC or BLM type models make very different predictions about the outcome of the response to these apparent motion stimuli, due to the differences in their output nonlinearities. If an HRC was implemented, one would expect a nonlinear amplification of signals moving into the PD, whereas a BLM would predict a nonlinear suppression of signals moving into the neuron's ND (Figure 2C).

Two separate studies used these apparent motion stimuli to analyze T4 and T5 properties. First of all, (Fisher et al., 2015b) showed apparent motion stimuli mimicking a moving edge by first activating one point in space by displaying a stripe, followed by activation of the same point as well as a neighboring point in space. When calcium signals were measured in T4 and T5 neurons, a significant nonlinear amplification of responses to this apparent motion into the neuron's PD was found, suggesting an HRC like mechanism (Fisher et al., 2015b). The same study had demonstrated that GABAergic mechanisms are important for direction-selective T4 and T5 responses, prompting to look for null direction suppression as suggested by the BLM. However, only weak signs of null direction suppression could be found, that often did not differ from an adaptation control (Fisher et al., 2015b). Subsequently, an apparent moving spot stimulus, that sequentially activated single points adjacent in space, could confirm the results obtained by (Fisher et al., 2015b), and also identified signs of null direction suppression in DS neurons (Haag et al., 2016). A precise stimulation technique might be important to activate the inhibitory subunit of the receptive field and thus the component leading to null direction suppression. This inhibitory subfield would then correspond to the side of the cell's receptive field that the motion stimulus reaches first, if traveling in the null direction of the cell. The results obtained using apparent motion stimuli are thus consistent with the direct measurement of T4 and T5 properties described above. The spatial extent of the receptive fields furthermore suggested that the DS cells get inputs from more than two columns, which was confirmed by visual stimulation of more than two adjacent points in visual space (Haag et al., 2016; Leong et al., 2016; Salazar-Gatzimas et al., 2016). Together, a picture emerges in which a combination of preferred direction amplification as suggested by the HRC, and null direction suppression as proposed by the BLM is used to establish direction-selective responses in early visual processing of the fly.

As previously introduced, the BLM model was strongly favored to describe direction-selectivity in ganglion

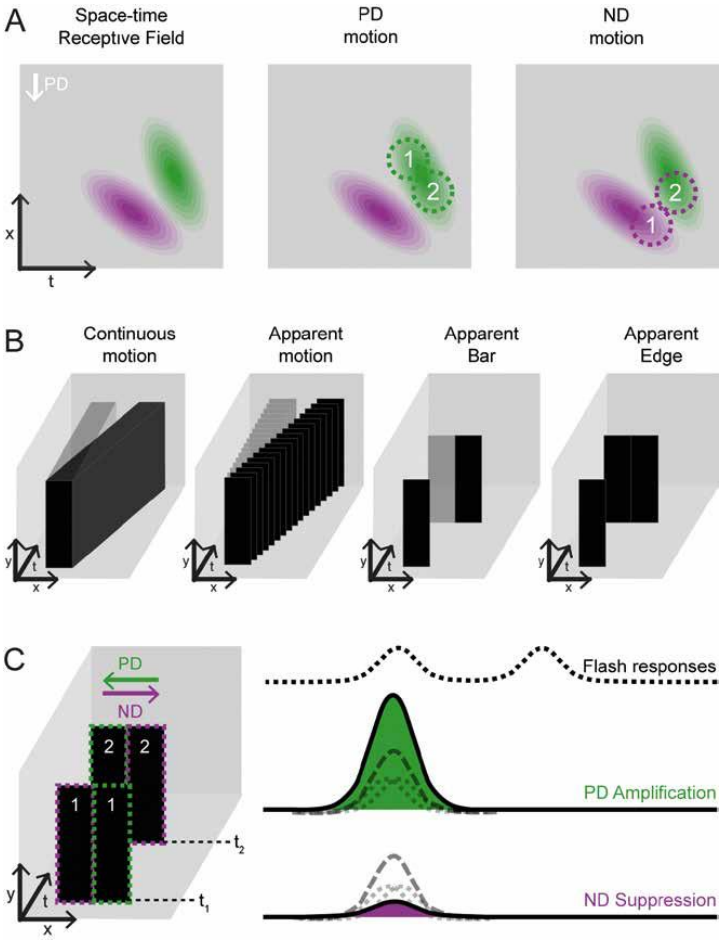

Fig. 2: A. Schematic drawing of a spatiotemporal receptive field of a direction-selective T4 or T5 neuron (after Leong et al. 2016). The receptive field contains excitatory (green) and inhibitory (purple) subfields, which are each tilted along the space-time axis. The preferred direction (PD) of this neuron is indicated. The middle panel shows the same receptive field, illustrating how motion in the preferred direction would sequentially activate the excitatory subfield. The right panels shows how motion in the null direction (ND) would sequentially hit the inhibitory and excitatory subfield, leading to suppression of signals moving in this direction. **B.** X-y-t plots illustrating how continuous motion can be decomposed into apparent motion stimuli. While the black boxes present motion to the right, the grey boxes illustrate a static object. The two rightmost panels illustrate apparent moving bar or edge stimuli that sequentially activate two neighboring points in space. **C.** An apparent moving bar stimulus can be moved in the PD (green) or ND (purple) of a cell. If the two time points are well separated in time, two individual flash responses are recorded (top trace). For short delays, these individual flash responses (dotted lines) can be shifted in time and summed to build a linear prediction (dashed line). If the response to a motion cue moving into the PD is nonlinearly amplified as shown in the middle panel (green, middle trace), this argues for a HRC type model. If the response to a motion cue moving into the ND in suppressed compared to the linear prediction (purple, bottom trace), this argues for the implementation of a BLM.

cells of the vertebrate retina. Presynaptic to these cells are the starburst amacrine cells, which are not only required for DS responses in ganglion cells, but whose dendrites are themselves direction-selective (Briggman et al., 2011; Euler et al., 2002). Interestingly, recent work on direction-selectivity in the dendrites of starburst amacrine cells also suggested that an HRC like mechanism is implemented at the bipolar cell to starburst amacrine cell synapse (Fransen and Borghuis, 2017; Kim et al., 2014) . This shows how the computational mechanisms used in verte-

brates and insects are much more similar than previously thought (see also Borst and Helmstaedter, 2015; Mauss et al., 2017).

Summary and Outlook

The circuits and mechanisms that extract visual motion cues have gotten a lot of attention, because the topic serves as a model to understand how basic computations are implemented in neuronal networks. Notably, the past years have not only seen fast progress in the identification of core motion detecting circuits in *Drosophila*, but have also revisited the algorithmic implementation of motion computation in the fly, and other systems. While the HRC has been a useful theoretical description of many properties of motion detection in insects, recent work showed that the fly visual system uses a combination of two mechanisms: feedforward amplification of preferred direction signals as proposed by the HRC, and null direction inhibition as suggested by the BLM.

To what degree which mechanism is implemented, and if certain algorithms are favored by specific stimulus conditions, is still an open question. One could imagine the existence of distinct circuits that implement either preferred direction amplification or null direction inhibition at different speed regimes. While so far isolated experiments have found evidence for both mechanisms, future studies will have to tell if both models serve together across a wide space of parameters. Especially, direct measurement of synaptic inhibition onto DS cells could probe under which stimulus conditions inhibitory mechanisms play a role.

The identification of neurons upstream of direction-selective cells now leaves the question open, which computational role is fulfilled by each of these cell types. This question can be tackled with the available genetic tools, not only by probing their physiological specialization, but also by defining their requirement for downstream circuit properties. Furthermore, the visual system contains ~100 cell types, many of which have not been studied. While most of the work in the fly visual system was done on motion detection, many other visual properties such as the size of objects could provide salient cues for the animal (Keleş and Frye, 2017; Wu et al., 2016). The circuits extracting these cues could be independent from motion-detection circuits, or share elements with them.

Finally, the molecular and cellular mechanisms implementing either aspect of the computations discussed throughout this review are still elusive. Given recent advances in identifying cell type specific expression profiles (Pankova and Borst, 2016; Tan et al., 2015), it will be interesting to see how many of the individual features of EMD properties are implemented at the biophysical level.

Acknowledgement: Work in the Silies lab is supported by grants of the Deutsche Forschungsgemeinschaft (DFG) through an Emmy Noether grant and the Collaborative Research Center 889 “Cellular Mechanisms of Sensory Processing” (project C08), as well by the European Research Council through ERC Starting Grant “MicroCyFly”.

References

Adelson, E. H., Bergen, J. R. (1985). Spatiotemporal energy models for the perception of motion. Journal of the Optical Society of America A: Optics 2, 284–299. doi:10.1364/JOSAA.2.000284

Ammer, G., Leonhardt, A., Bahl, A., Dickson, B. J., Borst, A. (2015). Functional Specialization of Neural Input Elements to the Drosophila ON Motion Detector. Curr Biol 25, 2247–2253. doi:10.1016/j.cub.2015.07.014

Amthor, F. R., Keyser, K. T., Dmitrieva, N. A. (2002). Effects of the destruction of starburst-cholinergic amacrine cells by the toxin AF64A on rabbit retinal directional selectivity. Visual Neuroscience 19, 495–509. doi:10.1017/S0952523802194119

Arenz, A., Drews, M. S., Richter, F. G., Ammer, G., Borst, A. (2017). The Temporal Tuning of the Drosophila Motion Detectors Is Determined by the Dynamics of Their Input Elements. Curr Biol 27, 929–944. doi:10.1016/j.cub.2017.01.051

Barlow, H. B., Levick, W. R. (1965). The mechanism of directionally selective units in rabbit’s retina. J Physiol (Lond) 178, 477–504.

Behnia, R., Clark, D. A., Carter, A. G., Clandinin, T. R., Desplan, C. (2014). Processing properties of ON and OFF pathways for Drosophila motion detection. Nature 1–15. doi:10.1038/nature13427

Borst, A. (2014). In search of the Holy Grail of fly motion vision. Eur J Neurosci 40, 3285–3293. doi:10.1111/ejn.12731

Borst, A., Egelhaaf, M. (1989). Principles of visual motion detection. Trends Neurosci 12, 297–306.

Borst, A., Euler, T. (2011). Seeing things in motion: models, circuits, and mechanisms. Neuron 71, 974–994. doi:10.1016/j.neuron.2011.08.031

Borst, A., Helmstaedter, M. (2015). Common circuit design in fly and mammalian motion vision. Nat Neurosci 18, 1067–1076. doi:10.1038/nn.4050

Briggman, K. L., Helmstaedter, M., Denk, W. (2011). Wiring specificity in the direction-selectivity circuit of the retina. Nature 471, 183–188. doi:10.1038/nature09818

Buchner, E. (1976). Elementary movement detectors in an insect visual system. Biol. Cybernetics 24, 85–101.

Caldwell, J. H., Daw, N. W. (1978). New properties of rabbit retinal ganglion cells. J Physiol (Lond) 276, 257–276.

Chen, T.-W., Wardill, T. J., Sun, Y., Pulver, S. R., Renninger, S. L., Baohan, A., Schreiter, E. R., Kerr, R. A., Orger, M. B., Jayaraman, V., Looger, L. L., Svoboda, K., Kim, D. S. (2013). Ultrasensitive

fluorescent proteins for imaging neuronal activity. Nature 499, 295–300. doi:10.1038/nature12354

Clark, D. A., Bursztyn, L., Horowitz, M. A., Schnitzer, M. J., Clandinin, T. R. (2011). Defining the computational structure of the motion detector in Drosophila. Neuron 70, 1165–1177. doi:10.1016/j.neuron.2011.05.023

Eckert, H. (1973). Optomotorische Untersuchungen am visuellen System der Stubenfliege Musca domestica L. Kybnertik 14, 1–23.

Egelhaaf, M., Reichardt, W. (1987). Dynamic response properties of movement detectors: Theoretical analysis and electrophysiological investigation in the visual system of the fly. Biological Cybernetics 56, 69–87.

Euler, T., Detwiler, P. B., Denk, W. (2002). Directionally selective calcium signals in dendrites of starburst amacrine cells. Nature 418, 845–852. doi:10.1038/nature00931

Fischbach, K., Dittrich, A. (1989). The optic lobe of Drosophila melanogaster. I. A Golgi analysis of wild-type structure. Cell Tissue Res 258, 441–475.

Fisher, Y. E., Leong, J. C., Sporar, K., Ketkar, M., Gohl, D., Clandinin, T. R., Silies, M. (2015a). A visual neuron class with wide field properties is required for local motion detection. Current Biology 1–6.

Fisher, Y. E., Silies, M., Clandinin, T. R. (2015b). Orientation Selectivity Sharpens Motion Detection inDrosophila. Neuron 1–16. doi:10.1016/j.neuron.2015.09.033

Fleishman, L. J., Pallus, A. C. (2010). Motion perception and visual signal design in Anolis lizards. Proc. Biol. Sci. 277, 3547–3554. doi:10.1098/rspb.2010.0742

Fransen, J. W., Borghuis, B. G. (2017). Temporally Diverse Excitation Generates Direction-Selective Responses in ON- and OFF-Type Retinal Starburst Amacrine Cells. Cell Rep 18, 1356–1365. doi:10.1016/j.celrep.2017.01.026

Gohl, D. M., Silies, M. A., Gao, X. J., Bhalerao, S., Luongo, F. J., Lin, C.-C., Potter, C. J., Clandinin, T. R. (2011). A versatile in vivo system for directed dissection of gene expression patterns. Nat Methods 8, 231–237.

Götz, K. G. (1964). Optomotorische Untersuchung des visuellen systems einiger Augenmutanten der Fruchtfliege Drosophila. Kybernetik 2, 77–92.

Haag, J., Arenz, A., Serbe, E., Gabbiani, F., Borst, A. (2016). Complementary mechanisms create direction selectivity in the fly. Elife 5. doi:10.7554/eLife.17421

Hassenstein, B., Reichardt, W. (1956). Systemtheoretische Analyse der Zeit-, Reihenfolgen- und Vorzeichenauswertung bei der Bewegungsperzeption des Rüsselkäfers Chlorophanus. Zeitschrift für Naturforschung 11, 513–524.

Hausen, K. (1982). Motion sensitive interneurons in the optomotor system of the fly. Biological Cybernetics 45, 143–156.

Heisenberg, M., Buchner, E. (1977). The role of retinula cell types in visual behavior of Drosophila melanogaster. J Comp Physiol 117, 127–162.

Hengstenberg, R., Hausen, K., Hengstenberg, B. (1982). The Number and Structure of Giant Vertical Cells (VS) in the Lobula Plate of the Blowfly Calliphora erythrocephala. J Comp Physiol A 149, 163–177.

Jenett, A., Rubin, G. M., Ngo, T.-T. B., Shepherd, D., Murphy, C., Dionne, H., Pfeiffer, B. D., Cavallaro, A., Hall, D., Jeter, J., Iyer, N., Fetter, D., Hausenfluck, J. H., Peng, H., Trautman, E. T., Svirskas, R. R., Myers, E. W., Iwinski, Z. R., Aso, Y., DePasquale, G. M., Enos, A., Hulamm, P., Lam, S. C. B., Li, H.-H., Laverty, T. R., Long, F., Qu, L., Murphy, S. D., Rokicki, K., Safford, T., Shaw, K., Simpson, J. H., Sowell, A., Tae, S., Yu, Y., Zugates, C. T. (2012). A GAL4-driver line resource for Drosophila neurobiology. Cell Rep 2, 991–1001. doi:10.1016/j.celrep.2012.09.011

Joesch, M., Plett, J., Borst, A., Reiff, D. F. (2008). Response properties of motion-sensitive visual interneurons in the lobula plate of Drosophila melanogaster. Curr Biol 18, 368–374. doi:10.1016/j.cub.2008.02.022

Joesch, M. M., Schnell, B. B., Raghu, S. V. S., Reiff, D. F. D., Borst, A. A. (2010). ON and OFF pathways in Drosophila motion vision. Nature 468, 300–304. doi:10.1038/nature09545

Keleş, M. F., Frye, M. A. (2017). Object-Detecting Neurons in Drosophila. Curr Biol 27, 680–687. doi:10.1016/j.cub.2017.01.012

Kim, J. S., Greene, M. J., Zlateski, A., Lee, K., Richardson, M., Turaga, S. C., Purcaro, M., Balkam, M., Robinson, A., Behabadi, B. F., Campos, M., Denk, W., Seung, H. S., EyeWirers, T. (2014). Space–time wiring specificity supports direction selectivity in the retina. Nature 1–17. doi:10.1038/nature13240

Klapoetke, N. C., Murata, Y., Kim, S. S., Pulver, S. R., Birdsey-Benson, A., Cho, Y. K., Morimoto, T. K., Chuong, A. S., Carpenter, E. J., Tian, Z., Wang, J., Xie, Y., Yan, Z., Zhang, Y., Chow, B. Y., Surek, B., Melkonian, M., Jayaraman, V., Constantine-Paton, M., Wong, G. K.-S., Boyden, E. S. (2014). Independent optical excitation of distinct neural populations. Nat Methods 11, 338–346. doi:10.1038/nmeth.2836

Leong, J. C. S., Esch, J. J., Poole, B., Ganguli, S., Clandinin, T. R. (2016). Direction Selectivity in Drosophila Emerges from Preferred-Direction Enhancement and Null-Direction Suppression. Journal of Neuroscience 36, 8078–8092. doi:10.1523/JNEUROSCI.1272-16.2016

Luan, H., Peabody, N. C., Vinson, C. R., White, B. H. (2006). Refined spatial manipulation of neuronal function by combinatorial restriction of transgene expression. Neuron 52, 425–436. doi:10.1016/j.neuron.2006.08.028

Maisak, M. S., Haag, J., Ammer, G., Serbe, E., Meier, M., Leonhardt, A., Schilling, T., Bahl, A., Rubin, G. M., Nern, A., Dickson, B. J., Reiff, D. F., Hopp, E., Borst, A. (2013). A directional tuning map of Drosophila elementary motion detectors. Nature 500, 212–216. doi:10.1038/nature12320

Mattis, J., Tye, K. M., Ferenczi, E. A., Ramakrishnan, C., O'Shea, D. J., Prakash, R., Gunaydin, L. A., Hyun, M., Fenno, L. E., Gradinaru, V., Yizhar, O., Deisseroth, K. (2011). Principles for applying optogenetic tools derived from direct comparative analysis of microbial opsins. Nat Methods 9, 159–172. doi:10.1038/nmeth.1808

Mauss, A. S., Vlasits, A., Borst, A., Feller, M. (2017). Visual Circuits for Direction Selectivity. Annu Rev Neurosci 40, 211–230. doi:10.1146/annurev-neuro-072116-031335

Meinertzhagen, I. A., O'Neil, S. D. (1991). Synaptic organization of columnar elements in the lamina of the wild type in Drosophila melanogaster. J Comp Neurol 305, 232–263. doi:10.1002/cne.903050206

Miesenböck, G., De Angelis, D. A., Rothman, J. E. (1998). Visualizing secretion and synaptic transmission with pH-sensitive green fluorescent proteins. Nature 394, 192–195. doi:10.1038/28190

Pankova, K., Borst, A. (2016). RNA-Seq Transcriptome Analysis of Direction-Selective T4/T5 Neurons in Drosophila. PLoS ONE 11, e0163986. doi:10.1371/journal.pone.0163986

Pfeiffer, B. D., Ngo, T.-T. B., Hibbard, K. L., Murphy, C., Jenett, A., Truman, J. W., Rubin, G. M. (2010). Refinement of tools for targeted gene expression in Drosophila. Genetics 186, 735–755. doi:10.1534/genetics. 110.119917

Reichardt, W. (1987). Evaluation of optical motion information by movement detectors. J Comp Physiol A 161, 533–547.

Rister, J., Pauls, D., Schnell, B., Ting, C.-Y., Lee, C.-H., Sinakevitch, I., Morante, J., Strausfeld, N. J., Ito, K., Heisenberg, M. (2007). Dissection of the peripheral motion channel in the visual system of Drosophila melanogaster. Neuron 56, 155–170. doi:10.1016/j.neuron.2007.09.014

Rivera-Alba, M., Vitaladevuni, S. N., Mishchenko, Y., Mischenko, Y., Lu, Z., Takemura, S.-Y., Scheffer, L., Meinertzhagen, I. A., Chklovskii, D. B., de Polavieja, G. G. (2011). Wiring economy and volume exclusion determine neuronal placement in the Drosophila brain. Curr Biol 21, 2000–2005. doi:10.1016/j.cub.2011.10.022

Salazar-Gatzimas, E., Chen, J., Creamer, M. S., Mano, O., Mandel, H. B., Matulis, C. A., Pottackal, J., Clark, D. A. (2016). Direct Measurement of Correlation Responses in Drosophila Elementary Motion Detectors Reveals Fast Timescale Tuning. Neuron 92, 227–239. doi:10.1016/j.neuron.2016.09.017

Schnell, B., Joesch, M., Forstner, F., Raghu, S. V., Otsuna, H., Ito, K., Borst, A., Reiff, D. F. (2010). Processing of horizontal optic flow in three visual interneurons of the Drosophila brain. J Neurophysiol 103, 1646–1657. doi:10.1152/jn.00950.2009

Serbe, E., Meier, M., Leonhardt, A., Borst, A. (2016). Comprehensive Characterization of the Major Presynaptic Elements to the Drosophila OFF Motion Detector. Neuron 89, 829–841. doi:10.1016/j.neuron.2016.01.006

Silies, M., Gohl, D. M., Clandinin, T. R. (2014). Motion-Detecting Circuits in Flies: Coming into View. Annu Rev Neurosci 37, 307–327. doi:10.1146/annurev-neuro-071013-013931

Silies, M., Gohl, D. M., Fisher, Y. E., Freifeld, L., Clark, D. A., Clandinin, T. R. (2013). Modular use of peripheral input channels tunes motion-detecting circuitry. Neuron 79, 111–127. doi:10.1016/j.neuron.2013.04.029

Simpson, J. H. (2009). Mapping and Manipulating Neural Circuit in the Fly Brain, 1st ed, Genetic Dissection of Neural Circuits and Behavior, Genetid Dissection of Neural Circuits. Elsevier Inc. doi:10.1016/S0065-2660(09)65005-7

Strother, J. A., Wu, S.-T., Wong, A. M., Nern, A., Rogers, E. M., Le, J. Q., Rubin, G. M., Reiser, M. B. (2017). The Emergence of Directional Selectivity in the Visual Motion Pathway of Drosophila. Neuron 94, 168–182.e10. doi:10.1016/j.neuron.2017.03.010

Takemura, S., Bharioke, A., Lu, Z., Nern, A., Vitaladevuni, S., Rivlin, P.K., Katz, W.T., Olbris, D.J., Plaza, S.M., Winston, P., et al. (2013). A visual motion detection circuit suggested by Drosophila connectomics. Nature 500, 175–181.

Takemura, S.-Y., Lu, Z., Meinertzhagen, I. A. (2008). Synaptic circuits of the Drosophila optic lobe: the input terminals to the medulla. J Comp Neurol 509, 493–513. doi:10.1002/cne.21757

Takemura, S.-Y., Nern, A., Chklovskii, D. B., Scheffer, L. K., Rubin, G. M., Meinertzhagen, I. A. (2017). The comprehensive connectome of a neural substrate for "ON" motion detection in Drosophila. Elife 6, 1–16. doi:10.7554/eLife.24394.001

Tan, L., Zhang, K. X., Pecot, M. Y., Nagarkar-Jaiswal, S., Lee, P.-T., Takemura, S.-Y., McEwen, J. M., Nern, A., Xu, S., Tadros, W., Chen, Z., Zinn, K., Bellen, H. J., Morey, M., Zipursky, S. L. (2015). Ig Superfamily Ligand and Receptor Pairs Expressed in Synaptic Partners in Drosophila. Cell 163, 1756–1769. doi:10.1016/j.cell.2015.11.021

van Santen, J. P., Sperling, G. (1985). Elaborated Reichardt detectors. J Opt Soc Am A 2, 300–321.

Wu, M., Nern, A., Williamson, W. R., Morimoto, M. M., Reiser, M. B., Card, G. M., Rubin, G. M. (2016). Visual projection neurons in the Drosophila lobula link feature detection to distinct behavioral programs. Elife 5. doi:10.7554/eLife.21022

Wyatt, H. J., Day, N. W. (1976). Specific effects of neurotransmitter antagonists on ganglion cells in rabbit retina. Science 191, 204–205.

Yang, H. H., St-Pierre, F., Sun, X., Ding, X., Lin, M. Z., Clandinin, T. R. (2016). Subcellular Imaging of Voltage and Calcium Signals Reveals Neural Processing In Vivo. Cell 166, 245–257. doi:10.1016/j.cell.2016.05.031

Yoshida, K., Watanabe, D., Ishikane, H., Tachibana, M., Pastan, I., Nakanishi, S. (2001). A key role of starburst amacrine cells in originating retinal directional selectivity and optokinetic eye movement. Neuron 30, 771–780.

Article note: German version available at https://doi.org/10.1515/nf-2017-0028

Bionotes

Dr. Marion Silies
European Neuroscience Institute Göttingen (ENI), University Medical Center Göttingen, Grisebachstr. 5, 37077 Göttingen, Germany
Phone: +49 551 3961331
Mail: **m.silies@eni-g.de**
Web: www.silieslab.com

Marion Silies is a group leader of the "Visual Processing" lab at the European Neuroscience Institute in Göttingen (ENI-G), which is a joined initiative of the University Medical Center Göttingen and the Max Planck Society. Before joining the ENI-G in 2015, she was a Postdoctoral Fellow in the laboratory of Thomas Clandinin at Stanford University (USA). She obtained her PhD in 2009 at the University of Münster in the lab of Christian Klämbt.

Giordano Ramos-Traslosheros
European Neuroscience Institute Göttingen (ENI), University Medical Center Göttingen, Grisebachstr. 5, 37077 Göttingen, Germany; International Max Planck Research School Neuroscience, University of Göttingen, Göttingen, Germany
Mail: **l.ramos@eni-g.de**

(Luis) Giordano Ramos-Traslosheros is a PhD student in the "Visual Processing" lab at the European Neuroscience Institute in Göttingen. He is a member of the International Max Planck Research School (IMPRS) for Neurosciences in Göttingen. He performed his MSc thesis work (2015) in Tim Gollisch's lab at the University Medical Center Göttingen. Before that, Luis studied physics at the Universidad Autónoma de Nuevo León (UANL, Mexico), and at the University of Göttingen (Germany).

Miriam Henning
European Neuroscience Institute Göttingen (ENI), University Medical Center Göttingen, Grisebachstr. 5, 37077 Göttingen, Germany
Mail: **m.henning@eni-g.de**

Miriam Henning is a PhD student in the "Visual Processing" lab at the European Neuroscience Institute in Göttingen. She is a member of the Göttingen Graduate School for Neurosciences, Biophysics and Molecular Biosciences (GGNB), and in particular of the Sensory and Motor Neuroscience (SMN) program. Miriam holds a BSc degree in Biology (2013) and a MSc degree (2016) in Neurobiology, Behaviour and Evolution from the University of Bielefeld, where she performed her thesis work in the lab of Martin Egelhaaf.

3 MANUSCRIPTS

3.1 Inhibitory columnar feedback neurons tune local motion detection

Manuscript in preparation:

The following manuscript 'Inhibitory columnar feedback neurons tune local motion detection' is in preparation.

Miriam Henning (M.H), Teresa Lüffe (T.L), Deniz Yüzak (D.Y), Daryl Gohl (D.G), Marion Silies (M.S)

Author contributions:

Conceptualization: M.H and M.S
Methodology: M.H, T.L
Software: M.H, D.Y
Investigation: M.H, T.L, D.G
Visualization: M.H
Supervision: M.S
Writing—original draft: M.H
Funding acquisition: M.S

Daryl Gohl and Marion Silies conducted the behavioral forward genetic screen using InSITE-Gal4 lines (basis for this study). Teresa Lüffe performed immunostainings for GABA colocalization and single cell Flp-out experiments (Fig.1). Deniz Yüzak helped with writing analysis code for the extraction of space-time-receptive fields (Fig.2, Fig.3, Fig.6). I performed all other experiments (Fig.1 – Fig.6), analyzed data, composed figures, and wrote this manuscript draft.

Inhibitory columnar feedback neurons tune local motion detection

Miriam Henning[1,2], Teresa Lüffe[3], Deniz Yüzak[2], Daryl Gohl[4] Marion Silies[1#]

[1] Institute of Developmental Biology and Neurobiology, Johannes-Gutenberg University Mainz, 55128 Mainz, Germany.

[2] Göttingen Graduate School for Neurosciences, Biophysics, and Molecular Biosciences (GGNB) and International Max Planck Research School (IMPRS) for Neurosciences at the University of Göttingen, 37077 Göttingen, Germany

[3] University Hospital Würzburg, Department for Human Genetics, Master of Science Developmental-, Neural- and Behavioral Biology

[4] Department of Genetics, Cell Biology, and Developmental Biology, University of Minnesota Genomics Center, Minneapolis, Minnesota,

[#]author for correspondence: msilies@uni-mainz.de

Keywords Motion vision, Direction selectivity, Feedback inhibition, ND suppression, neural circuits, *Drosophila*

Abstract

Visual motion information is essential for many living organisms to guide through their environment. The underlying neuronal circuits compute motion signals using a combination of enhancing preferred directions (PD) as well as suppressing non-preferred (null-directions, ND) in both the vertebrate retina and invertebrate visual systems. GABAergic signaling plays a crucial role in the direction-selective T4/T5 neurons of the Drosophila visual system, as well as retinal ganglion cells. However, the GABAergic neurons required for direction selectivity are unknown. Here we show that in the *Drosophila* visual system two GABAergic neurons, C2 and C3, provide inhibitory feedback to upstream circuitry of motion processing. Blocking output of C2 or C3 leads alters the receptive field organization of T4/T5 neurons and block of C2 leads to a loss of null direction suppression in T4. Together, this reduces direction-selectivity of T4 and T5. This inhibitory feedback mechanism thus constitutes an essential pathway for the computation of direction selectivity, supporting direct feedforward mechanisms described previously.

Introduction

The computation of direction-selectivity (DS), a hallmark of motion detection, is a canonical example to understand the implementations of specific computations in neural networks. More than 60 years ago, two now famous models have been formulated that algorithmically explain how direction-selective signals can be extracted: The Hassenstein-Reichardt Correlator (HRC) has been the key model to explain DS in the fly visual system, relying solely on the temporal and spatial comparison of two neighbouring excitatory inputs to enhance responses to motion in the preferred direction (PD) (Von Hassenstein and Reichardt, 1956b). Proposed to explain DS of retinal ganglion cells in the rabbit retina, the Barlow-Levick model (BLM) uses inhibitory inputs to suppress motion into the nonpreferred, or null direction (ND) (Barlow and Levick, 1965). More recent studies proposed combinations of PD enhancement and ND suppression to explain DS in both the fly visual system and the mammalian retina (Arenz et al., 2017; Badwan et al., 2019; Haag et al., 2016; Leong et al., 2016; Mauss et al., 2017; Pei et al., 2015). In both the vertebrate and invertebrate visual system direction-selective responses of the first local motion detectors rely on GABAergic signalling, as a pharmacological block of GABAergic inhibition leads to a loss of direction-selectivity (Ariel and Daw, 1982; Fisher et al., 2015a). Direction selective ganglion cells (DSGCs) in the vertebrate retina receive lateral GABAergic inhibition from starburst amacrine cells (SACs) during motion into the ND leading to a suppression of responses as proposed by the BL model (Fried et al., 2002; Wei, 2018; Wei et al., 2011; Yoshida et al., 2001). Similarly, it has recently been shown that the first direction-selective cells in the visual system of the fruit fly, the T4 and T5 cells do not only integrate excitatory inputs for PD enhancement but additionally receive inhibitory signals that lead to ND suppression (Gruntman et al., 2018, 2019; Haag et al., 2016; Leong et al., 2016). However, it is unknown whether this inhibitory signal for ND suppression is also mediated by direct GABAergic signals onto T4 and T5 cells.

In the visual system of *Drosophila*, light information is transmitted from photoreceptors to lamina cells which further convey information in a retinotopic fashion to medulla neurons of the dark-sensitive OFF pathway or light-sensitive ON pathway (Clark et al., 2011; Joesch et al., 2010; Molina-Obando et al., 2019; Silies et al., 2013) In the ON pathway, T4 neurons receive input from the two cholinergic medulla neurons Mi1 and Tm3 and two inhibitory neurons, the GABAergic neuron Mi4 and the glutamatergic neuron Mi9 (Shinomiya et al., 2019b; Strother et al., 2017; Takemura et al., 2017). Together these neurons synapse onto the dendrites of T4, with Mi1 and Tm3 providing fast excitation in the central part of the dendrite and Mi9 and Mi4 providing slow inhibition on the flanking sides of the dendrite, such that they could implement both PD enhancement and ND suppression as suggested by a combination of an HRC and a BLM (Ramos-Traslosheros et al., 2018; Takemura et al., 2017). While genetic silencing experiments showed that the two excitatory inputs Mi1 and Tm3 together are required for T4 responses, silencing the GABAergic Mi4 neuron had only a little effect on T4 responses (Strother et al., 2017). In the OFF pathway, four cholinergic and thus excitatory neurons Tm1, Tm4, Tm2, and Tm9, constitute the main inputs to the direction selective T5 neuron (Shinomiya et al., 2014, 2019b). This suggests that the GABAergic inhibitory signal required for DS in T4 and T5 neurons may not be implemented at the level of T4/T5 dendrites but in upstream circuitry of motion vision.

Several GABAergic neurons in the visual system have been described by means of different techniques, including immunostainings and RNA sequencing (Datum et al., 1986; Davie et al., 2018; Davis et al., 2020; Kolodziejczyk et al., 2008; Konstantinides et al., 2018;

Raghu et al., 2013; Takemura et al., 2017). These include two GABAergic columnar feedback neurons C2 and C3, some distal and proximal medulla neurons Dm10, Pm3 and Pm4 and the large amacrine cell CT1. CT1 exhibits strong compartmentalization and processes ON information locally in the medulla, and OFF information locally in the lobula. It was therefore suggested to provide local inhibitory input to both T4 and T5 cells (Meier and Borst, 2019; Shinomiya et al., 2019b; Takemura et al., 2017). However, neither CT1 nor any of the other GABAergic cell types have been shown to be required for the computation of direction-selectivity in the local motion detectors T4 and T5. Thus, the identity of the GABAergic neurons that are relevant for motion computation remain unknown.

Here we identified GABAergic neurons that are required for motion guided behaviour based on data from a behavioural forward genetic screen (Gohl et al., 2011; Silies et al., 2013). This analysis frequently revealed the two GABAergic columnar feedback neurons C2 and C3. Using *in vivo* two photon calcium imaging we show that C2 and C3 are ON selective. Blocking the synaptic output of C2 or C3 releases suppression of T4 neurons to full-field ON stimuli impacts spatiotemporal filtering properties of T4 and T5 neurons and significantly reduces direction selectivity. Both neurons do not interact with the motion-sensitive neurons directly, but alter the physiological response properties of lamina and medulla neurons of both ON and OFF pathways, upstream of T4/T5. Therefore, our data suggest that, in addition to feedforward excitation or inhibition, feedback inhibition mediated by the two GABAergic C2 and C3 neurons is required for direction-selective signals in T4 and T5 cells and thus motion computation in the fly visual system.

Results

GABAergic C2 neurons are required for behavioral responses to motion cues

The computation of motion relies on GABAergic signalling, but it is unclear which neurons provide this inhibitory component and how it is implemented. To identify GABAergic neurons required for motion detection, we used data from a behavioural forward genetic screen (Silies et al., 2013). Different neuronal cell types, marked by a large collection of InSITE Gal4 driver lines, were tested for a role in motion-guided behaviors (Gohl et al., 2011; Silies et al., 2013). When the Gal4 lines were used to block synaptic activity, 25 driver lines showed a pronounced deficit in OFF edge motion detection, indicated by decreased turning to motion stimuli (**Fig.1a**). To identify GABAergic cell types, we marked the Gal4 expression patterns with GFP and co-labeled brains with anti-GABA (**Fig. 1a, b**). Out of the 25 lines, seven lines contained GABA-positive neurons (**Fig. 1b** and **Supplementary Fig. 1a**). Using a Flp-out strategy to sparsen the GFP-expression pattern, we then identified cell types within those driver lines based on their unique projection patterns (**Fig.1c** and **Supplementary Fig. 1a**). Out of the seven lines, expression in four lines marked the GABAergic columnar neuron C2, which is clearly recognizable based on its arborizations in the medulla (M) layer M1, M5, M8 and M10 and the distinct position of its cell body between medulla and lobula plate cortex (**Fig. 1c, f** and **Supplementary Table1**) (Fischbach and Dittrich, 1989; Kolodziejczyk et al., 2008). In some driver lines the expression pattern was clean and housed only one or two different cell types including C2, (InSITE 0787 and InSITE 0564), whereas the expression pattern of InSITE 0301 revealed broad expression in different cell types (**Fig. 1c**). C2 neurons

were found in 70% (0787), 60% (0564, 0301) and 100% (0940) of all Flp-out clones, indicating that in all four InSITE lines the expression pattern was dominated by C2.

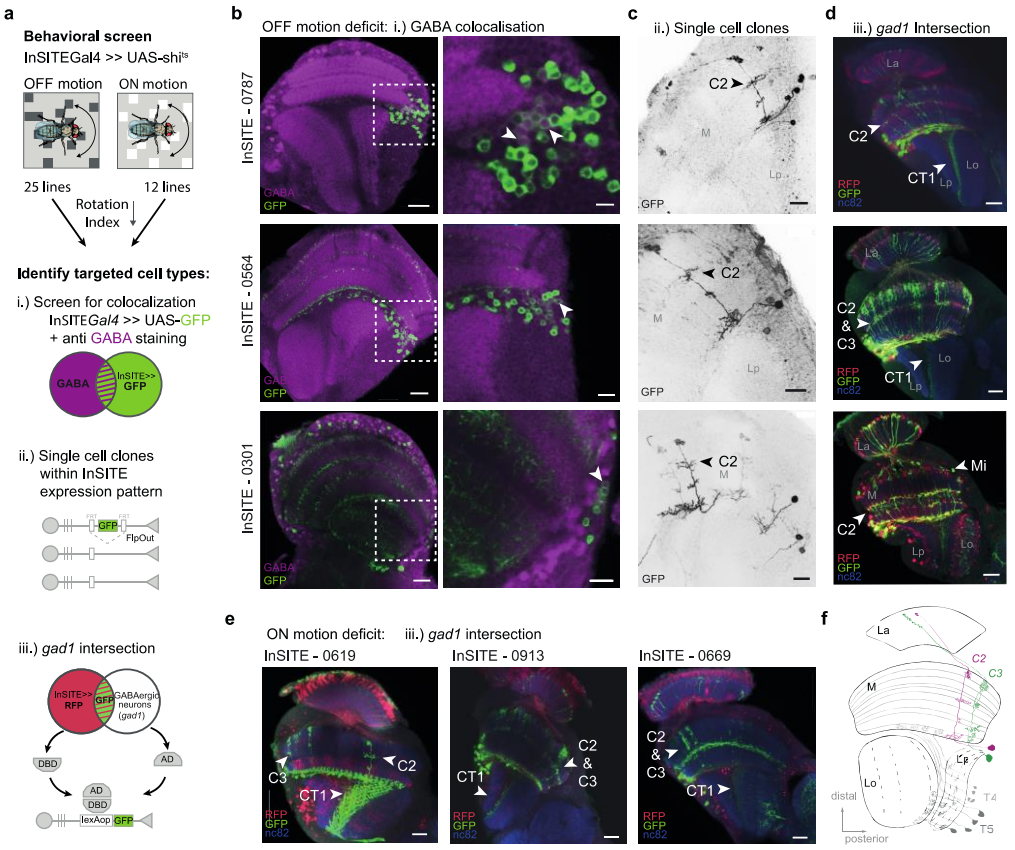

Fig. 1. C2 dominates the expression pattern of driver lines with deficits in motion vision upon neuronal silencing. a) Schematic illustrating the procedure of screening for behaviourally relevant GABAergic neurons in the visual system of Drosophila. InSITE Gal4 driver lines were selected based on a reduced rotation behaviour to moving ON or OFF stimuli when the targeted neurons were silenced. GABAergic neurons within the expression pattern were identified by i) screening for colocalization of the InSITE expression pattern (GFP, green) with anti-GABA (purple) staining, ii) visualizing single cells within the expression pattern using a FlpOut strategy and iii) a gad1 intersection strategy, labelling solely GABAergic neurons within the expression pattern with GFP (green) and the whole expression pattern with RFP (red). **b, c, d)** Three examples of InSITE lines with behavioural deficits to OFF motion stimuli screened for GABA colocalization (b, scale bar = 20µm, 10µm), single cell clones (c, scale bar = 10µm) and the gad1 intersection pattern (d, scale bar = 20µm), where the neuropil is marked with nc82 (blue). **e)** Three examples of InSITE lines with behavioural deficits to ON motion stimuli screened for neurons within the gad1 intersection pattern. **f)** Drawing of the two GABAergic neurons C2 (purple) and C3 (green) in the fly visual system including the four neuropiles: lamina (La), medulla (M), lobula (Lo) and lobula plate (Lp). The local motion detectors T4 and T5 are additionally visualized in grey.

To validate the expression of the GABAergic C2 cell in the selected InSITE lines, we used an intersectional strategy with cells expressing a split-LexA driver half under the promotor of *glutamic acid decarboxylase 1 (gad1)* (**Fig. 1a**), a key enzyme for GABA synthesis (Featherstone et al., 2000). Only cells that were marked by both the InSITE Gal4 line and *Gad1* expressed GFP. The full Gal4-expression pattern was additionally visualized with RFP (**Fig. 1d** and **Supplementary Fig. 1a**). This confirmed that the GABAergic C2 cell was dominantly expressed in the InSITE lines with behavioral deficits for ON motion detection. This strategy also revelaed other GABAergic cell types, including the columnar neuron C3 and the large

amacrine cell CT1 (Meier and Borst, 2019), however these two neuron types also expressed GFP when only the p65-Gal4 activation domain expressed under the control of the *gad1* promotor was present, indicating unspecific labelling independent of the InSITE driver lines (data not shown).

To also identify GABAergic neurons that may be important for ON edge motion computation we next intersected 12 InSITE-Gal4 lines with deficits in ON-edge detection (**Fig.1e** and **Supplementary Fig. 1b**) with the *Gad1* pattern. This again identified 4 lines labelling C2. All driver lines additionally labelled C3 and CT1 (**Supplementary Table 1**). Furthermore, we found a large tangential cell (LT) located in the lobula and a medulla neuron, with a branching pattern reminiscent to the medulla intrinsic neuron Mi^{new}1 (**Supplementary Fig. 1b** and **Supplementary Table 1,** Raghu et al., 2011). Taken together, we repeatedly found the GABAergic neuron C2 to be dominantly expressed by the selected InSITE Gal4 lines, suggesting that the observed behavioral phenotype for ON and OFF motion detection is strongly affected by the loss of function of C2 neurons. This indicates that C2 is likely relevant for the computation of motion. Although CT1 and C3 were found in the *gad1* intersection patterns of almost all tested InSITE lines, their role for the measured behavioral phenotypes remains obscure.

C2 & C3 are ON selective, multicolumnar neurons

The two GABAergic columnar feedback neurons C2 and C3 both have been suggested to be important for motion guided behaviours (Triphan et al., 2016; Tuthill et al., 2013). To understand how they contribute to the computation of motion we first characterized the response properties of the two cells using *in vivo* two photon calcium imaging. We expressed the calcium indicator GCaMP6f specifically in one of the two cell types and recorded responses from arborizations in the first layer of the medulla (M1) to ON and OFF light flashes. Both neurons showed a transient increase in calcium signal followed by a sustained plateau response to the onset of light and a return to baseline to the offset of light (**Fig. 2a**). Calcium responses from C2 and C3 showed similar kinetics but lower amplitudes in other medulla layers (**Supplementary Fig. 2b**). Probing responses of these neurons to ON and OFF edges moving into eight different directions, both neurons responded to the ON edge but not to the OFF edge and showed no preference to any particular direction (**Fig. 2b**). To investigate the spatial and temporal filter properties of C2 and C3 we extracted their spatiotemporal receptive fields (STRFs) based on responses to horizontal and vertical ternary noise bars (**Fig. 2c**). Both C2 and C3 temporal filters showed a fast ON and a delayed OFF response component, where the timing of the ON peak tended to be slower for C3 compared to C2 for both the vertical and the horizontal STRF (**Fig. 2d**). The horizontal spatial filter size of ~18°, estimated by the full width half maximum (FWHM) of a Gaussian fit, was similar between C2 and C3, whereas the vertical spatial filter for C3 tended to be slightly narrower with ~15° compared to ~18° for C2 (**Fig 2e**). Together these data show that the GABAergic C2 and C3 neurons are multicolumnar and ON selective neurons that might shape responses of T4 or T5 neurons within the ON or OFF pathways.

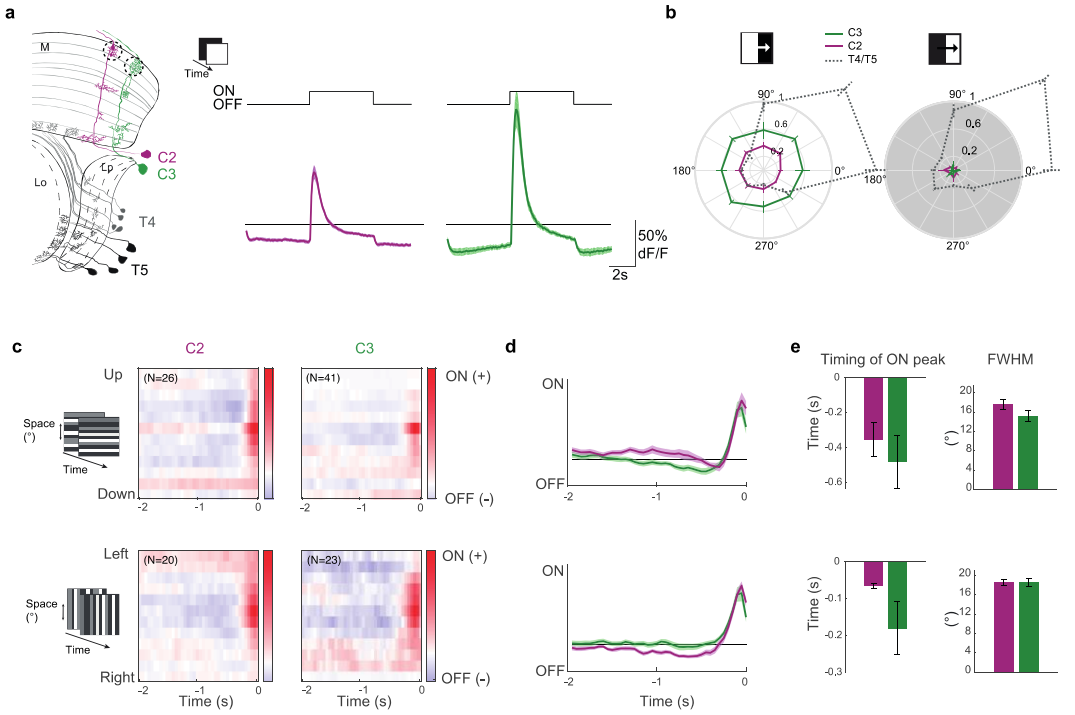

Fig. 2. Response properties of C2 and C3 to visual stimulation. a) Calcium responses of C2 (purple, N=16 flies, 181 cells) and C3 (green, N=12 flies, 149 cells) neurons in medulla layer M1 to full field ON and OFF flashes. **b)** Polar plots showing response intensities of C2 (N=6 flies) and C3 (N=8 flies) to ON and OFF edges moving onto eight different directions. Dotted lines show responses of the direction selective T4 and T5 cells (N=6 flies) for comparison. c) Average aligned spatiotemporal receptive fields (STRFs) of C2 and C3 cells extracted from responses to horizontal or vertical ternary noise bars. Red and blue colour indicate a positive and negative correlation with the stimulus, respectively. Sample size (N) equals number of cells. **d)** Temporal filter extracted from averaging single STRFs along the time axis of the horizontal and vertical STRFs. **e)** Timing of the ON peak of the temporal filter (left) and the full width half maximum (FWHM) of a gaussian fit extracted along the spatial dimension of maximal response of single STRFs (right). Shown are mean ± standard error. Significances are based on Wilcoxon rank sum test.

C2 & C3 shape temporal and spatial filtering of T4 and T5 neurons

C2 and C3 are presynaptic to lamina and medulla neurons of known motion-detection circuitry, and C3 also directly synapses onto T4 (**Fig. 3a**, Takemura et al., 2013). To examine if C2 and C3 affect response properties of T4 and T5 neurons, we recorded T4/T5 GCaMP6f responses while genetically blocking neuronal activity in C2 and C3 by expressing the inward rectifying potassium channel Kir2.1 (**Fig. 3a**, Baines et al., 2001). To distinguish responses of single T4 and T5 axon terminals, we extracted regions of interest based on their unique response properties to moving ON and OFF edges (methods, **Supplementary Fig. 3a**).The motion-selective neurons T4 and T5 hardly respond to full field ON and OFF flashes (Fisher et al., 2015a), but silencing either C2, C3, or both neurons simultaneously elicited strong increases in calcium signal in T4 neurons to the onset of a full field light stimulus (**Fig. 3a, b** and **Supplementary Fig. 3c, d**). While C2 silencing led to a fast and transient ON response in T4, the ON response caused by C3 silencing reached its peak value significantly later (**Fig. 3c**). The ON response elicited by C2 silencing rapidly decreased back to baseline while the decay rate (λ) tended to be slightly smaller for the ON response caused by C3 silencing (**Fig. 3c**). The increased ON response of T4 neurons upon C2 or C3 block was observed within T4 neurons of the four distinct layers of the lobula plate (**Supplementary**

Fig. 3f). However, the effect of C2 silencing was more pronounced for cells from layer 3 and 4, while C3 silencing had a more pronounced effect on T4 cells from layer 1 and 4 (**Supplementary Fig. 3f**). Responses of T5 neurons to the offset of light were not affected by C2 or C3 silencing (**Fig. 3b**), but T5 neurons showed a significant increase of calcium responses to the onset of light when C2 was blocked (**Supplementary Fig. 3e**). Although we cannot fully exclude that these responses are due to artefacts of T4 responses within T5 clusters, this could also constitute a dis-inhibited ON response of T5 when blocking C2. This ON response of T5 upon silencing C2 was especially increased for the T5 subtype positioned in layer 4 of the lobula plate (**Supplementary Fig. 3f**). Notably, the number of T4 and T5 cells extracted was drastically reduced when silencing both C2 and C3 together (**Supplementary Fig. 3b**). This can be attributed to a reduced contrast selectivity index (CSI) of individual pixels used to separate clean T4 or T5 pixel for the analysis (data not shown), indicating that data shown in Supplementary Fig. 3c-e likely underestimate the true phenotype. Together, our data show that both C2 and C3 suppress responses of the ON-selective T4 neuron to stationary full field ON stimuli and a possible role of C2 for suppression of ON responses in T5.

The responses of T4/T5 to non-moving stimuli upon blocking C2 or C3 could reflect a critical role of C2 and C3 for the computation of motion- or direction-selective responses in T4/T5. To understand the specific contribution of C2 and C3 to the spatial and temporal filter properties of T4 and T5 neurons we extracted the space time receptive fields (STRFs) of T4 and T5 neurons. Using horizontal and vertical ternary noise bars we obtained receptive fields of cells that are tuned to upward, downward, front-to-back or back-to-front motion. The STRFs of single T4 and T5 neurons show the two oppositely signed subfields, tilted along the neurons preferred direction that are characteristic for these directions-selective cells (**Fig. 3d**, Leong et al., 2016) These space-time filters can be well fit by a Differences-of-Gaussians (**Fig. 3d** and **Supplementary Fig. 4b**, Leong et al., 2016). When blocking C2, the STRFs of all T4 subtypes showed a significantly reduced amplitude of the positive (ON) subfield and a significant increase in amplitude of the negative (OFF) subfield of the STRF, such that the OFF subfield was much more prominent in the average STRF (**Fig. 3e,f** and **Supplementary Fig.4c**). C2 silencing thus creates an imbalance of the ON and OFF subfields of T4 neurons. The OFF subfield was further compressed in both its temporal and spatial extent, such that only a fast OFF subfield remained (**Fig. 3e, f** and **Supplementary Fig.4c**). The effect on the STRF structure of T5 cells was less prominent, but C2 silencing reduced the peak amplitude of both the ON and OFF subfields. When blocking C3, the peak timing of the ON and OFF subfields of T4 STRFs became more variable and the average STRFs of all T4 subtypes appears temporally shifted (**Fig. 3e,f** and **Supplementary Fig.4c**). T5 STRFs were predominantly reduced in size along the spatial axis (minor axis) of the OFF subfield (**Fig. 3f**). The slope of either the ON or OFF subfields for T5 and T4 STRFs were not affected by C2 or C3 silencing (**Fig. 3f**). Together these data show that both C2 and C3 impact the temporal and spatial filtering of T4 and T5 neurons.

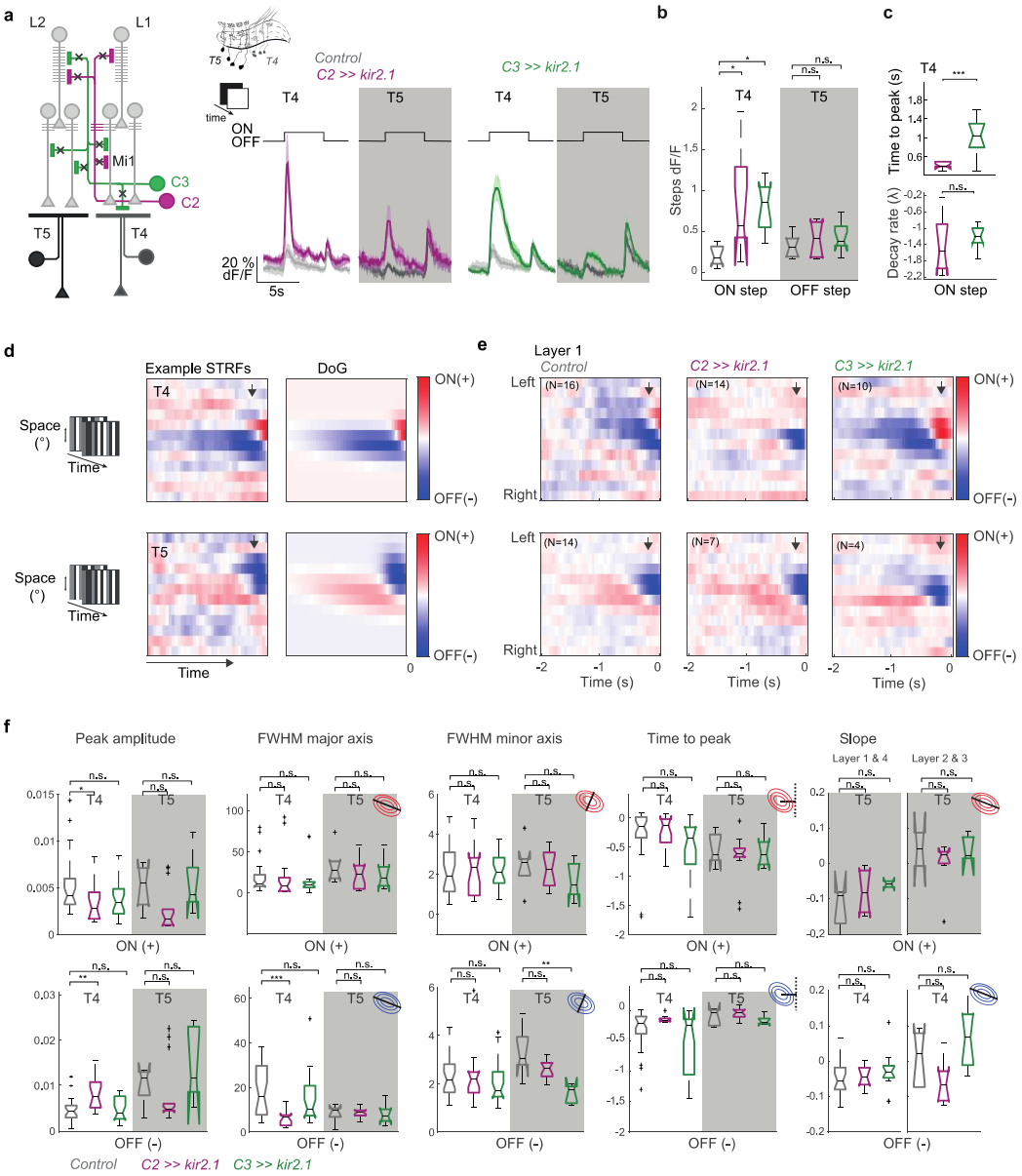

Fig. 3. C2 and C3 shape response properties of the motion detectors T4 and T5. a) Schematic of C2 and C3 interactions in upstream circuitry of T4 and T5 silenced by expression of the rectified potassium channel Kir 2.1 and in vivo calcium responses of T4 and T5 neurons to full field ON and OFF light flashes for control condition (grey, N=9 flies), C2 silencing (purple, N=8 flies) or C3 silencing (green, N=10 flies). **b)** Response change of T4 neurons to the onset of light (ON step) and T5 neurons to the offset of light (OFF step) quantified from (a). **c)** Time to peak of the ON response of T4 upon C2 and C3 silencing (a) and decay rate quantified from fitting an exponential function to the decay of the ON response. **d)** Spatiotemporal receptive field (STRF) examples of one T4 and one T5 cell extracted by reverse correlation of the cells response to a ternary white noise bar stimulus of vertical orientation and the fitted Difference-of-Gaussians (DoG). Red and blue colour indicate a positive and negative correlation with the stimulus, respectively. Black errors are aligned with the neurons PD. **e)** Average aligned spatiotemporal receptive fields (STRFs) of several T4 and T5 cells from lobula plate layer 1 for the control, C2 silencing, and C3 silencing conditions. Sample size (N) equals number of cells. **f)** Statistics from fitting DoGs on extracted STRFs for individual T4 and T5 cells from each subtype. Upper row: Parameters of DoG for the ON (positive) subfield, including the peak amplitude, the half width maximum for the major and minor axis, the time to peak and the slope. Lower row: same for DoG parameters of the OFF (negative) subfield. Sample size refers to number of cells with N=29 for T4 Control, N=16 for T4 C2 silencing, N=26 for T4 C3 silencing condition and N=6 for T5 Control, N=14 for T5 C2 silencing, N=5 for T5 C3 silencing condition. Shown are mean ± standard error. Significances are based on ANOVA (b, c) or Kruskal-Wallis Test (f) (p≤0.05 *, p≤0.01**, p≤0.001***, + Bonferroni correction for multiple testing).

C2 & C3 neurons sharpen direction selectivity of T4 and T5 neurons.

Because direction-selective neurons correlate visual input across space and time, the temporal and spatial filtering properties are critical for precise motion estimation. The effect of C2 and C3 silencing might thus also impact direction selectivity in T4/T5. To test this, we recorded T4/T5 responses to stripes moving into eight different directions and quantified the tuning direction (direction of vector) and the direction selectivity (DS = length of vectors) of single T4 or T5 neurons. Blocking the activity of both C2 and C3 significantly reduced DS of T4 neurons (**Fig. 4a, b**). The impact of blocking C2 alone on T4 neurons was more drastic than blocking C3 alone. A loss of direction selectivity can be allocated to either an increase of responses to the neuron's non-preferred directions or a decrease of the response to the preferred directions. To differentiate these two, we plotted the peak responses of T4/T5 neurons to the different motion directions. Blocking C2 increased responses to motion directions that differed from the PD by more than 45°, while a C3 block less specifically enhanced responses to all directions of motion (**Fig. 4c**). Blocking the activity of C2 and C3 simultaneously further decreased PD direction responses in T4 and lead to an even more drastic reduction of DS. DS of T5 neurons was less affected and only significantly reduced when both C2 and C3 neurons were silenced together (**Fig 4. a,b**). This phenotype was again associated with a significant increase of responses to non-preferred directions of motion (**Fig. 4c**). Silencing C2 and C3 had similar effects for T4/T5 subtypes of any lobula plate layer (**Supplementary Fig. 5**). Taken together, our data show that the two columnar neurons C2 and C3 strongly impact motion processing, especially in T4 neurons.

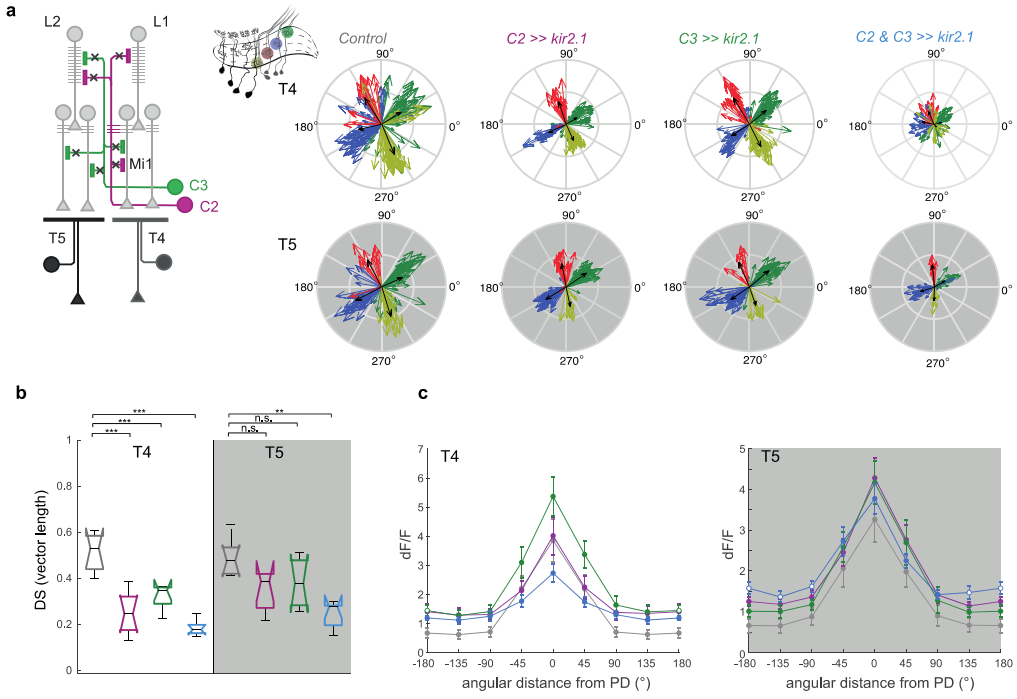

Fig. 4. C2 and C3 are required for direction-selective responses of T4 and T5 cells. a) Compass plots showing direction tuning of T4 and T5 neurons extracted from responses to ON and OFF edges moving into eight different directions for the control (UAS-Kir2.1), C2 silencing (C2>>Kir2.1), C3 silencing(C3>>Kir2.1) and C2/C3 double silencing (C2&C3>>Kir2.1) conditions. Vector length corresponds to the strength of the tuning. Black arrow indicates the average vector of the population. **b)** Direction selectivity averaged across cells and flies for control condition (grey, N=7 flies, 370 T4 cells, 196 T5 cells), C2 silencing (purple, N=8 flies 170 T4 cells, 196 T5cells), C3 silencing (green, N=6 flies, 188 T4 cells, 117 T5 cells) or double C2/C3 silencing (blue, N=7 flies, 132 T4 cells, 78 T5

cells). **c)** Response amplitude (dF/F) of T4 and T5 cells in relation to the angular distance of stimulus motion direction to the neurons PD. Shown are mean ± standard error. Significances are based on ANOVA (p≤0.05 *, p≤0.01**, p≤0.001***) (b) or Kruskal Wallis test (c) + Bonferroni correction for multiple testing. In (c) significant comparisons are indicated by open circles.

C2 & C3 neurons shape processing in medulla and lamina neurons

We next asked how C2 and C3 could shape the temporal and spatial filter properties of neurons upstream of T4 and T5 neurons. While C3 forms direct synaptic contacts with T4 cells, it only indirectly connects to T5 via medulla and lamina neurons of the OFF pathway. C2 is entirely lacking direct connections to the motion-sensitive T4 and T5 cells. Expressing the dendritic marker DenMark and a GFP-tagged Synaptotagmin (sytGFP) to label pre-synapses in C2 confirmed that C2 forms both postsynaptic and presynaptic contacts in the lamina and medulla (**Fig. 5a**). To reveal the neurons with the most frequent postsynaptic contacts of C2 and C3 we extracted synapse counts from a seven column EM dataset (Shinomiya et al., 2019b). This revealed that C2 for example forms several presynaptic contacts to the lamina neurons L5, L1, and L2 or the medulla neurons Mi1 and Tm1, while C3 mainly targets T1, L2 and L5, the trans-medulla neurons Tm1 and Tm4, and the medulla neuron Mi9 (**Fig. 5b**). Except of T1, all these neurons are known to be important components of the ON and OFF motion-detection circuits (**Fig. 5c, d**), suggesting that C2 and C3 indirectly affect processing in T4 and T5 by shaping upstream circuitry.

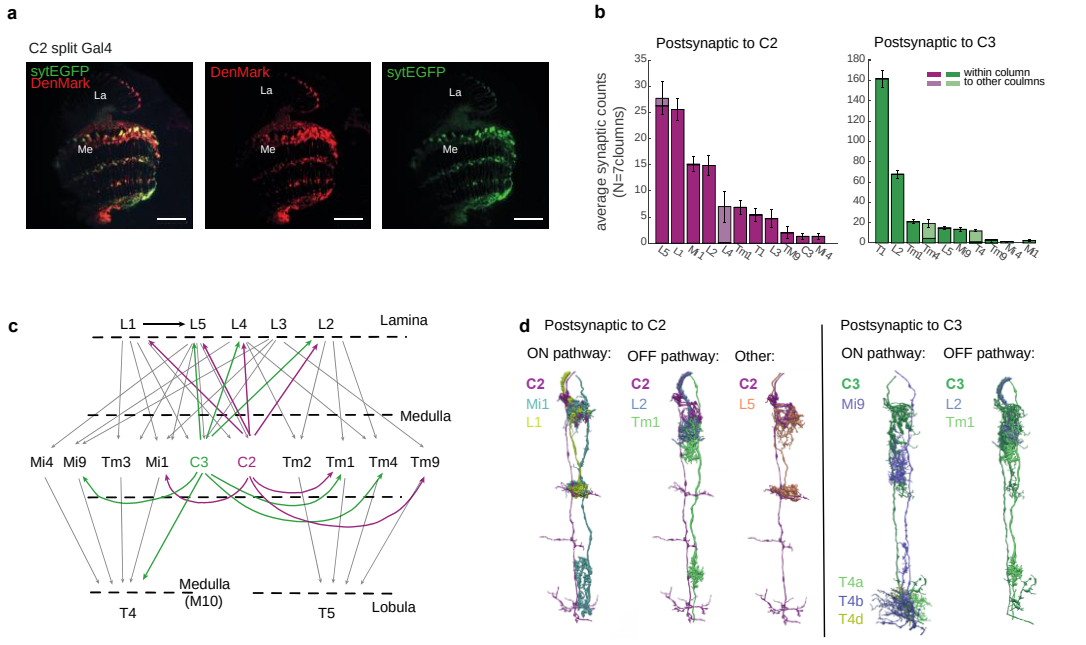

Fig. 5. C2 and C3 connect to upstream circuitry relevant for motion detection. a) Confocal images of C2 cells labelled with the dendritic marker DenMark and a GFP-tagged Synaptotagmin (sytGFP) to label pre-synapses in C2 (scale bar = 20µm). **b)** Counts of synapses with neurons postsynaptic to C2 or C3 within the same or neighbouring columns from EM data. **c)** Illustration of the C2 and C3 circuitry within the motion detection pathway. **d)** EM reconstructions of main postsynaptic neurons downstream of C2 and C3 from the ON and OFF pathway. Data in (b-d) were extracted from the 7column EM dataset (neuprint-examples.janelia.org), recently published in (Shinomiya et al., 2019b).

To next examine if C2 already sets the physiological properties of neurons in circuitry presynaptic to T4/T5, we tested the effect of C2 silencing on two example neurons of the ON and OFF pathways: the lamina neuron L2, which is one of the main inputs to the OFF pathway, and the ON pathway medulla neuron Mi1, one of the main direct inputs to T4 (**Fig. 5c**). Similar to C2 and C3 neurons, Mi1 responded with a transient increase in calcium signal to the onset of light that decreased to a sustained plateau response (**Fig. 6a**). At light offset, the calcium signal returned back to baseline. C2 silencing enhanced the Mi1 ON responses and the ON plateau response of Mi1 slowly decreased throughout the stimulus presentation. When measuring spatiotemporal receptive fields of Mi1, C2 silencing significantly delayed the biphasic temporal filter (**Fig. 6b**).

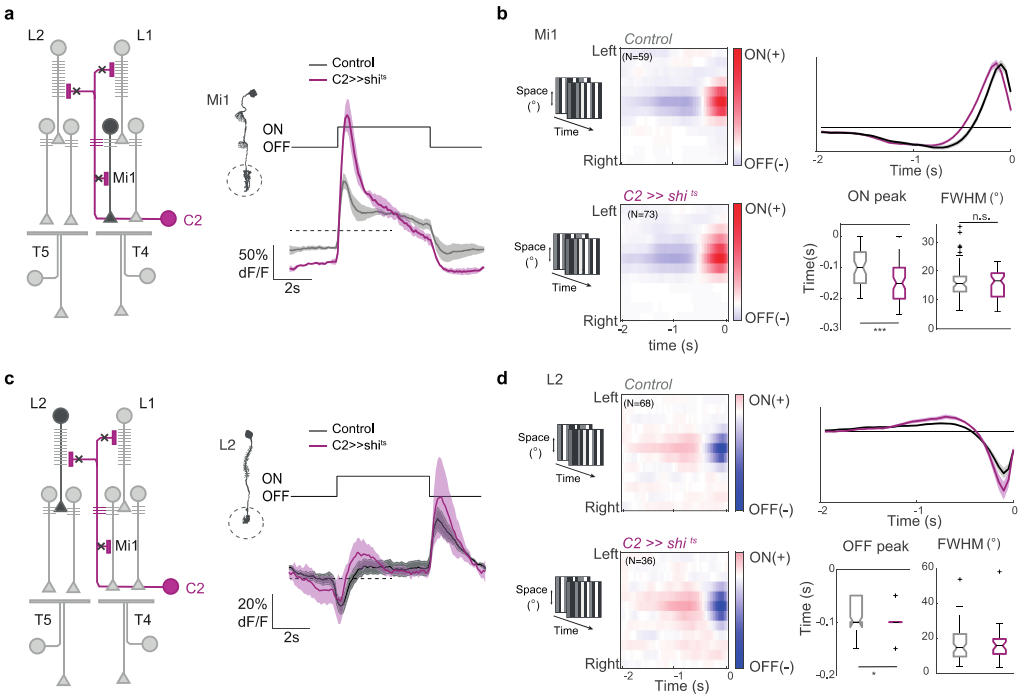

Fig. 6. C2 shapes physiological properties of neurons from ON and OFF pathway. a) Calcium responses of Mi1 axon terminals for control condition (grey, N=5 flies, 24 cells) or while genetically silencing C2 using shibire^{ts} (purple, N=3 flies, 20 cells). **b)** Left: Average aligned spatiotemporal receptive fields (STRFs) of Mi1 cells extracted from responses to horizontal or vertical ternary noise bars. Sample size (N) equals number of cells. Right: Temporal filter extracted from averaging single STRFs along the time axis of the horizontal and vertical STRFs. Timing of the ON peak of the temporal filter (top) and the full width half maximum (FWHM) of a gaussian fit extracted along the spatial dimension of maximal response of single STRFs (bottom). Shown are mean ± standard error. Significances are based on Wilcoxon rank sum test. **c, d)** Same as (a, b) for calcium responses of L2. Shown are control condition (N=8 flies, 59 cells) and C2 silencing condition (purple, N=4 flies, 26 cells).

L2 responded with a decrease in calcium signal to the ON step and an increase to the OFF step of the full field light stimulus (**Fig. 6c**). C2 silencing caused a more biphasic response to the ON step and slightly enhanced the OFF response. The spatiotemporal filter of L2 was also slightly, although not significantly affected, in a way that C2 silencing again increased both the positive and the negative filter amplitudes (**Fig. 6d**). Taken together these data show that C2 shapes the response properties of neurons in upstream circuitry in both the lamina and the medulla and thus indirectly impacts processing in downstream circuitry. C2 has a bigger influence on the physiological properties of the ON pathway neuron Mi1, which is in line with the more pronounced effect of C2 silencing on T4 vs. T5 (**Fig. 4**). Considering the many postsynaptic targets of C2 and also C3, these results might generalize such that the

GABAergic C2 and C3 shape properties of other lamina and medulla neurons and constitute a so far unknown inhibitory feedback pathway that is required for motion computation.

Discussion

In this study we have shown that the two GABAergic feedback neurons, C2 and C3, are novel, critical components of motion computation. Both neurons are ON selective and connect to several lamina and medulla neurons of both the ON and OFF pathway. Silencing C2 and C3 affects filter properties of the local motion detector neurons, T4 and T5, and leads to a reduced direction-selectivity. Whereas C2 silencing specifically increased T4 responses to ND stimuli and induces an imbalance in the ON and OFF receptive field components of T4 neurons, C3 silencing leads to more general enhancement of both T4 and T5 signals. The impact of C2 silencing on physiological properties of neurons upstream of the direction-selective T4/T5 cells suggests an indirect effect via feedback inhibition of upstream circuitry to be required for motion computation.

C2 and C3 are GABAergic, ON selective and multicolumnar

A forward genetic screen repeatedly identified driver lines whose expression pattern was dominated by the two columnar neurons C2 and C3. Both neurons are required for motion computation in T4 and T5 cells. During development C2/C3 and T4/T5 cells develop from the same progenitor cells in two competence windows, further arguing that these cells are intricately linked (Apitz and Salecker, 2016, 2018). Both neurons were found to be GABAergic by GABA colocalizations and a *gad1* intersection strategy, in line with previous studies (Datum et al., 1986; Kolodziejczyk et al., 2008; Meyer et al., 1986). The fast ON and the delayed OFF component of the C2/C3 filters well explain the transient ON responses to a full field light stimulus. The spatial receptive field of more than 15° suggests that C2 and C3 are multicolumnar and pool information from at least three neighbouring columns (Götz, 1964). This is in line with their broad arborisations into neighbouring columns of the medulla where C2 receives 30% of its total inputs, and C3 receives 15% of its total inputs from medulla neurons outside of their home column (neuprint, 7column data, Fischbach and Dittrich, 1989; Shinomiya et al., 2019). Interestingly the arborizations of C3 in medulla layer M5 and M9 into one direction along the anterior-posterior axis of the medulla is very stereotypic (Tuthill et al., 2013) and matches the wider receptive field size of C3 along the horizontal visual axis (Fig. 2c). Taken together, inhibitory C2 and C3 neurons integrate visual information across several visual units that are further processed by lamina and medulla neurons to inform motion processing.

The functional role of C2 and C3 for the ON pathway

C2 and C3 both define the spatial and temporal filtering properties of the motion detectors T4 and T5. There is a severe decrease of direction selectivity when either C2, C3, or both neurons are silenced. This is line with previous pharmacological experiments blocking GABA receptors in the whole brain (Fisher et al., 2015a). Given that other GABAergic inputs to T4/T5 are not required for DS responses, this suggests that C2 and C3 constitute a key

GABAergic circuit component required for motion detection. C2 and C3 neurons are ON selective and may thus have a greater impact on the processing of ON motion. This is consistent with the effect of C2 and C3 silencing on direction-selectivity being especially prominent for T4 neurons.

The loss of the delayed negative (OFF) subfield upon C2 silencing argues for a missing ON-selective inhibitory input and can be explained by indirect inhibition from C2. This imbalance in the ON and OFF subfield, and especially the compressed temporal extent of the OFF subfield can explain the observed loss of direction-selectivity in T4. A stimulus moving into the neurons non-preferred or null direction (ND) and thus normally hitting both the ON and OFF subfield simultaneously will not be cancelled. This idea is further in line with the increased responses of T4 to non-preferred stimuli when C2 is blocked. Together, this suggest that C2 implements ND suppression as suggested by the Barlow Levick model. However, C2 does not connect to T4 and can thus only indirectly mediate the ND suppression via medulla neurons that connect to T4. One prominent candidate would be Mi1 as it is one of the main inputs to T4 and receives synaptic input from C2 (Shinomiya et al., 2019; Takemura et al., 2017, illustrated in **Fig.5**). Furthermore, increased Mi1 responses to a full field light stimulus upon C2 block indicate ON suppression by C2. How could Mi1, which was shown to predominantly synapse at the centre of the T4 dendrite implement ND suppression? Notably, the negative subfield of T4 neurons extends from the trailing side to the centre of the STRF (**Fig. 3e**). C2 silencing diminished the delayed negative subfield in the centre of the T4 STRF, in line with the central input of Mi1 to T4. This argues that in addition to inhibition on the trailing side of the receptive field (RF), a delayed inhibition in the centre of the RF may be important for ND suppression. In line with this, the spatiotemporal filter of Mi1 revealed a biphasic temporal filter with a late negative component, as also shown previously (Arenz et al., 2017; Yang et al., 2016). This filter was temporally delayed upon C2 silencing, which could affect the filtering properties of the downstream T4 neuron but would not explain the loss of the negative delayed subfield or the diminished positive subfield of T4. However, Mi1 is not the only T4 input that receives synaptic input from C2. C2 also strongly connects to L1, the main input to all ON pathway neurons, and L5, the main input to Mi4, and could thus indirectly affect the filtering properties of almost all T4 inputs (**Fig. 5**). As such, Tm3 responses also exhibits fast positive and a late negative temporal filter component and could mediate both the positive and the delayed negative subfield of T4 (Arenz et al., 2017). In this way an indirect contribution of C2 to the negative and positive temporal filter of medulla neurons could shape ND suppression in T4 neurons.

C3 makes direct synaptic contacts with T4 and was therefore previously suggested to implement ND suppression in T4 together with Mi4 (Shinomiya et al., 2019b; Takemura et al., 2017). However, our data suggest another broader role of C3 for motion detection by interactions in upstream circuitry. Similar to C2, C3 inhibits flash responses in T4, but the slightly different response kinetics of T4 upon C2 or C3 silencing suggest different mechanisms by which C2 and C3 act. Indeed, C3 suppressed T4 responses not only to non-preferred motion directions but also to PD directions and affected the timing of the ON and OFF filter components of T4 neurons. This suggests a potential role of C3 for temporal tuning of the ON pathway. Notably, C3 connects to Mi4 and Mi9, which both have previously been suggested to contribute to temporal frequency tuning of the ON motion pathway and to be relevant at different behavioural states of the fly (Strother et al., 2017, 2018).

The functional role of C2 and C3 for the OFF pathway

Although C2 and C3 additionally connect to several lamina and medulla neurons of the OFF pathway, the impact on motion computation in T5 is less pronounced. Both C2 and C3 significantly affected the spatiotemporal filtering of T5 neurons, but only silencing C2 and C3 together significantly reduced direction-selectivity and contrast-selectivity in T5. Notably, C2 silencing induced ON responses of T5 to the full field light stimulus (**Fig. 3**), which could be explained by connections from C2 via Tm9 to T5 (Fisher et al., 2015c; Ramos-Traslosheros and Silies, 2021; Shinomiya et al., 2019b). On the other hand, C2 slightly affects responses of L2, the main input neuron to most major OFF pathway neurons, Tm1, Tm2 and Tm4 (Shinomiya et al., 2014, 2019b), which could together amplify the effect and affect T5 responses. Interestingly, both C2 and C3 connect to L2, which could explain the rather subtle phenotypes of blocking C2, and also explain previous data on GABAergic signalling setting up an L2 inhibitory surround (Freifeld et al., 2013). Furthermore, C2 and C3 were together but not individually required for direction-selectivity of T5, arguing that C2 and C3 may play a redundant role for shaping responses of the OFF pathway.

Taken together, we hypothesize a specific role of C2 for mediating inhibition for ND suppression to the ON pathway and another more global role of both C2 and C3 for balancing neuronal activity in upstream circuitry of the ON and OFF pathway.

C2 and C3 are relevant for motion guided behaviours

C2 was identified for its behavioral loss of function phenotype for ON and OFF motion detection. Additionally, both C2 and C3 neurons are relevant for direction-selective responses in the motion detectors T4 and T5. As T4 and T5 neurons are required for responses in downstream wide field motion detectors and optomotor turning to visual stimuli (Bahl et al., 2013; Maisak et al., 2013; Strother et al., 2017), this suggests that both C2 and C3 are required for motion guided behaviours. C2 and C3 have not been considered to be part of core-motion detection circuits so far, although some studies have suggested distinct roles of C2 and C3 for motion guided behaviours. For example, silencing C2 or C3 had individual effects on the amplitude and timing of behavioural responses to apparent motion stimuli with reversed contrast, so called reverse-phi stimuli (Tuthill et al., 2013). In behaving flies these stimuli elicit a turning response opposite to the direction of motion, which is reversed at higher temporal frequencies. Reverse-phi responses are already prominent in T4/T5 responses likely due to the temporal decorrelation of inputs from the ON and OFF pathways (Salazar-Gatzimas et al., 2018; Wienecke et al., 2018). The role of C2 and C3 on the balance and especially the timing of the ON and OFF components of the T4 filter will drastically impact the decorrelation of the two components and can thus explain the behavioural phenotypes to reverse-phi stimuli. Opposite effects of C2 and C3 silencing suggest differential mechanisms of C2 and C3 for motion processing, in line with the specific effects on T4 and T5 response properties. Additionally, C3 was suggested to provide asymmetric luminance signals to enhance regressive but not progressive motion information (Tuthill et al., 2013). This could suggest a specific effect of C3 on T4 and T5 cells that encode regressive but not progressive motion. However, we found a smaller effect of C3 on full field flash responses of T4 and T5 neurons from layer 2 that preferentially respond to regressive motion (**Supplementary Fig. 3f**) and no layer specific effect on filter properties or direction-selectivity of T4 and T5 neurons (**Supplementary Fig. 4c** and **Supplementary Fig. 5**). C2 and C3 have also been discussed to be important for distance estimation based on parallax-

motion (Triphan et al., 2016). Taken together these behavioural phenotypes of C2 and C3 silencing highlight the relevant role of C2 and C3 not only for direction selective responses at the level of T4 and T5 cells but for visual processing per se.

Potential role of upstream inhibitory signalling for motion computation

Several studies recently proposed a combination of direct excitatory and inhibitory mechanisms to compute direction selectivity in T4 and T5 cells (Badwan et al., 2019; Fisher et al., 2015a; Gruntman et al., 2018, 2019; Haag et al., 2016; Leong et al., 2016). Our data now suggest that motion computation relies on indirect feedback inhibition to upstream circuitry. Although EM studies and genetic profiling showed that both T4 and T5 cells receive direct inhibitory inputs within the ON and OFF pathways (Davis et al., 2020; Shinomiya et al., 2019b; Takemura et al., 2015, 2017) none of these inhibitory inputs have so far been shown to be relevant for motion detection. For example, the prominent input Mi4 was suggested to provide ND suppression on the trailing side of T4 (Arenz et al., 2017; Shinomiya et al., 2019b) but blocking Mi4 output did not change responses of T4 and only affected ON motion behavior at higher temporal frequencies (Strother et al., 2017). In contrast, our data suggest that C2 provides inhibitory feedback to lamina and medulla neurons that is utilized further downstream to implement ND suppression in T4 neurons. Although our data suggest that neither C2 nor C3 implement ND suppression in T5, a similar mechanism of upstream inhibition could explain the delayed inhibitory signals measured in T5 cells (Gruntman et al., 2019). This inhibitory feedback mechanism would be different from computations described in the vertebrate retina, where GABAergic starburst amacrine cells directly mediate ND suppression to direction-selective retinal ganglion cells (Fried et al., 2002; Wei, 2018; Wei et al., 2011; Yoshida et al., 2001). However, the idea of upstream inhibitory signalling required for DS reminds of the motion energy model that was suggested for motion-selective cells in cat visual cortex (Adelson and Bergen, 1985). Here, the inhibitory surround of upstream circuitry is utilized further downstream to compute direction-selective responses. The resulting Gabor-like filters of the motion detector highly resemble the tilted filter of T4 and T5 neurons (Leong et al., 2016; Salazar-Gatzimas et al., 2016). Notably, most inputs to T4 and T5 have centre-surround receptive fields or show negative temporal filtering (Arenz et al., 2017; Bahl et al., 2015; Fisher et al., 2015c; Meier et al., 2014; Salazar-Gatzimas et al., 2018; Serbe et al., 2016; Strother et al., 2017). Furthermore, we could show that C2 has a broad receptive field, suitable for inhibitory surround inhibition. A modified version of the motion energy model, where the complex spatial and temporal filters were replaced with filters describing T4 responses, has also recently been used to explain DS responses in Drosophila (Gruntman et al., 2018), however this model still utilizes a direct inhibitory connection for ND suppression. It thus remains to be seen if the inhibition implemented in upstream circuitry alone is sufficient to mediate ND suppression in T4 cells. ND suppression could additionally be supported by direct inhibition from Mi4 in the ON pathway or CT1 in both the ON and OFF pathway. (Meier and Borst, 2019; Shinomiya et al., 2019b; Strother et al., 2017, 2018). Such an apparently degenerate system, employing two different mechanisms to implement the same function may be more robust against external or internal disturbances (Tononi et al., 1999).

Broad impact of feedback inhibition on upstream processing

Both C2 and C3 extensively connect to neurons in upstream circuitry which express different types of ionotropic $GABA_A$ but also metabotropic $GABA_B$ receptors (Davis et al., 2020). Both receptor types mediate mainly inhibition to postsynaptic cells, by either gating chloride or G-protein coupled potassium channels (Wilson and Laurent, 2005). Additionally, our functional data suggests a more general role of C2 and especially C3 for inhibiting the activity of the entire network. In the vertebrate retina, horizontal cells (HCs) provide GABAergic feedback signals to photoreceptors, bipolar cells and retinal ganglion cells and have been proposed to be involved in multiple mechanisms of retinal processing including global light adaptation, spatial frequency tuning and the centre surround organization of retinal ganglion cells (Chaya et al., 2017; Diamond, 2017; Shelley et al., 2006; Tatsukawa et al., 2005; Thoreson and Mangel, 2012; Wu, 1992). In the salamander retina broadly distributed GABAergic inhibitory feedback synapses from the OFF amacrine cell highly influences sensitivity of ganglion cells (de Vries et al., 2011). Similarly, C2 could provide negative feedback to lamina and medulla neurons to return the membrane potential to baseline levels, increasing sensitivity to subsequent luminance changes. Such GABAergic inhibitory feedback interaction with an excitatory network of cells has been proposed to be important for network stabilization in higher mammalian brain regions (Avoli et al., 1995; Mann et al., 2009; Tsodyks et al., 1997). In the mouse retina excitation/inhibition balance has been suggested to be important for reliable computation of direction selectivity (Poleg-Polsky and Diamond, 2011). Thus, similar to HCs of the vertebrate retina, C2 and C3 provide inhibitory feedback to several neurons and could additionally play a more general role for balancing excitation and inhibition in the entire network of motion processing.

Taken together, our data demonstrate that C2 and C3 are essential to compute direction-selective outputs at the level of the local motion detectors T4 and T5. This work illustrates a novel feedback mechanism, adding to the feedforward circuitry to compute DS signals in T4 and T5 cells.

Acknowledgements

We are grateful to Christine Gündner and Jonas Chojetzki for great technical support and to all members of the Silies lab for valuable discussions. This project has received funding from the European Research Council (ERC) under the European Union's Horizon 2020 research and innovation program (grant agreement No 716512).

Author contributions

MH and MS conceived the experiments. MS and DG conducted the initial behavioral screen. MH and TL performed experiments and analyzed data. DY helped with data analysis. MH wrote the manuscript.

Methods

CONTACT FOR REAGENT AND RESOURCE SHARING

Further information and requests for resources and reagents should be directed to and will be fulfilled by the Lead Contact, Marion Silies (msilies@uni-mainz.de).

EXPERIMANTAL MODEL AND SUBJECT DETAILS

Drosophila strains and fly husbandry

Drosophila melanogaster were raised on molasses-based food at 25°C and 55% humidity in a 12:12 hr light-dark cycle. For all experiments female flies were used. For imaging experiments flies were recorded 3-5 days after eclosion at room temperature (RT, 20°C). Genotypes used in all experiments are given in the Key Resources Table.

Table 1 KEY RESOURCES TABLE

REAGENT or RESOURCE	SOURCE	IDENTIFIER	Designation	Additional information
Experimental Models: Organisms/Strains : *D. melanogaster*				
InSITE- 0301	BDSC	RRID:BDSC_62767	Immunostaining	Fig.1
InSITE- 0564	BDSC	RRID:BDSC_63411	Immunostaining	Fig.1
InSITE- 0787	BDSC	RRID:BDSC_63782	Immunostaining	Fig.1
InSITE- 0940	BDSC	RRID:BDSC_63911	Immunostaining	Supplementary Fig. 1
InSITE- 0470	BDSC	RRID:BDSC_63341	Immunostaining	Supplementary Fig. 1
InSITE- 0096	T.Clandinin		Immunostaining	
InSITE- 0396	BDSC	RRID:BDSC_64718	Immunostaining	
InSITE- 0619	BDSC	RRID:BDSC_63449	Immunostaining	Fig.1
InSITE- 0913	BDSC	RRID:BDSC_63892	Immunostaining	Fig.1
InSITE- 0669	BDSC	RRID:BDSC_64737	Immunostaining	Fig.1
InSITE- 0974	T.Clandinin		Immunostaining	Supplementary Fig.1
InSITE- 1037	BDSC	RRID:BDSC_63975	Immunostaining	Supplementary Fig.1
InSITE- 0980	BDSC	RRID:BDSC_63936	Immunostaining	Supplementary Fig.1
InSITE- 0518	T.Clandinin		Immunostaining	Supplementary Fig.1
InSITE- 0756	BDSC	RRID:BDSC_63499	Immunostaining	Supplementary Fig.1
InSITE- 0081	BDSC	RRID:BDSC_62703	Immunostaining	Supplementary Fig.1

InSITE- 0168	BDSC	RRID:BDSC_62706	Immunostaining	Supplementary Fig.1
InSITE- 0651	BDSC	RRID:BDSC_63731	Immunostaining	Supplementary Fig.1
UAS-FRT-CD2y+-RFT-mCD8::GFP; UASFlp	(Wong et al., 2002)		FlpOut clones	Fig.1, Supplementary Fig.1
UAS-mCD8::GFP	(Fisher et al., 2015c)		Immunostaining	Fig.1,Supplementary Fig.1
UAS-eGFP	(Fisher et al., 2015c)		Immunostaining	Fig.1, Supplementary Fig.1
UAS-DenMark, UAS-syt.eGFP	BDSC	RRID:BDSC_33065	C2/C3 label dendrites & synaptic axons	Fig.5
UAS-mCD8::RFP^{attP8};lexAop-mCD8::GFP^{attP16}	(Fisher et al., 2015c)		*Gad1* intersection	Fig.1, Supplementary Fig.1
UAS-lexADBD	BDSC	RRID:BDSC_56528	*Gad1* intersection	Fig.1, Supplementary Fig.1
Gad1^{MI09277}-p65AD	BDSC	RRID:BDSC_60322	*Gad1* intersection	Fig.1, Supplementary Fig.1
lexAop-GCaMP6f-p10$^{su(Hw)attp5}$	BDSC	RRID:BDSC_44277	T4/T5>>GCaMP 6f, Mi1>>GCaMP6f, L2>>GCaMP6f	Fig.3, 6, Supplementary Fig.3
20xUAS-IVS-GCaMP6f^{attP40}	BDSC	RRID:BDSC_42747	C2/C3>>GCaMP 6f	Fig.2, Supplementary Fig.2
R59E08-LexA^{attP40}	BDSC	RRID:BDSC_52832	T4/T5>>GCaMP 6f	Fig.3,4
R20C11-p65.AD^{attP40}	BDSC	RRID:BDSC_70106	C2 split Gal4, C2/C3 split Gal4	Fig.2, 3, 4, 5 Supplementary Fig.2,3, 4
R25B02-Gal4.DBD^{attP2}	BDSC	RRID:BDSC_68969	C2 split Gal4	Fig.2, 3, 4, 5, Supplementary Fig.2,3, 4
R26H02-p65.AD^{attP40}	(Tuthill et al., 2013)	RRID:BDSC_70159	C3 split Gal4	Fig.2, 3, 4, Supplementary Fig.2,3, 4
R29G11-Gal4.DBD^{attP2}	Tuthill et al., 2013)		C3 split Gal4	Fig.2, 3, 4, Supplementary Fig.2,3, 4
R48D11-Gal4.DBD^{attP2}	BDSC	RRID:BDSC_69028	C2/C3 split Gal4	Fig.4, Supplementary Fig.3, 4
R19F01-lexA^{attp40}	BDSC	RRID:BDSC_52547	Mi1>> GCaMP6f	Fig.6

R19D12-lexA^{attp40}	BDSC	RRID:BDSC_52545	L2>> GCaMP6f	Fig.6
UAS-KCNJ2.EGFP(Kir 2.1)[7]	BDSC	RRID:BDSC_6595	C2/C3 >>Kir2.1	Fig.3,4, Supplementary Fig.3, 4
UAS-shi^{ts}	BDSC	RRID:BDSC_44222	C2/C3 >>shibire^{ts}	Fig.6
Software				
ImageJ	National Institutes of Health	http://imagej.nih.gov/ij		Fig.1, Supplementary Fig.1
Imaris	Oxford Instruments			Fig.1, Supplementary Fig.1
Adobe Photoshop 2021				Fig.1, Supplementary Fig.1
MATLAB	Mathworks	http://ww.mathworks.com/		All (except Fig.1)
Python 2.7	Python	https://python.org		All (except Fig.1)

METHOD DETAILS

Immunohistochemistry and confocal microscopy

Fly brains were dissected and simultaneously fixed in 2% paraformaldehyde in phosphate-buffered lysine (PBL) for 1hr at RT. Next, brains were washed 3x in phosphate-buffered saline containing 0.3% triton X-100 (PBT, pH:7.2) and blocked for 30 min in 10% normal goat serum (NGS, Fisher Scientific GmbH, Schwerte, Germany) in PBT at RT. The primary antibody solution was incubated for 24hr at 4°C and removed by washing 3x for 5 min in PBT. Subsequently the secondary antibody solution was incubated at 4°C overnight. The primary and secondary antibodies used for the different experiments are listed below. Last the samples were again washed with PBT 3x and embedded in Vectashield (Vector Laboratories, Burlingame) until further use but no longer that 7 days.

Table 2 List of primary and secondary antibodies used for stainings

Primary antibody	**species**	**Conc.**	**company**	**Product nr.**
Polyclonal anti-GFP	chicken	1:2000	Abcam (Cambridge, UK)	Ab13970
Monoclonal anti-Bruchpilot (nc82)	mouse	1:25	DSHB (Iowa City, US)	
Polyclonal anti-GABA	rabbit	1:200	Sigma-Aldrich (Darmstadt, G)	A2052 Sigma
Polyclonal Anti-DsRed	rabbit	1:400	Clontech (California, US)	632475

Secondary antibody	**species**	**Conc.**	**company**	**Product nr.**
Alexa Fluor anti-chicken-Alexa 488	goat	1:200	Dianova (Hamburg, G)	103-545-155
Alexa Fluor anti-mouse-Alexa 647	goat	1:200	DSHB (Iowa City, US)	115-605-003
Alexa Fluor anti-rabbit-Alexa 594	goat	1:200	Sigma-Aldrich (Darmstadt, G)	111-585-003

For confocal microscopy brains were mounted with a small drop of Vectashield on a microscope slide and covered with a cover slip (Thermo Fisher Scientific GmbH, Schwerte, Germany). Serial Z-stacks were taken on a Zeiss LSM10 microscope (Carl Zeiss Microscopy GmbH, Germany) using the Zen 2 Blue Edition software (Carl Zeiss Microscopy, LLC, United States). Z-stack images were taken at 1 µm steps and 512x512 pixel resolution using three different Plan-Apochromat objectives (20x/0.8 M27 (air), DIX(UV)VIS-IR 40x/1.3 M27 (oil), DIX(UV)VIS-IR 63x/1.4 M27 (oil)). Confocal stacks were further rendered into two-dimensional images using *Imaris* (Oxford Instruments) and later edited using *Adobe Photoshop 2021.*

Identification of GABAergic cell types

To identify GABAergic cell types required for motion vision, we tested 25 InSITE Gal4 lines that were previously identified in a behavioral screen to be motion blind and showed extensive expression in the visual system (Silies et al., 2013). We expressed *UAS-eGFP* and *UAS-mCD8::GFP* under the control of the InSITE-Gal4 line and visualized the expression pattern using confocal microscopy. To localize GABAergic neurons within the expression pattern, we stained the brains with anti-GABA antibodies and screened for colocalization of GFP and GABA.

To identify cell types in the expression pattern of the InSITE Gal4 lines, we used a single cell Flpout strategy by which GFP expression was restricted to random cells of the targeted pattern. By expressing *UAS>CD2,y^{+}>mCD8::GFP* Flpout as well as *UAS-Flp* under control of the respective Gal4 driver line.

Identifying pre and postsynaptic sites of C2 and C3

To identify the dendrites and synaptic axons of C2, we expressed the dendritic marker DenMark and the GFP-tagged Syt1 to label synaptic vesicles. Brain dissections and Confocal imaging was done as described above. Synaptic counts of C2 and C3 with postsynaptic cells and reconstructions of C2 and C3 and their postsynaptic partners were extracted from the 7column EM dataset (neuprint-examples.janelia.org), recently published in (Shinomiya et al., 2019b).

Two-photon calcium imaging

Prior to two-photon imaging, flies were anesthetized on ice and fit into a small hole in stainless-steel foil, located in a custom-made holder. The head was tilted approximately 30° to expose the back of the head. To fix the head of the fly, a small drop of UV-sensitive glue (Bondic) was used on the left side of the brain and the thorax. The cuticle on the right eye, fat bodies and tracheae were removed using breakable razor blades and forceps. To ensure constant nutrients and calcium supply flies were perfused with a carboxygenated saline containing 103 mM NaCl, 3 mM KCl, 5 mM TES, 1mM NaH_2PO_4, 4 mM $MgCl_2$ 1.5 mM $CaCl_2$, 10mM trehalose, 10mM glucose, 7mM sucrose, and 26mM $NaHCO_3$ (pH~7.3). To record

calcium activity, a two-photon microscope (Bruker Investigator, Bruker, Madison, WI, USA), equipped with a 25x/1.1 objective (Nikon, Minato, Japan) was used. For excitation of GCaMP6f, the excitation laser (Spectraphysics Insight DS+) was tuned to a wavelength of 920nm with <20mW of laser power measured at the objective. Emitted light was filtered through an SP680 short pass filter, a 560 lpxr dichroic filter and a 525/70 emission filter and detected by PMTs set to a gain of 855V. Imaging frames were acquired at a frame rate of ~15-20 Hz and 4-7 optical zoom using PrairieView software.

Visual stimulation

Visual stimuli were presented on a 8 cm x 8 cm rear projection screen in front of the fly covering a visual angle of 60 deg in azimuth and elevation. Stimuli were filtered through a 482/18 bandpass filter (Semrock) and ND1.0 neutral density filter (Thorlabs) and projected using a LightCrafter 4500 DLP (Texas Instruments, Texas, USA) with a frame rate of 100 Hz and synchronized with the recording of the microscope as described previously (Freifeld et al., 2013).

All visual stimuli were generated using custom-written software using C++ and OpenGL. T4 and T5 recordings always started by showing ON and OFF edges moving into four directions of motion used for the automated ROI selection. Subsequent stimuli were randomized. If the fly moved, the moving edge stimulus was repeated in between recordings.

Moving OFF and ON edges

Full contrast dark or bright edges moving with a velocity of 20°/s across the full screen to four or eight different directions. Each stimulus direction was presented at least two times in semi random order. A four-direction stimulus was used for the later mathematical identification of T4 and T5 axon terminals. An eight-direction stimulus was shown to C2 and C3 to quantify direction-selectivity.

Periodic full-field flashes

The full-field flash stimulus consisted of full-contrast ON and OFF flashes covering the whole screen. Each flash lasted for 5 s and thus 10 s for one stimulus epoch, presented for ~2 min per fly. This stimulus was shown to flies while recording C2/C3, T4/T5, Mi1 or L2 cells.

Moving OFF and ON stripes

Full contrast dark or bright stripes of 5° width moving with a velocity of 20°/s to eight different directions in semi-randomized order. This stimulus was repeated at least three times per fly and was used to quantify tuning preferences of T4 and T5 neurons.

Ternary white noise

Each frame consisted of 12 bars of 5° x 60° size tilted along either azimuth or elevation and spanning the whole screen of 60° x 60°. Each bar changed its contrast from frame to frame

with equal probability of having either minimal, maximal or intermediate contrast independent of all other bars. Frames were updated every 50 ms. The duration of one epoch was 500s with 3s of grey interleave. Per fly the stimulus epoch was repeated twice for T4 and T5 recordings and once for medulla and lamina neurons. This stimulus was used to extract the spatiotemporal receptive fields (STRFs) of all neuron types.

QUANTIFICATION AND STATISTICAL ANALYSIS

Preprocessing

All data analysis was performed using MATLAB R2017a (The MathWorks Inc, Natrick, MA) or Python 2.7. Motion artifacts were corrected using Sequential Image Alignment SIMA, applying an extended Hidden Markov Model (Kaifosh et al., 2014).

Manual ROI selection

For manual ROI selection the average intensity of all frames was used to guide the manual selection of axon terminals using a custom written user interface with Matlab. Responses of pixels belonging to one ROI were averaged and saved for further analysis.

Automated ROI selection

For the extraction of single T4 or T5 axon terminals we made use of their contrast- and direction-selective responses to ON and OFF edges moving into four directions. First, the aligned images were averaged across time and the average image intensity was Gaussian filtered (s=1.5) and then threshold-selected by Otsu's method (Otsu, 1979) to find foreground pixels suitable for further analysis. After averaging responses across stimulus repetitions, we selected pixels that showed a peak response larger than the average response plus two (three, for STRFs) times the standard deviation of the full trace. These pixels were grouped based on their contrast preference (ON or OFF pixels) and further assigned to four categories based on their anatomical location within the lobula plate (layers A, B, C, or D). We further calculated a direction-selectivity index (DSI) and contrast selectivity index (CSI) for each pixel as follows:

$$DSI = \frac{PD_{max} - ND_{max}}{PD_{max}},$$

$$CSI = \frac{PC_{max} - NC_{max}}{PC_{max}}.$$

where PD_{max} and ND_{max} denote the maximal response into the preferred direction (PD) and null direction (ND) and PC_{max} and NC_{max} denote the maximum responses for the preferred contrast (PC) and the non-preferred or inverse contrast (NC). We excluded all pixels that did not exceed the CSI threshold of 0.2 or 0.5 for STRF calculation to obtain clean T4 or T5 responses. For the final clustering we used the x and y location of pixel and the timing of the response to the PD. Based on these parameters the Euclidean distance between each pair of pixels was calculated and average-linkage agglomerative hierarchical clustering was performed. We further evaluated the optimal distance threshold that yielded most clusters of the appropriate size between 1 and 6.5 μm^2. All resulting clusters that fell outside this

range were excluded from further analysis. Cluster locations were saved and matched with subsequent recordings of the same cells to other stimulus types.

Response quantification

dF/F clalculation

After subtracting a background signal, the response of a cell was calculated as dF/F using the following formula:

$$\frac{dF}{F} = \frac{F - F_0}{F_0},$$

For T4 and T5 responses F_0 was defined as the baseline fluorescence, computed from averaging responses to gray interleaves. For C2, C3, Mi1 and L2 F_0 was defined as the average of the whole response trace. Responses of single ROIs were averaged for each fly and interpolated to 10Hz before averaging across flies.

Full-field flashes

Responses of single cells to full-field flashes were extracted by matching the location of the extracted clusters from the cluster analysis. For T4 and T5 responses ON or OFF step responses were calculated as the difference of a response to an epoch 2s before the onset or offset of light and the peak response in an epoch 2s after the onset or offset of light, respectively. The time to peak was quantified solely for the two silencing conditions as the time delay from the onset of light to the timing of the peak response. The time to decay was extracted from the decay constant of a single term exponential fit to the response in an epoch 3s after the onset of light. A decay constant was only taken into account if it was negative.

Moving OFF and ON stripes

To quantify direction selectivity (DS) of single cells, responses were trial averaged and the peak response to the eight different directions of either increment or decrement bars was extracted for T4 and T5 cells respectively. We further quantified the tuning of single cells by computing vector spaces as follows (Mazurek et al., 2014):

$$L_{dir} = \left| \frac{\sum_k R(\theta_k) \exp(i\theta_k)}{\sum_k R(\theta_k)} \right|.$$

where $R(\theta_k)$ is the response to angle θ_k. The direction of the vector L_{dir} denotes the tuning angle of the cell and the normalized length of the vector is related to the circular variance and thus represents the selectivity of the cell.

Space-time receptive field mapping

Space-time receptive fields (STRFs) were extracted from responses of single cell ROIs to the ternary white noise stimulus. The raw fluorescence (F) traces of single clusters were extrapolated to 20Hz matching the update rate of the ternary white noise stimulus. The response changes of the cell (dF/F) was extracted as described above for the full-field flash

stimulus. Here (F_0) denotes the baseline fluorescence, computed from averaging responses to gray interleaves. The extracted cell response was further centered around its mean and averaged across two stimulus epochs if it was repeated twice. The stimulus was normalized to have values of -1, 0 and 1 for dark, gray and bright bars.

STRFs were extracted by computing a weighted stimulus average also known as reverse correlation. For this a sliding average of two seconds length was propagated backwards in time and weighted by the response of the cell at the start of the window. Given the response of the cell at time point t (r_t), the time window of the stimulus (τ), the amount of total time points (T) and the stimulus snippet $s(t-\tau)$ the STRF is computed as follows:

$$STRF = \frac{1}{T-\tau} \sum_{t=\tau}^{T} r_t s(t-\tau).$$

To evaluate how well STRFs predicted the real cell response we convoluted the extracted STRFs with the stimulus. This prediction of the cell response was then correlated with the real cell response. The correlation value R^2 was used to discard non-valid STRFs. The R^2 threshold was chosen by visual inspection to be 0.2 for STRFs of T4 and T5 neurons and 0.26 for C2, C3, Mi1 and L2 STRFs. Furthermore, we extracted a reliability measure of the cell response by correlating the responses two the two epochs of stimulus repetition for responses from T4 and T5. The threshold was again chosen empirically to be 0.1 (**Supplementary Fig. 4a**). For medulla and lamina neurons one repetition of white noise was sufficient, so that no reliability measure could be calculated.

The weighted average STRF was computed by averaging all STRFs of one subtype of cell and weighting each STRF by the R^2 value. Therefore, STRFs that well predicted the cell response had a higher impact on the average.

To further extract statistics of the STRFs for T4 and T5 neurons we fit Differences-of-Gaussians (DoG) models with two opposite signed components to each STRF (Leong et al., 2016). DoG fits were initialized at the location of the minimum and maximum of the STRF with a width of 10° in space and 250 ms in time. The angular orientation was set to 0 radians. The fitting was repeated 10 times with random perturbations of the initial parameters to improve robustness to initialization. Based on Euclidean distance the best fitting model was selected (Leong et al., 2016). We further applied a fitting threshold of 0.3 to filter for valid STRFs. From the best fitting linear DoG filter, we extracted the peak amplitude to be the maximum and minimum values of the filter and the time to peak from the distance of the maximum and minimum to 0 time. The spatial and temporal extends were approximated by extracting the half width of the principal and minor axis of the two subfields separately and the slope of the two subfields was calculated as the tangens from the angular orientation of fits (θ). For C2, C3, Mi1 and L2 the temporal filter was extracted from averaging single STRFs along the time axis of the horizontal or vertical STRFs. Timing of the ON peak was calculated as the time of highest correlation of the temporal filter and the full width half maximum (FWHM) was extracted from a gaussian fit along the spatial dimension of maximal response of single STRFs.

Statistics

All statistics were done in Matlab. For comparisons between C2 and C3 response characteristics (**Fig. 2d,e**) a two-sided Wilcoxon signed rank test was calculated.

For multiple comparisons of T4 and T5 or Mi1 and L2 response characteristics from control and C2/C3 silencing conditions all samples were first tested for normal distribution with a Kolmogorov–Smirnov test. If all samples were normally distributed a oneway ANOVA with subsequent pairwise comparison was calculated (an exception was made for Data in (**Fig. 4b**), where only the double C2 and C3 silencing condition for T5 was not normally distributed). Bonferroni correction was applied for multiple testing. In the case of non-normally distributed data, a Kruskal-Wallis Test was calculated. All statistics are listed in the following tables:

Response properties of C2 and C3

Table 3 *Statistical summary of Wilcoxon rank sum test. Sample Size (N) is given in number of cells (C)*

Fig. 2		**Group 1: C2** (purple)			**Group 2: C3** (green)		
	p-value G1-G2	Mean	Std	N	Mean	Std	N
Timing ON peak Elevation (e)	0.1164	-0.353	0.50	26C	-0.543	0.80	36C
Timing ON peak Azimuth (e)	0.2648	-0.065	0.02	20C	-0.180	0.34	23C
FWHM Elevation (e)	0.0515	17.580	7.66	26C	14.764	8.32	36C
FWHM Azimuth (e)	0.8742	18.532	4.43	20C	18.539	5.91	23C

Response properties of T4 and T5 to full field flashes

Table 4 *Statistical summary of ANOVA*

T4-ONResps (Fig. 3b & Supplmentary Fig.3d)

Source	SS	dF	MS	F	Prob>F
Groups	2.39505	3	0.79835	4.26	0.012
Error	6.18794	33	0.18751		
Total	8.58299	36			

T5-OFFResps (Fig. 3b & Supplmentary Fig.3d)

Source	SS	dF	MS	F	Prob>F
Groups	0.10164	3	0.03388	0.86	0.4715
Error	1.30002	33	0.03939		
Total	1.40166	36			

T5-ONResps (Supplementary Fig. 3e)

Source	SS	dF	MS	F	Prob>F
Groups	0.57289	3	0.19096	5.02	0.0056
Error	1.25588	33	0.03806		
Total	1.82877	36			

 # Cells T4 (Supplementary Fig. 3b)

Source	SS	dF	MS	F	Prob>F
Groups	4868.62	3	1622.87	13.74	4.95355e-06
Error	4017.2	34	118.15		
Total	8885.82	37			

 # Cells T5 (Supplementary Fig. 3b)

Source	SS	dF	MS	F	Prob>F
Groups	163.53	3	54.5101	2.01	0.1313
Error	923.02	34	27.1477		
Total	1086.55	37			

Table 5 *Statistical summary of multi comparisons with Bonferroni correction. Sample Size (N) is given in number of cells (C) or flies (F).*

Fig. 3				**G1: Control** (grey)			**G2: C2 block** (purple)			**G3: C3 block** (green)		
	p-value G1-G2	p-value G1-G3	p-value G2-G3	Mean	Std	N	Mean	Std	N	Mean	Std	N
Steps dF/F T4 ON (b)	0.02745	0.02156	1	0.1908	0.11	9F	0.8310	0.65	8F	0.8146	0.27	10 F
Steps dF/F T5 OFF (b)	1	1	1	0.3167	0.13	9F	0.3999	0.22	8F	0.4350	0.18	10 F
Time to peak (c)	-	-	0.00032	-	-	-	0.4250	0.07	8F	1.0500	0.38	10 F
Decay rate (c)	-	-	0.15063	-	-	-	0.6938	0.27	7F	0.8685	0.20	10 F

Supplmentary Fig.3				**G1: Control** (grey)			**G2: C2block** (purple)			**G2: C3 block** (green)			**G2: C2C3 block** (blue)		
	p-val G1-G2	p-val G1-G3	p-val G1-G4	Mean	Std	N	Mean	Std	N	Mean	Std	N	Mean	Std	N
# Cells T4 (b)	1	0.087025	0.000018	42.666	13.0	9F	41.666	13.6	9F	29.800	10.4	10F	14.800	4.49	10F
# Cells T5 (b)	1	1	1	11.000	4.55	9F	7.5556	6.94	9F	13.400	5.35	10F	10.400	3.53	10F
Steps dF/F T4 ON (d)	See T1	See T1	0.19447	0.1908	0.11	9F	See T1	-	-	See T1	-	-	0.6352	0.51	10F
Steps dF/F T5 OFF (d)	See T1	See T1	1	0.3167	0.13	9F	See T1	-	-	See T1	-	-	0.3181	0.23	10F
Steps dF/F T5 ON(e)	0.00301	0.46976	0.76674	0.1082	0.09	9F	0.4739	0.31	8F	0.2711	0.12	10F	0.2483	0.19	10F

T4 and T5 STRFs

Table 6 *Statistical summary of Kruskal-Wallis Test*

T4 R2- goodness of gauss fit (Supplementary Fig. 4b)

Source	SS	dF	MS	Chi-sq	Prob>Chi-sq
Groups	2701.3	2	1350.65	6.34	0.042
Error	27118.7	68	398.8		
Total	29820	70			

T5 R2- goodness of gauss fit (Supplementary Fig. 4b)

Source	SS	dF	MS	Chi-sq	Prob>Chi-sq
Groups	40.61	2	20.3048	0.75	0.6874
Error	1259.39	22	57.245		
Total	1300	24			

Peak amplitude T4 ON (Fig.3f)

Source	SS	dF	MS	Chi-sq	Prob>Chi-sq
Groups	2876.1	2	1438.05	6.75	0.0342
Error	26943.9	68	396.23		
Total	29820	70			

Peak amplitude T5 ON (Fig.3f)

Source	SS	dF	MS	Chi-sq	Prob>Chi-sq
Groups	389.967	2	194.983	7.2	0.0273
Error	910.033	22	41.365		
Total	1300	24			

Peak amplitude T4 OFF (Fig.3f)

Source	SS	dF	MS	Chi-sq	Prob>Chi-sq
Groups	5496.3	2	2748.13	12.9	0.0016
Error	24323.7	68	357.7		
Total	29820	70			

Peak amplitude T5 OFF (Fig.3f)

Source	SS	dF	MS	Chi-sq	Prob>Chi-sq
Groups	260.25	2	130.126	4.8	0.0905
Error	1039.75	22	47.261		
Total	1300	24			

FWHM major axis T4 ON

Source	SS	dF	MS	Chi-sq	Prob>Chi-sq
Groups	1182.8	2	591.397	2.78	0.2495
Error	28637.2	68	421.135		
Total	29820	70			

FWHM major axis T5 ON

Source	SS	dF	MS	Chi-sq	Prob>Chi-sq
Groups	79.44	2	39.719	1.47	0.4803
Error	1220.56	22	55.4801		
Total	1300	24			

FWHM major axis T4 OFF

Source	SS	dF	MS	Chi-sq	Prob>Chi-sq
Groups	8084.3	2	4042.14	18.98	7.57113e-05
Error	21735.7	68	319.64		
Total	29820	70			

FWHM major axis T5 OFF

Source	SS	dF	MS	Chi-sq	Prob>Chi-sq
Groups	66.31	2	33.1548	1.22	0.5422
Error	1233.69	22	56.0768		
Total	1300	24			

FWHM minor axis T4 ON

Source	SS	dF	MS	Chi-sq	Prob>Chi-sq
Groups	12.8	2	6.391	0.03	0.9851
Error	29807.2	68	438.341		
Total	29820	70			

FWHM minor axis T5 ON

Source	SS	dF	MS	Chi-sq	Prob>Chi-sq
Groups	83.59	2	41.7929	1.54	0.4623
Error	1216.41	22	55.2916		
Total	1300	24			

FWHM minor axis T4 OFF

Source	SS	dF	MS	Chi-sq	Prob>Chi-sq
Groups	1014.7	2	507.332	2.38	0.3039
Error	28805.3	68	423.608		
Total	29820	70			

FWHM minor axis T5 OFF

Source	SS	dF	MS	Chi-sq	Prob>Chi-sq
Groups	671.51	2	335.755	12.4	0.002
Error	628.49	22	28.568		
Total	1300	24			

Time to peak T4 ON

Source	SS	dF	MS	Chi-sq	Prob>Chi-sq
Groups	2572.4	2	1286.18	6.04	0.0488
Error	27247.6	68	400.7		
Total	29820	70			

Time to peak T5 ON

Source	SS	dF	MS	Chi-sq	Prob>Chi-sq
Groups	3.51	2	1.7548	0.06	0.9681
Error	1296.49	22	58.9314		
Total	1300	24			

Time to peak T4 OFF

Source	SS	dF	MS	Chi-sq	Prob>Chi-sq
Groups	2856.8	2	1428.4	6.71	0.035
Error	26963.2	68	396.52		
Total	29820	70			

Time to peak T5 OFF

Source	SS	dF	MS	Chi-sq	Prob>Chi-sq
Groups	242.84	2	121.421	4.48	0.1063
Error	1057.16	22	48.053		
Total	1300	24			

Slope Layer 1&4 T4 OFF

Source	SS	dF	MS	Chi-sq	Prob>Chi-sq
Groups	402.43	2	201.213	2.33	0.3115
Error	7187.57	42	171.133		
Total	7590	44			

Slope Layer 2&3 T4 OFF

Source	SS	dF	MS	Chi-sq	Prob>Chi-sq
Groups	476.79	2	238.393	8.15	0.017
Error	985.71	23	42.857		
Total	1462.5	25			

Slope Layer 1&4 T5 ON

Source	SS	dF	MS	Chi-sq	Prob>Chi-sq
Groups	30.393	2	15.1964	2	0.3672
Error	151.607	10	15.1607		
Total	182	12			

Slope Layer 2&3 T5 ON

Source	SS	dF	MS	Chi-sq	Prob>Chi-sq
Groups	2.976	2	1.4881	0.23	0.8918
Error	140.024	9	15.5582		
Total	143	11			

Table 7 *Statistical summary of multi comparisons with Bonferroni correction. Sample Size (N) is given in number of cells (C) or flies (F).*

Fig. 3				**G1: Control** (grey)			**G2: C2 block** (purple)			**G3: C3 block** (green)		
	p-value G1-G2	p-value G1-G3	p-value G2-G3	Mean	Std	N	Mean	Std	N	Mean	Std	N
Peak amplitude T4 ON (f)	0.04414	0.20788	1	0.0050	0.0029	29 C	0.0033	0.0019	16 C	0.0037	0.0019	26 C
Peak amplitude T5 ON (f)	0.08749	1	0.1039	0.0050	0.0024	6C	0.0050	0.0024	14 C	0.0054	0.0033	5C
Peak amplitude T4 OFF (f)	0.00307	1	0.0041	0.0043	0.0023	29 C	0.0079	0.0036	16 C	0.0045	0.0024	26 C
Peak amplitude T5 OFF (f)	0.6904	1	0.1078	0.0094	0.0038	6C	0.0074	0.0063	14 C	0.0136	0.0076	5C
HWHM major T4 ON	0.36603	0.69035	1	18.451	19.0	29 C	18.880	28.2	16 C	12.008	12.1	26 C
HWHM major T5 ON (f)	0.71385	1	1	31.437	21.9	6C	21.516	16.6	14 C	21.539	20.7	5C
HWHM major T4 OFF (f)	0.00005	0.86526	0.0029	21.862	19.6	29 C	6.093	3.03	16 C	16.804	14.8	26 C
HWHM major T5 OFF (f)	1	0.83438	1	8.6434	4.04	6C	8.8525	2.09	14 C	8.3158	5.24	5C
HWHM minor T4 ON (f)	1	1	1	3.0726	4.38	29 C	3.1608	3.58	16 C	2.2373	1.20	26 C
HWHM minor T5 ON (f)	1	0.67689	0.9815	2.4164	1.17	6C	2.2316	0.87	14 C	1.6506	0.93	5C
HWHM minor T4 OFF (f)	1	0.41408	0.8865	2.3314	0.87	29 C	2.5014	1.53	16 C	2.0424	1.53	26 C
HWHM minor T5 OFF (f)	0.75417	0.00205	0.0122	3.2766	1.00	6C	3.2766	0.39	14 C	1.5815	0.39	5C
Time to peak T4 ON (f)	1	0.0522	0.3161	-0.275	0.44	29 C	-0.266	0.30	16 C	-0.541	0.53	26 C
Time to peak T5 ON (f)	1	1	1	-0.577	0.26	6C	-0.702	0.38	14 C	-0.602	0.29	5C
Time to peak T4 OFF (f)	0.45985	0.49823	0.0299	-0.312	0.31	29 C	-0.149	0.04	16 C	-0.489	0.50	26 C
Time to peak T5 OFF (f)	1	0.7030	0.1049	-0.095	0.13	6C	-0.043	0.08	14 C	-0.164	0.08	5C
Slope Layer1&4 T4 OFF (f)	1	0.38495	1	-0.173	0.56	21 C	0.4428	1.46	9C	0.0475	0.30	15 C
Slope Layer1&4 T5 ON (f)	1	0.47706	1	-0.125	0.07	4C	-32.98	87.3	7C	-0.05	0.01	2C
Slope Layer2&3 T4 OFF (f)	0.63933	0.36518	0.0144	-0.145	0.47	8C	1.556	4.00	7C	0.1293	0.22	11 C
Slope Layer2&3 T5 ON (f)	1	1	1	0.0404	0.06	2C	-0.002	0.07	7C	0.042	0.04	3C

Supplmentary Fig. 4				**G1: Control** (grey)			**G2: C2 block** (purple)			**G3: C3 block** (green)		
	p-value G1-G2	p-value G1-G3	p-value G2-G3	Mean	Std	N	Mean	Std	N	Mean	Std	N
R2- goodness of gauss fit T4 (b)	0.39505	0.66545	-	0.5242	0.10	29 C	0.4661	0.11	16 C	0.5564	0.11	26 C
R2- goodness of gauss fit T5 (b)	1	1	-	0.5915	0.13	6F	0.6283	0.13	14 F	0.6440	0.19	5F

Direction tuning T4 and T5

Table 8 *Statistical summary of ANOVA*

DS (vector length) all layers: multiway analysis ANOVAN

Source	SS	dF	MS	F	Prob>F
Conditions	2.17782	3	0.72594	60.18	0
Layer	0.13956	3	0.04652	3.86	0.0104
T4/T5	0.02321	1	0.02321	1.92	0.167
Error	2.34025	194	0.01206		
Total	4.67595	201			

DS (vector length) averaged across layers T4

Source	SS	dF	MS	F	Prob>F
Groups	0.43445	3	0.14482	29.78	2.93772e-08
Error	0.11671	24	0.00486		
Total	0.55116	27			

DS (vector length) averaged across layers T5

Source	SS	dF	MS	F	Prob>F
Groups	827.81	3	275.937	13.14	0.0043
Error	810.19	23	35.226		
Total	1638	26			

Table 9 *Statistical summary of multi comparisons with Bonferroni correction. Sample Size (N) is given in number of cells (C) or flies (F).*

Fig.4				**G1: Control** (grey)			**G2: C2block** (purple)			**G2: C3 block** (green)			**G2: C2C3 block** (blue)		
	p-val G1-G2	p-val G1-G3	p-val G1-G4	Mean	Std	N	Mean	Std	N	Mean	Std	N	Mean	Std	N
DS T4 (b)	0.00000	0.00028	0.00000	0.5165	0.08	7F	0.2517	0.08	8F	0.3245	0.05	6F	0.1852	0.03	7F
DS T5 (b)	0.0244	0.1894	0.0001	0.4880	0.08	7F	0.3463	0.08	7F	0.3822	0.10	6F	0.2495	0.06	7F
dF/F -180AD T4 (c)	0.1292	0.0249	0.2850	0.6751	0.44	7F	1.4116	0.70	8F	1.4518	0.43	6F	1.1939	0.22	7F
dF/F -135AD T4 (c)	0.1130	0.0974	0.2255	0.6233	0.40	7F	1.2933	0.65	8F	1.2765	0.45	6F	1.1196	0.30	7F
dF/F -90AD T4 (c)	0.2515	0.1219	0.3842	0.7187	0.42	7F	1.3122	0.55	8F	1.4167	0.54	6F	1.2521	0.45	7F
dF/F -45AD T4 (c)	1	1	1	2.2096	1.10	7F	2.1420	0.91	8F	3.1046	1.32	6F	1.7718	0.53	7F
dF/F 0AD T4 (c)	1	0.5452	1	3.8594	1.93	7F	4.0212	1.86	8F	5.3724	1.66	6F	2.7353	0.82	7F
dF/F 45AD T4 (c)	1	0.3177	1	2.1960	1.22	7F	2.2547	1.11	8F	3.3790	1.15	6F	1.7469	0.44	7F
dF/F 90AD T4 (c)	0.4993	0.1437	0.2850	0.7076	0.48	7F	1.3867	0.75	8F	1.6395	0.79	6F	1.3073	0.36	7F
dF/F 135AD T4 (c)	0.1143	0.0708	0.3842	0.6250	0.42	7F	1.3499	0.71	8F	1.4048	0.56	6F	1.1209	0.31	7F
dF/F -180AD T5 (c)	0.0401	0.6768	0.0010	0.6593	0.45	7F	1.2500	0.34	8F	1.0113	0.35	6F	1.5759	0.38	7F
dF/F -135AD T5 (c)	0.0749	0.6488	0.0104	0.6537	0.43	7F	1.1803	0.34	8F	1.0035	0.36	6F	1.3635	0.35	7F
dF/F -90AD T5 (c)	0.2801	1	0.0276	0.8763	0.55	7F	1.3589	0.48	8F	1.1756	0.30	6F	1.6191	0.35	7F
dF/F -45AD T5 (c)	1	1	1	2.0625	1.19	7F	2.4539	0.96	8F	2.5859	0.88	6F	2.7355	0.94	7F
dF/F 0AD T5 (c)	0.8391	1	1	3.2665	1.45	7F	4.2833	1.37	8F	4.1690	1.27	6F	3.7727	0.97	7F
dF/F 45AD T5 (c)	0.8175	1	1	1.9791	1.00	7F	2.7670	1.02	8F	2.6985	1.32	6F	2.2519	0.45	7F
dF/F 90AD T5 (c)	1	1	0.8102	0.8989	0.68	7F	1.4130	0.54	8F	1.2793	0.78	6F	1.4200	0.30	7F
dF/F 135AD T5 (c)	0.1324	0.8234	0.0030	0.6688	0.45	7F	1.1418	0.29	8F	0.9882	0.31	6F	1.4702	0.41	7F

Supplmentary Fig. 5				**G1: Control** (grey)			**G2: C2block** (purple)			**G2: C3 block** (green)			**G2: C2C3 block** (blue)		
	p-val G1-G2	p-val G1-G3	p-val G1-G4	Mean	Std	N	Mean	Std	N	Mean	Std	N	Mean	Std	N
DS Layer 1 T4 (b)	0.2761	1	0.0112	0.4743	0.18	7F	0.2762	0.10	8F	0.3346	0.08	6F	0.2135	0.05	6F
DS Layer 1 T5 (b)	0.5212	1	0.0058	0.4786	0.12	7F	0.3510	0.07	7F	0.3923	0.11	6F	0.2220	0.09	7F
DS Layer 2 T4 (b)	0.0838	1	0.0147	0.4587	0.14	7F	0.2411	0.13	8F	0.3886	0.12	6F	0.1869	0.06	6F
DS Layer 2 T5 (b)	0.0346	0.2933	0.0058	0.4909	0.12	7F	0.3230	0.07	7F	0.3695	0.11	6F	0.2873	0.09	7F
DS Layer 3 T4 (b)	0.0550	1	0.0064	0.5411	0.09	7F	0.3467	0.11	6F	0.4763	0.10	5F	0.2427	0.10	5F
DS Layer 3 T5 (b)	0.0825	0.9529	0.0159	0.5393	0.09	5F	0.3598	0.09	7F	0.4398	0.12	6F	0.3188	0.08	6F
DS Layer 4 T4 (b)	0.0631	1	0.0002	0.5944	0.12	7F	0.3051	0.11	6F	0.4207	0.07	5F	0.1721	0.10	7F
DS Layer 4 T5 (b)	0.3688	0.3864	0.0178	0.5127	0.13	7F	0.3291	0.17	6F	0.3286	0.14	5F	0.2339	0.09	6F

Response properties of Mi1 and L2 cells

Table 10 *Statistical summary of Wilcoxon rank sum test. Sample Size (N) is given in number of cells (C)*

Fig.6		**Group 1: Control** (gray)			**Group 2: C2 block** (purple)		
	p-value G1-G2	Mean	Std	N	Mean	Std	N
Timing ON peak Mi1 (b)	0.0000	-0.113	0.15	59C	-0.195	0.23	73C
FWHM Mi1 (b)	0.8332	16.366	5.65	59C	15.447	5.01	73C
Timing OFF peak L2 (b)	0.0119	-0.136	0.22	68C	-0.140	0.22	36C
FWHM L2 (b)	0.8994	24.808	44.4	68C	16.414	9.65	36C

DATA AND SOFTWARE AVAILABILITY

Correspondance and requests for materials should be addressed to Marion Silies (msilies@uni- mainz.de)

References

References of this manuscripts can be found in the reference list at the end of this thesis.

Supplemental Information

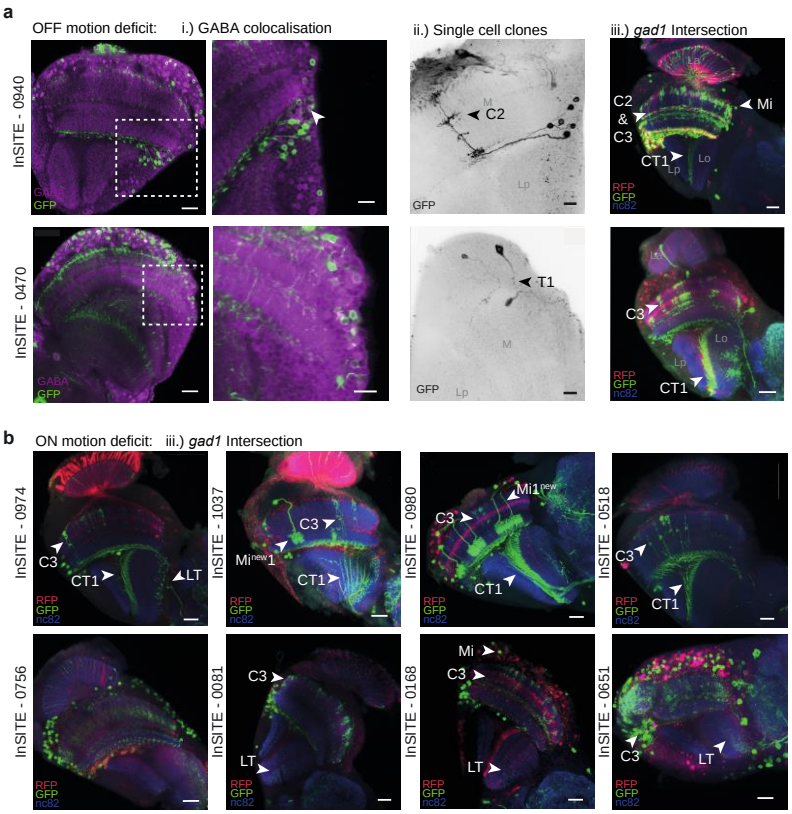

Supplementary Fig. 1. **Screen for behaviorally relevant GABAergic neurons. a)** Two more examples of InSITE lines with behavioral deficits to OFF motion stimuli screened for GABA (purple) colocalization with the InSITE expression pattern labeled with GFP (green) (I, scale bar = 20µm, 10µm), single cell clones (ii, scale bar = 10µm) and the gad1 intersection pattern (iii, scale bar = 20µm), where the neuropil is marked with nc82 (blue), the InSITE expression pattern is marked with RFP (red) and the GABAergic neurons are additionally labeled with GFP (green). **b)** Examples of InSITE lines with behavioral deficits to ON motion stimuli screened for neurons within the gad1 intersection pattern (scale bar = 20µm).

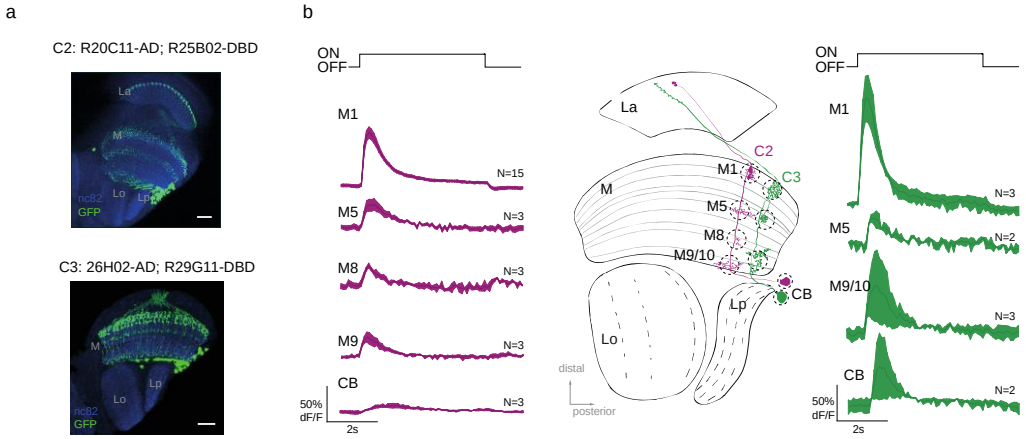

Supplementary Fig. 2. C2 and C3 responses are weaker in proximal medulla layers. a) Confocal image of C2 and C3 split gal4 driver lines expressing GFP (green). The neuropil is marked with nc82 (blue). **b)** Calcium responses of C2 (purple, N=16 flies, 181 cells) and C3 (green, N=12 flies, 149 cells) neurons in different medulla layers M1, M5, M8, M9 and the cell bodies (CB) to full field ON and OFF flashes.

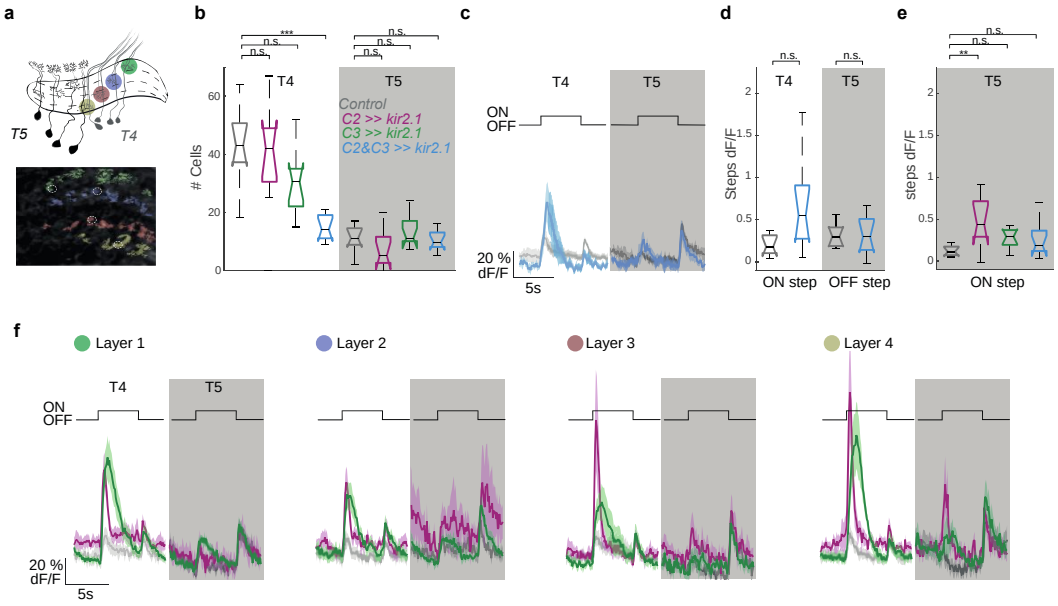

Supplementary Fig. 3. C2 and C3 silencing specifically shape ON responses of T4 and T5 neurons from different lobula plate layers a) ROIs of single T4 and T5 axon terminals extracted mathematically from calcium imaging data. **b)** Number of ROIs (cells) extracted for all flies for control condition (grey, N=9 flies), C2 silencing (purple, N=9 flies), C3 silencing (green, N=10 flies) and C2/C3 double silencing (blue, N=10 flies). **c)** Calcium responses of T4 and T5 neurons to full field ON and OFF light flashes for C2/C3 double silencing. **d)** Response change of T4 neurons to the onset of light (ON step) and T5 neurons to the offset of light (OFF step) quantified from (c). **e)** Response change of T5 neurons to the onset of light (ON step). **f)** Calcium responses of T4 and T5 neurons extracted from different layer of the lobula plate to full field ON and OFF light flashes. Shown are mean ± standard error. Significances are based on ANOVA (p≤0.05 *, p≤0.01**, p≤0.001***, + Bonferroni correction for multiple testing).

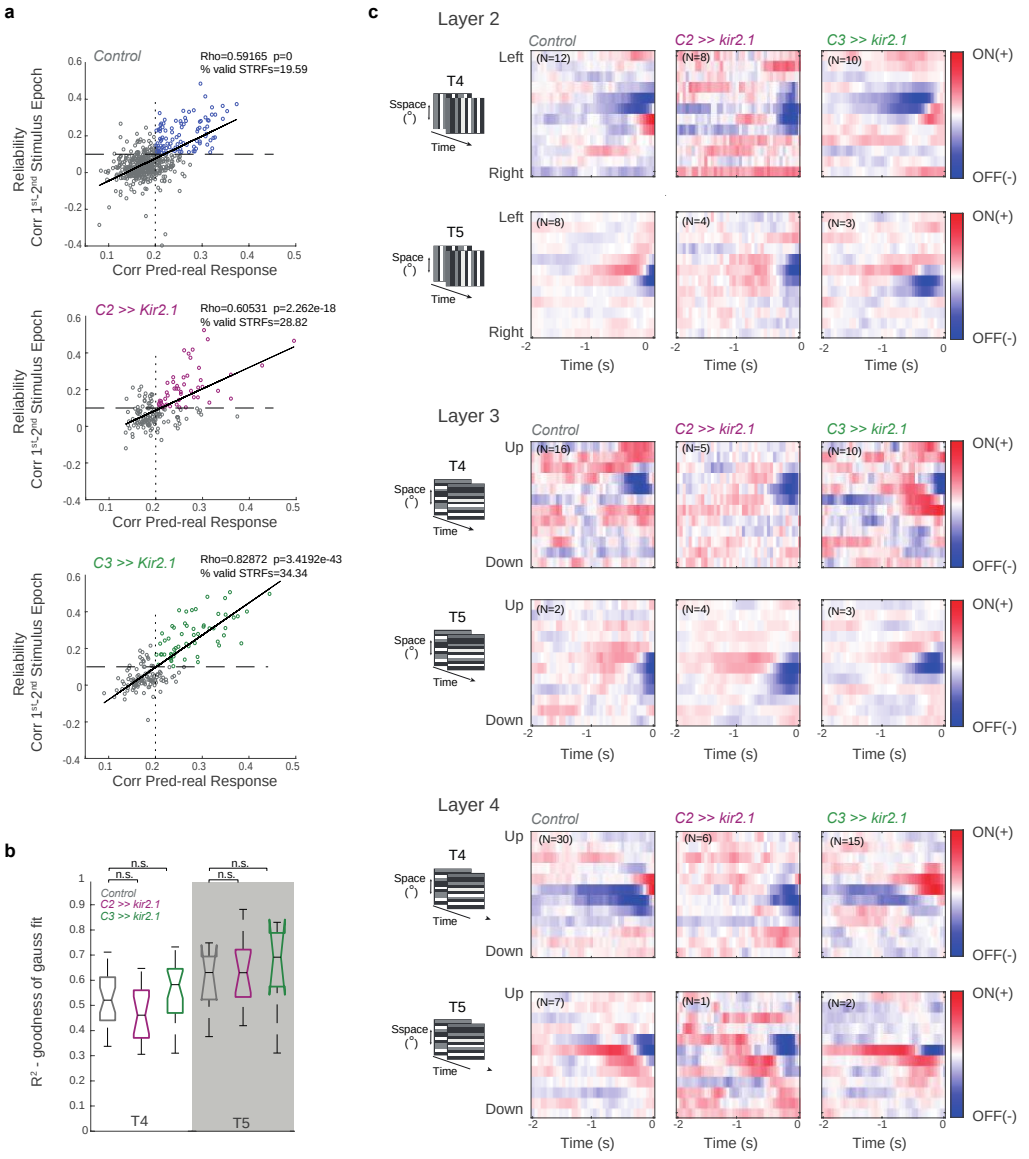

Supplementary Fig. 4. Effect of C2 and C3 silencing on T4/T5 filter properties is not layer specific a) Spatiotemporal receptive fields (STRFs) of T4 and T5 cells were extracted by reverse correlation of responses to a ternary white noise bar stimulus of vertical or horizontal orientation. Good quality STRFs (colored circles) were filtered based on the correlation of the predicted and the real response of the cell (x-axis) and a correlation of responses to the first and the second repetition of the stimulus (y-axis). **b)** R^2 values of fitting difference of Gaussians (DoGs) on extracted STRFs for T4 and T5 cells. Sample size refers to number of cells with N=29 for T4 Control, N=16 for T4 C2 silencing, N=26 for T4 C3 silencing condition and N=6 for T5 Control, N=14 for T5 C2 silencing, N=5 for T5 C3 silencing condition. Shown are mean ± standard error. Significances are based on KKW (p≤0.05 *, p≤0.01**, p≤0.001***, + Bonferroni correction for multiple testing). **c)** Average aligned spatiotemporal receptive fields (STRFs) of several T4 and T5 cells from layers 2, 3 and 4 of the lobula plate for the control, C2 silencing, and C3 silencing conditions. Sample size (N) equals number of cells.

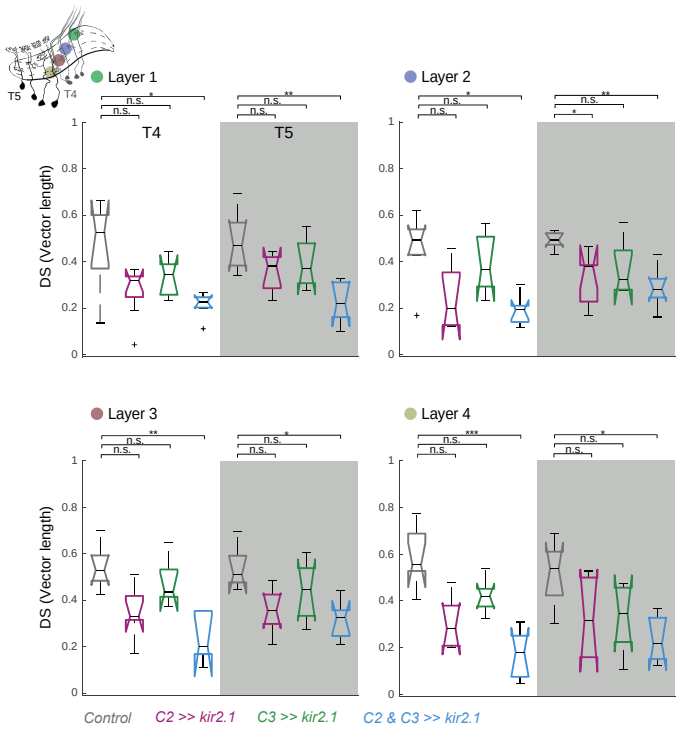

Supplementary Fig. 5. C2 and C3 are required for direction-selective responses of T4 and T5 cells from all lobula plate layer. Direction selectivity averaged across cells and flies, for different layer of the lobula plate. Control condition (grey, N=7 flies), C2 silencing (purple, N=8), C3 silencing (green, N=6 flies) and double C2/C3 silencing (blue, N=7). Significances are based on KKW (p≤0.05 *, p≤0.01**, p≤0.001***, + Bonferroni correction for multiple testing).

Supplementary Table 1. *List of behaviourally relevant neurons identified from the expression pattern of InSITE lines with behavioural deficits to either OFF- or ON edge motion stimuli. Neurons were identified based on either colocalization of the InSITE expression pattern with GABA and single cell Flp-Out experiments, or a Gad1-intersection strategy.*

INSITE OFF-motion deficit	GABA coloc/Flp-Out **GABA pos**	**– GABA neg**	Gad1-intersection	Figure
0787	C2	Tm9	C2, (CT1)	Fig. 1 b-d
0564	C2		C2, (C3,CT1)	Fig. 1 b-d
0301	C2		C2, Mi	Fig. 1 b-d
0940	C2		C2,(C3,CT1),Mi	Suppl. Fig 1a
0470		T1, TM4	(C3, CT1)	Suppl. Fig 1a
0396	C2 (no Flp-Out clone found)	T1, L4, Tm2		(not shown)
0096		Tm9	-	(not shown)

INSITE ON-motion deficit	GABA coloc/Flp-Out **GABA pos**	**– GABA neg**	Gad1-intersection	
0619	-	-	C2, (C3, CT1)	Fig. 1 e
0913	-	-	C2, (C3, CT1)	Fig. 1 e
0669	-	-	C2, (C3, CT1)	Fig. 1 e
0974	-	-	(C3, CT1), LT	Suppl. Fig 1b

1037	-	-	Mi1^{new}, (C3, CT1)	Suppl. Fig 1b
0756	-	-	-	Suppl. Fig 1b
0518	-	-	(C3, CT1)	Suppl. Fig 1b
0980	-	-	Mi1^{new}, (C3, CT1)	Suppl. Fig 1b
0564	-	-	C2, (C3, CT1)	Suppl. Fig 1b
0081	-	-	(C3), LT	Suppl. Fig 1b
0168	-	-	(C3), Mi, LT	Suppl. Fig 1b
0651	-	-	(C3), LT	Suppl. Fig 1b

3.2 Populations of local direction-selective cells encode global motion patterns generated by self-motion

Manuscript in peer review:

The previous version of this manuscript was recently published on bioRxiv: https://doi.org/10.1101/2021.03.17.435642 with the title: 'An optimal population code for global motion estimation in local direction-selective cells.'

This manuscript is currently being peer-reviewed by Science Advances.

Miriam Henning, Giordano Ramos-Traslosheros, Burak Gür, Marion Silies

Author contributions:

Conceptualization: M.H and M.S
Methodology: M.H, G.R-T, B.G
Software: M.H, G.R-T, B.G
Investigation: M.H
Visualization: M.H, G.R-T
Supervision: M.S
Writing—original draft: M.H and M.S
Writing—review & editing: all authors
Funding acquisition: M.S

Giordano Ramos-Traslosheros coded the model (Fig. 4). Burak Gür helped with writing analysis code for the extraction of receptive field centers (Fig. 4). I performed all experiments, analyzed data, composed figures, and wrote a first draft of the manuscript with guidance by Marion Silies, which was finalized with input from all authors.

Science Advances
AAAS

Manuscript Template

FRONT MATTER

Populations of local direction-selective cells encode global motion patterns generated by self-motion

Miriam Henning[1,2], Giordano Ramos-Traslosheros[1,2], Burak Gür[1,2], Marion Silies[1*]

Affiliations

[1] Institute of Developmental Biology and Neurobiology, Johannes-Gutenberg University Mainz, 55128 Mainz, Germany.

[2] Göttingen Graduate School for Neurosciences, Biophysics, and Molecular Biosciences (GGNB) and International Max Planck Research School (IMPRS) for Neurosciences at the University of Göttingen, 37077 Göttingen, Germany

*Corresponding author. Email: msilies@uni-mainz.de

Abstract

Self-motion generates visual patterns on the eye that are important for navigation. These optic flow patterns are different in flying animals as compared to walking animals because of maneuvers in three dimensions during flight. Whether this difference is reflected in neural processing is unknown. We show that the population of local direction-selective T4/T5 cells in *Drosophila* encodes global motion patterns generated during flight, similar to a population code in the mouse retina. Whereas the retina encodes four types of optic flow, the fly visual system encodes six. This matches the larger number of degrees of freedom and the increased complexity of possible translational and rotational motion patterns during flight. The four uniformly tuned T4/T5 subtypes described previously represent a local subset of the population. Thus, a population code for global motion patterns appears to be a general coding principle of visual systems that matches the individual ethological constraints of the animal.

Teaser

Local direction-selective cells encode six types of global motion patterns, matching different types of motion generated by fly behavior.

MAIN TEXT

Introduction

Animals that use the visual system to navigate through their environment need to detect and compute global motion patterns elicited on the eye. Such optic flow patterns are generated by locomotion, such as during walking, riding, or flying, where different types of behavior will elicit different optic flow patterns. In vertebrates, such optic flow generated by self-motion is represented by the population of local motion-sensitive retinal ganglion cells (1). Here, directional tuning of retinal ganglion cells changes gradually across visual space, together matching four different types of global motion patterns generated during walking. Thus, the first direction-selective cells in the mammalian visual pathway employ a code for visual cues generated by self-motion. Flying animals are exposed to more complex optic flow fields, but how the additional degrees of freedom in behavior impact neuronal processing is not known.

In flies, the first direction-selective cells that encode local motion are the T4 and T5 neurons, that are sensitive to moving ON (T4) or OFF (T5) contrast signals. In contrast to the local direction selective ganglion cells of the vertebrate retina, T4/T5 neurons are thought to be uniformly tuned throughout the visual field, representing the four cardinal directions: upward, downward, front-to-back and back-to-front motion (2–4). These direction-selective T4/T5 cells compute local motion by comparing inputs from neighboring points in space along one axis (3–9). Neighboring columnar units in the fly visual system are organized in a hexagonal array (10), following the hexagonal arrangement of ommatidia in the fly eye. Yet how these hexagonal interactions can yield four orthogonal motion axes represented by T4/T5 is unknown.

One synapse downstream of T4/T5 cells, optic flow patterns are encoded by wide-field neurons that sample information globally across visual space (11–13). The general importance of this coding strategy is supported by the widespread presence of such flow-field sensitive cells, covering for instance moths (14–16), locusts (17–19) and dragonflies(20). In blow flies, different wide-field lobula plate tangential cells (LPTCs) are tuned to specific optic flow patterns generated by forward movement or turns of the animal (13, 21, 22). LPTCs with a similar receptive-field organization have been mapped in *Drosophila* (23–25), and are thought to be involved in the control of head optomotor responses, as well as in stabilizing gaze and forward walking (26–28).

To extract optic-flow information, wide-field neurons pool information from presynaptic local motion detectors. In *Drosophila*, this is achieved by LPTCs receiving strong input from the columnar T4 and T5 neurons (2, 29). Four T4/T5 subtypes can be distinguished by axonal projections terminating in one of four layers of the lobula plate. Here, T4/T5 provide excitatory input to downstream LPTCs within the same layer and indirect inhibitory input to LPTCs of the adjacent lobula plate layer with opposite tuning, thus establishing motion opponency (29, 30). Most LPTCs extend their dendrites along one layer of the lobula plate and thus pool information from one subtype of T4/T5 neurons (23, 24, 31), although some LPTCs also project to more than one layer (25). Additionally, local motion signals are selectively amplified within the LPTC dendrites if they match the preferred global motion pattern (32). This suggests that the coding of optic flow is fundamentally different between vertebrate and invertebrate visual systems. It is unclear why flies would have evolved a system in which optic flow has to be computed through complex transformations from local motion detectors with uniform tuning, to ultimately match the motion patterns generated during flight. To understand how the four subtypes contribute to downstream optic flow fields, it is necessary to have a detailed map of T4/T5 direction tuning across retinotopic space.

Here, we use *in vivo* two-photon calcium imaging to characterize the direction tuning distribution of T4/T5 neurons across anatomical and visual space. We demonstrate that directional preference of T4/T5 subtypes changes gradually, forming continuous maps of tuning. At the population level, T4/T5 cells in fact do not fall into four but six subgroups that encode six diagonal directions of motion, matching the hexagonal lattice of the eye. The six topographic tuning maps match optic flows field generated by self-motion of the fly. Therefore, the organization of local direction-selective cells that represents self-motion parallels the retinal code for optic flow, providing a striking example of convergent evolution. The specific types of optic flow that are encoded differ between the mouse retina and the *Drosophila* visual system, arguing that evolution matched neural resources to the different physical distribution of information encountered during walking or flight.

Results

T4/T5 population tuning clusters around hexagonal directions of motion

To understand how the T4/T5 neurons contribute to downstream optic flow fields, it is necessary to have a detailed map of T4/T5 direction tuning across retinotopic space. We used *in vivo* two-photon calcium imaging to record motion responses from large populations of T4/T5 neurons in individual flies. We imaged GCaMP6f responses to ON and OFF edges moving in eight directions at different fly orientations relative to the screen, together subtending ~150° in azimuth and ~60° in elevation (**fig. S1, A and B**). Tuning across 3537 individual cells (1376 T4, 2161 T5), recorded in 14 flies was broad, together spanning 360º of motion. Neurons in both layer A and B covered more than 120° of tuning direction, and thus twice the range of cells in layers C and D, which were tuned to a range of ~60° (**Fig. 1A**). Dorsoventral location strongly impacted tuning direction in layers A and B (**Fig. 1A**). In layer A, cells that were more dorsally located in the lobula plate preferentially covered the 300°- 360° range, whereas more ventral cells of the lobula plate showed tuning directions in the 0°- 60° range. In layer B, more dorsally located cells were tuned to the 120°- 180° range, and more ventrally located cells were tuned to 180°- 240° (**Fig. 1A**). Although the population of T4/T5 cells covered all directions of motion, the tuning distribution was non-uniform (*Circular Rayleigh test*: $p<0.0001$).

Looking at the number of neurons sensitive to a certain motion direction, most neurons in layers A and B were tuned to the diagonal directions of motion, flanking the overall average orthogonal tuning of these layers (**Fig. 1B**). Cells in layers C and D each showed a unimodal directional tuning distribution in the upward or downward direction, respectively (**Fig. 1B**). The bimodal distribution in layers A and B were well fit by two Gaussians (**fig. S1C**). When thus assigning each cell to one of six subtypes, tuning of two subtypes in layer A and B split at 0° or 180°, respectively (**fig. S1D**). The population average of the A.I subtypes was tuned to diagonal upward motion (~30°) and the A.II subtype was tuned to diagonal downward motion (~330°). Layer B subtypes encoded the two opposite axes of motion direction (**fig. S1D**). Taken together, our data show that at the population level, T4/T5 neurons fall into six functional subtypes (**Fig. 1C** and **fig. S1D**) Average motion tuning within individual subtypes reveals sensitivity to six directions with each subtype spanning a 60°-range, matching the hexagonal arrangement of the fly compound eye (**Fig. 1**, **C and D**).

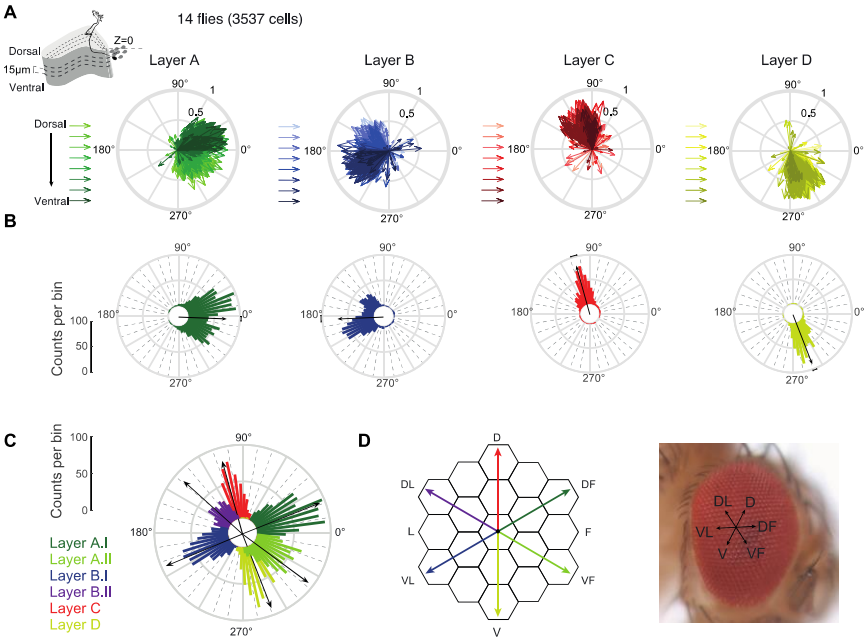

Fig. 1. Directional tuning clusters around hexagonal directions of motion. (**A**) Directional tuning of individual neurons from 3537 cells (Layer A: 479/926 T4/T5. Layer B: 252/662 T4/T5. Layer C: 365/220 T4/T5. Layer D: 280/353 T4/T5) in 14 flies. Motion responses were represented by a vector(33), whose direction depicts tuning, whereas its length indicates selectivity. Hue illustrates z-depth relative to a reference (the outermost T4/T5 cell bodies). (**B** and **C**) Circular histograms of neuronal tuning preference. Black vectors depict average tuning per layer (B) or subtype (C). (**D**) On average, tuning of the six subtypes matches the hexagonal arrangement of the fly eye.

To understand the spatial organization of six T4/T5 subtypes projecting to four anatomically distinguishable lobula plate layers, we plotted cellular subtype identity back onto the anatomical structure of the lobula plate (**Fig. 2A** and **fig. S2**). T4/T5 cells of one subtype dominated one lobula plate layer recorded in one plane along the dorsoventral axis. At more ventral planes, subtype A.I and B.I as well as the single respective subtypes of layers C and D were found more frequently. Dorsal planes more prominently housed subtypes A.II and B.II, but hardly showed any layer C or D cell responses (**Fig. 2, A and B** and **fig. S2**). This argues for a spatial separation of layer A and B subtypes at the level of T4/T5 axon terminals. Importantly, local T4/T5 recordings in an individual fly preferentially showed either four subtypes (as e.g. described in(2, 3)), or two subtypes, each representing snapshots of the T4/T5 population (**Fig. 2, A to D**). Only a global analysis of tuning revealed the six T4/T5 subtypes encoding six diagonal directions of motion (**Fig. 2e**).

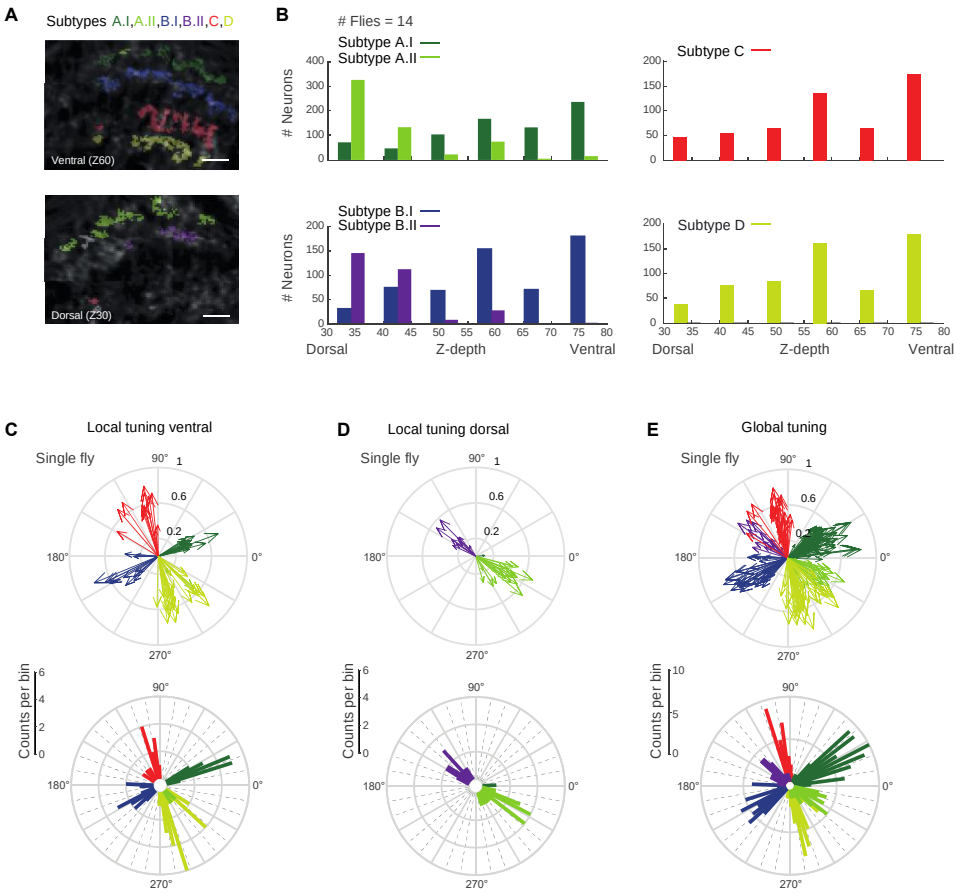

Fig. 2. Layer A and B subtype projections separate along the dorsoventral axis. (**A**) *In vivo* two photon calcium images of the lobula plate at two planes along the dorsoventral axis (Z30/Z60 = z-depth 30/60 ∝m). ROIs are color coded based on their subtype identity. (**B**) Histograms displaying number of neurons from the different classes along the dorsoventral axis (z-depth). Scale bar 10 µm. (**C** and **D**) Tuning of individual neurons from one fly recorded in a ventral (Z60) (C), or dorsal (Z30) (D) plane of the lobula plate. Below: Same data plotted as circular histograms. (**E**) Tuning of all neurons recorded at different dorsoventral planes within one fly.

T4/T5 neurons form topographic maps of directional tuning

We next asked if the ~60º distribution of directional tuning within one subtype was random, or topographically organized. Color coding axon terminals based on their directional preference revealed that the tuning of neighboring cells was similar and gradually changed along the distal-to-proximal axis. As such, recording in one ventral plane of layer A (group A.I) revealed T4/T5 tuning ranging from diagonally upward on the proximal end to front-to-back motion on the distal end of the lobula plate (**Fig. 3, A and B**). T4/T5 cells of other subtypes also gradually changed tuning from proximal to distal. Subtler changes in the tuning of neighboring cells within one subtype were also apparent along the dorsoventral axis (**fig. S3, A and B**). This gradually distributed tuning existed for both T4 and T5 when analyzed separately (**Fig. 3, C and D** and **fig. S3C**). Because T4/T5 neurons are retinotopically organized, this directional tuning map suggests that the population of T4/T5 cells is sensitive to specific global motion patterns.

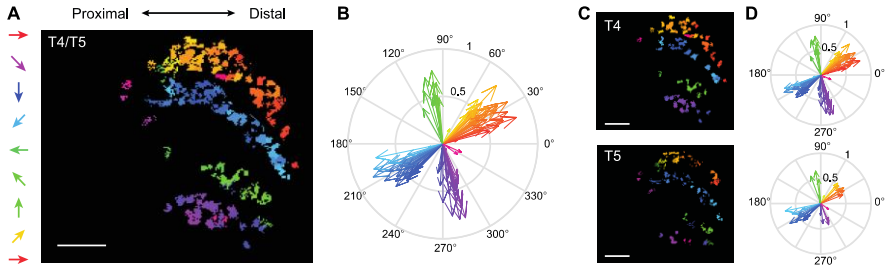

Fig. 3. T4/T5 neurons form topographic maps of directional tuning. (**A**) Image of one layer of the lobula plate with ROIs color coded according to their directional tuning. (**B**) Data from (A) shown in vector space. (**C** and **D**) Data shown separately for T4 and T5 neurons. Scale bar = 10 μm.

The six T4/T5 subtypes encode optic flow induced by self-motion

The local differences in the tuning preference within one T4/T5 subtype are reminiscent of direction-selective ganglion cells in the vertebrate retina, where the population of cells encodes translational optic flow generated by self-motion of the animal(1). We hypothesized that the differential tuning measured within each subtype of T4/T5 cells in the fly visual system serves a similar function. To relate tuning to the visual input, we mapped receptive-field centers (**fig. S4, A and B**) and plotted tuning at each receptive-field location on the screen (**fig. S4, C and D**). This revealed that cells of one subtype do not encode a uniform direction of motion, but rather that direction tuning of all cells within one subtype change gradually across visual space (**Fig. 4A** and **fig. S4E**). These topographic tuning maps resemble flow fields generated by different directions of self-motion in the fly. T4/T5 neurons in layers C and D appear to encode optic flow generated by downward or upward movement of the fly, whereas T4/T5 neurons in layers A and B seem to be tuned to diagonally upward or downward motion. The two flow fields encoded by the two subtypes of layers A or B are vertically flipped versions of each other (**Fig. 4A**). The successive change of tuning along azimuth and elevation matches the change of tuning seen in the topographic maps in the lobula plate (**Fig. 4A**, **Fig. 3**, and **fig. S4, E and F**).

To investigate the type of self-motion encoded by the different subtypes, we trained an optic flow model (34) to match the population receptive fields of T4/T5 neurons. We fitted the parameters for the three axes of motion for both translation (Tx,Ty,Tz) and rotation (Rx,Ry,Rz) (**Fig. 4B**). Although the population data did not fully cover the visual field of one eye (**fig. S5A**), optic flow fields were well-matched filters for each of the six T4/T5 subtypes (**Fig. 4C** and **fig. S5B**). We compared performance including models where the fly only turned (rotational optic flow) or moved straight (translational optic flow). Across the six subtypes, only the model combining rotations and translations outperformed the null model consisting of a uniform vector field, with larger performance in layers A.I, B.II, C and layer D (**Fig. 4D** and **fig. S4C**). Thus, T4/T5 subtypes are tuned to optic flow generated by mixtures of translational and rotational motion. For each T4/T5 subtype, a single component tended to dominate the translational axis of motion, whereas the rotational axis was more distributed across the three components (**Fig. 4C** and **fig. S5A**). Together, our data show that local direction-selective T4/T5 neurons display a population code for different types of self-motion of the fly. Populations of T4/T5 cells are tuned to optic flow patterns, similar to their vertebrate counterparts(1), but representing six instead of four types of self-motion.

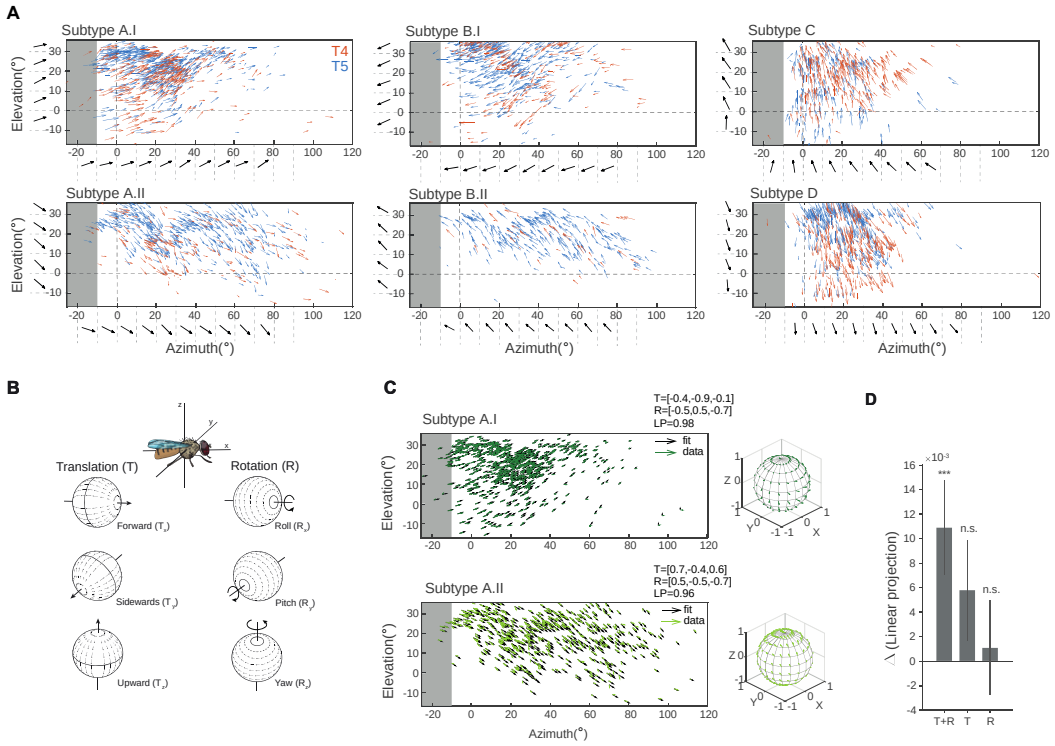

Fig. 4. The population of T4/T5 neurons encode optic flow induced by self-motion. (**A**) Arrows indicate tuning direction of individual neurons plotted at their receptive field center coordinates in visual space. Length of vectors indicates direction selectivity of T4 (red) or T5 neurons (blue), n=14 flies. Horizontal and vertical dashed lines mark the split between left and right visual hemispheres and the horizon, respectively. Black tuning vectors show mean across 10 degree-wide bins. Gray shaded areas indicate the visual space in the left hemisphere that cannot be seen by the right eye. (**B**) Schematic of rotational and translational flow fields around the three body axes of the fly (modified after(35)). (**C**) Flow fields of data from two subtypes and the fitted normalized optic-flow model. Model vectors are shown for each corresponding data vector. (**D**) Differences of the fit quality for three model types (translation + rotation [T+R], pure translation [T], pure rotation [R]) compared to a uniform vector field model (***Wilcoxon: $p<0.001$).

Discussion

In this study, we have demonstrated that optic flow is encoded by the local motion detectors in the *Drosophila* visual system: The direction-selective T4/T5 neurons are divided into six subtypes that encode specific optic flow pattern. Anatomically, these six direction match the hexagonal arrangement of the fly compound eye. Within each of the six subtypes, individual tuning preference is gradually distributed across the lobula plate such that the population of T4/T5 neurons of each subtype together forms a retinotopic tuning map that encodes flow fields containing information about translational and rotational self-motion of the fly.

Direction-selective T4/T5 neurons in *Drosophila* have been described to encode four cardinal directions of motion (2, 3). Population T4/T5 recordings now reveal average tuning to diagonal rather than cardinal motion directions, such that six subtypes of T4/T5 neurons exist. Only a global analysis of directional tuning reveals these six subtypes, but tuning to diagonal motion has been observed in electrophysiological recordings of an individual T4 neuron (8), and in optical recordings of T4/T5 (3, 36). T4/T5 neurons compute direction-selective signals across neighboring columns within the eye (5, 37). Thus, motion can simply be computed along the internal

organization of the fly eye, and the hexagonal arrangement of the eye does not need to be transformed into a cardinal coordinate system.

Individual directional preference of a T4/T5 neuron correlates with its dendrite orientation, which manifests during development (10, 38, 39). Interestingly, developmental dendrite orientation for subtypes A and B reveal two peaks of diagonal rather than orthogonal orientation of dendrites (39), consistent with their distribution of direction selectivity. Our data show that each T4/T5 subtype retinotopically covers overlapping regions in visual space. A comprehensive analysis of T4/T5 dendrite anatomy across the visual system will be needed to clarify how adult dendrite orientation is distributed across the visual system to represent the six subtypes. Furthermore, single-cell transcriptomics has assigned developing T4/T5 cells to distinct clusters based on their genetic profiles (39–42), but genes involved in dendrite development or the differentiation are expressed in narrow time windows (42). Interestingly, one recent study identified a genetic subpopulation of T4 neurons, restricted to lobula plate layers A and B (40). While it remains to be determined whether this corresponds to the functional layer A/B subtypes, genetic access will help to better understand the development and anatomy of the individual subtypes.

While downstream of T4/T5, wide-field LPTCs are thought to encode self-motion (21, 24), our data show that the population of T4/T5 cells already encodes optic flow generated by a combination of rotational and translational self-motion of the fly. Within an optic flow field, single T4/T5 tuning changes along the retinotopic map. This could be inherited by the spatial distribution of ommatidia along the optical axis which varies with the curvature of the eye (43, 44). T4/T5 can then pass this information to downstream LPTCs, which do to not need to transform cardinal motion information into complex flow fields. Therefore, T4/T5 population tuning might be organized to encode optic flow in a way that facilitates downstream processing of diverse complex flow fields represented by a repertoire of LPTCs. Further internal dendritic processing, such as suppression of adjacent local motion signals, electrical coupling between LPTCs (24) and feedforward inhibition from lobula plate intrinsic neurons (30) will support the computation of diverse optic flow fields (29, 30, 32).

The encoding of optic flow generated by self-motion at the level of local motion detectors has also recently been described in the mouse retina (1), where any kind of self-motion will activate different retinal ganglion cell types from both eyes in a unique pattern that will be decomposed into translational and rotational components further downstream. The fly eye and the vertebrate retina both show differences between local and global directional tuning (1, 45), and similarly compute visual signals generated by self-motion at the population level (1). A population code for optic flow generated by self-motion might therefore be a canonical strategy of visual systems, and evolved convergently during evolution. However, mice and flies differ in the number and directions of optic flow encoded by local direction-selective cells. Flying animals encode more motion axes than walking animals, likely to match the higher degrees of freedom encountered during flight. This difference might highlight adaptation to the visuoecological niches of flying and walking animals. We are just starting to understand how a population code in visual systems matches the statistics of the visual environment (1, 46–49), or animal behavior. Thus, this work is an important step towards understanding how anatomy, ethological constraints, and neuronal function are ultimately linked.

Materials and Methods

Drosophila strains and fly husbandry

Drosophila melanogaster were raised on molasses-based food at 25°C and 55% humidity in a 12:12 hr light-dark cycle. For all imaging experiments female flies of the genotype w^{+}; *R59E08-LexA^{attP40}, lexAop-GCaMP6f-p10$^{su(Hw)attp5}$/ R59E08-LexA^{attP40}, lexAop-GCaMP6f-p10$^{su(Hw)attp5}$* were recorded 3-5 days after eclosion at room temperature (RT, 20°C). *R59E08-LexA^{attP40}* and *lexAop-GCaMP6f-p10$^{su(Hw)attp5}$* were obtained from the Bloomington Drosophila Stock Center (BDSC #52832 and #44277), recombined, and crossed into a w^{+} background.

In vivo two-photon calcium imaging

Fly preparation, experimental setup and data acquisition

Prior to two-photon imaging, flies were anesthetized on ice and fit into a small hole in stainless-steel foil, located in a custom-made holder. The head was tilted approximately 30° to expose the back of the head. To fix the head of the fly, a small drop of UV-sensitive glue (Bondic) was used on the left side of the brain and the thorax. The cuticle on the right eye, fat bodies and tracheae were removed using breakable razor blades and forceps. To ensure constant nutrients and calcium supply flies were perfused with a carboxygenated saline containing 103 mM NaCl, 3 mM KCl, 5 mM TES, 1mM NaH_2PO_4, 4 mM $MgCl_2$ 1.5 mM $CaCl_2$, 10mM trehalose, 10mM glucose, 7mM sucrose, and 26mM $NaHCO_3$ (pH~7.3). To record calcium activity, a two-photon microscope (Bruker Investigator, Bruker, Madison, WI, USA), equipped with a 25x/1.1 objective (Nikon, Minato, Japan) was used. For excitation of GCaMP6f, the excitation laser (Spectraphysics Insight DS+) was tuned to a wavelength of 920nm with <20mW of laser power measured at the objective. Emitted light was filtered through an SP680 short pass filter, a 560 lpxr dichroic filter and a 525/70 emission filter and detected by PMTs set to a gain of 855V. Imaging frames were acquired at a frame rate of ~15-20 Hz and 4-7 optical zoom using PrairieView software. Each fly was recorded in at least three to five different focal planes (z-depth). We determined z-depth position relative to cell bodies and started the first recording at a z-depth of 30μm from there. Planes were then imaged every 15μm from there (**fig. S1B**).

Visual stimulation

Visual stimuli were presented on an 8 cm x 8 cm rear projection screen in front of the fly covering a visual angle of 60° in azimuth and elevation. To cover a larger part of the horizontal visual field of 150° we rotated the fly with respect to the screen two times by 45° (**fig. S1A**). Stimuli were filtered through a 482/18 bandpass filter (Semrock) and ND1.0 neutral density filter (Thorlabs) and projected using a LightCrafter 4500 DLP (Texas Instruments, Texas, USA) with a frame rate of 100 Hz and synchronized with the recording of the microscope as described previously(50). All visual stimuli were generated using custom-written software using C++ and OpenGL.

Moving OFF and ON edges

Full-contrast dark or bright edges moving with a velocity of 20°/s across the full screen to four or eight different directions. Each stimulus direction was presented at least twice in pseudo-random order. The four-direction stimulus was merely used for the subsequent identification of T4 and T5 axon terminals.

Data analysis

Preprocessing

All data analysis was performed using MATLAB R2017a (The MathWorks Inc, Natrick, MA) or Python 2.7. Motion artifacts were corrected using Sequential Image Alignment SIMA, applying an extended Hidden Markov Model(51).

Automated ROI selection

For the extraction of single T4 or T5 axon terminals we made use of their contrast- and direction-selective responses to ON and OFF edges moving into four directions. First, the aligned images were averaged across time and the average image intensity was Gaussian filtered (s=1.5) and then threshold-selected by Otsu's method (52) to find foreground pixels suitable for further analysis. After averaging responses across stimulus repetitions, we selected pixels that showed a peak response larger than the average response plus two times the standard deviation of the full trace. These pixels were grouped based on their contrast preference (ON or OFF pixels) and further assigned to four categories based on their anatomical location within the lobula plate (layers A, B, C, or D). We further calculated a direction-selectivity index (DSI) and contrast selectivity index (CSI) for each pixel as follows:

$$DSI = \frac{PD_{max} - ND_{max}}{PD_{max}},$$
$$CSI = \frac{PC_{max} - NC_{max}}{PC_{max}}.$$

where PD_{max} and ND_{max} denote the maximal response into the preferred direction (PD) and null direction (ND) and PC_{max} and NC_{max} denote the maximum responses for the preferred contrast (PC) and the non-preferred or inverse contrast (NC). We excluded all pixels that did not exceed the CSI threshold of 0.2 to obtain clean T4 or T5 responses. For the final clustering we used the quantified DSI and CSI parameter and the timing of the response to the PD. Based on these parameters the Euclidean distance between each pair of pixels was calculated and average-linkage agglomerative hierarchical clustering was performed. We further evaluated the optimal distance threshold that yielded most clusters of the appropriate size between 1 and 2.5 μm^2. All resulting clusters that fell outside this range were excluded from further analysis. Custer locations were saved and matched with subsequent recordings of the same cells to other stimulus types.

Moving OFF and ON stripes

For dF/F calculation, baseline responses to ~ 0.5s gray epoch were used. To quantify direction selectivity (DS) of single cells, responses were trial averaged and the peak response to the eight different directions of either increment or decrement bars was extracted for T4 and T5 cells respectively. We further quantified the tuning of single cells by computing vector spaces as follows(33):

$$L_{dir} = \left| \frac{\sum_k R(\theta_k) \exp(i\theta_k)}{\sum_k R(\theta_k)} \right|.$$

where $R(\theta_k)$ is the response to angle θ_k. The direction of the vector L_{dir} denotes the tuning angle of the cell and the normalized length of the vector is related to the circular variance and thus represents the selectivity of the cell.

Receptive-field center extraction

To extract receptive-field centers, we used a back-propagation algorithm to map the receptive fields of T4 and T5 cells and to locate the center of the receptive fields(53). First, we imaged neural responses to eight different directions and created two-dimensional images from one-dimensional response traces. Neural latency and indicator dynamics introduce delays that will decrease the precision of receptive-field position estimation. To account for this delay, we measured the spatial difference of the response peaks between a static and a moving stimulus. We found an average of 9.6° delay for both T4 and T5 cells and shifted the traces for 9.6° before calculating the receptive-field map in our back-propagation algorithm (**fig. S4, A and B**). These were rotated according to their corresponding direction and averaged to obtain a receptive-field map. To find the center of the receptive field, we fitted a two-dimensional gaussian and took its peak coordinate.

Z-stack generation

Images representing the location of single ROIs color coded by their directional preference were generated in Matlab. Images containing data from different z-depth layers within the same fly were then further processed in Illustrator to create pseudo z-stacks. For this, ROIs from the same lobula plate layer were first compiled in a 3D structure and ROIs from different z-depth layers were stacked to better represent the third dimension of the lobula plate.

Statistics

All statistics were done in Matlab using Circular Statistics Toolbox(54).

SNOB analysis

To extract underlying classes from the population of neurons found in layers A and B, we converted data of each population to be linear in the range of directions that most neurons where selective to, resulting in a scale from - π to π for layer A, C and D and a scale from 0 to 2π for the data from layer B. We used the finite mixture model SNOB (55) to predict the number of underlying Gaussians using minimum message length criterion. We further used the statistical prediction from the model to assign individual neurons to each of the underlying classes by choosing the class with the highest probability of the neuron's tuning preference (**fig. S1, C and D**).

Model

We fitted an optic flow field elicited from self-motion on the field of view at a constant distance from the observer, i.e., a spherical surface. Two coordinates describe the viewing direction: the azimuth θ and the elevation ϕ angles.

The self-motion flow-field vectors $\vec{p}_i$ at each viewing location $\vec{d}_i$ on the unit sphere were specified by the translation and rotation vectors, $\vec{v}_T = (v_{Tx}, v_{Ty}, v_{Tz})$ and $\vec{v}_R = (v_{Rx}, v_{Ry}, v_{Rz})$, respectively (34):

$$\vec{p_i} = -(\vec{v}_T - (\vec{v}_T \cdot \vec{d}_i)\,\vec{d}_i) - \vec{v}_R \times \vec{d}_i$$

The flow-field vectors were then represented in spherical coordinates $\vec{p}_i = u_i\,\hat{e}_\theta + v_i\,\hat{e}_\phi + r\,\hat{e}_r$ to extract a vector tangential to the spherical surface $\vec{q_i} = (u_i, v_i)$ that could be matched to the direction-selectivity vectors from T4/T5 data. The uniform flow-field tangent to the spherical surface was specified by a single vector $\vec{v}_U = \vec{q_i} = (u, v)$ at every viewing position.

The comparison of data to model was done using the following *loss* function

$$\begin{aligned}\mathcal{L}(\{\vec{q}_{i,data}, \vec{q}_{i,model} | i \in [1, N]\}) &= \frac{\sum_{i=1}^{N} \vec{q}_{i,model} \cdot \vec{q}_{i,data}}{\sum_{i=1}^{N} || \vec{q}_{i,model} || \cdot || \vec{q}_{i,data} ||} \\ &= \frac{\sum_{i=1}^{N} || \vec{q}_{i,model} || \cdot || \vec{q}_{i,data} || \cos\eta_i}{\sum_{i=1}^{N} || \vec{q}_{i,model} || \cdot || \vec{q}_{i,data} ||}\end{aligned}$$

where η_i is the angle between the model and the data flow vectors at the location $\vec{d}_i$, for all N vectors in the dataset, and $||\cdot||$ indicates the magnitude of the vector. When all vectors match in both magnitude and direction this quantity is 1 and when all vectors match in magnitude but are in opposite directions this quantity is -1. To optimize for the vectors $\vec{v}_T = (v_{Tx}, v_{Ty}, v_{Tz})$ and $\vec{v}_R = (v_{Rx}, v_{Ry}, v_{Rz})$, and $\vec{v}_U = \vec{q_i} = (u, v)$ that maximize $\mathcal{L}$, the MATLAB function fmincon was used. The positive of the loss function is the linear projection (LP), shown in (**Fig. 4**, **C and D**) and (**fig. S5, A and C**).

Four model variations were considered: fitting both $\vec{v}_R$ an $\vec{v}_T$; fitting $\vec{v}_R$ with $\vec{v}_T = \vec{0}$; $\vec{v}_T$ with $\vec{v}_R = \vec{0}$; and fitting the uniform model $\vec{v}_U$. For all cases the model was constrained to vectors of unit magnitude, to focus on the direction rather than the speed of self-motion, and because the T4/T5 vectors (direction-selectivity index) had magnitudes between zero and one.

The data was fitted using ten-fold cross-validation (CV), dividing the data into ten random subsets. In each fold, nine subsets were used for training and the remaining subset was used for testing the model fit. For each CV fold, the same training data was fit ten times starting from ten different random conditions, and the best fit was stored and used to calculate the performance on the test set. The same training and testing data were used for all models, resulting in repeated measures of the test performance across models. Statistical testing was done on the ten test-performance values obtained per model. A one-tailed nonparametric Wilcoxon signed-rank test was used to determine whether the performance of each of the self-motion models was higher than the performance of the uniform model, for tests pooling all subtypes (**Fig. 4D**) and tests of individual subtypes (**fig. S5C**). A signed-rank test accounted for repeated measures, and a Bonferroni correction was applied to account for multiple testing ($p < 0.05/3$).

Code and data are available on github.com/silieslab/DS_tuning_Henning

References

1. S. Sabbah, *et al.*, A retinal code for motion along the gravitational and body axes. *Nature* **546**, 492–497 (2017).
2. M. S. Maisak, *et al.*, A directional tuning map of Drosophila elementary motion detectors. *Nature* **500**, 212–216 (2013).
3. Y. E. Fisher, M. Silies, T. R. Clandinin, Orientation Selectivity Sharpens Motion Detection in Drosophila. *Neuron* **88**, 390–402 (2015).
4. G. Ramos-Traslosheros, M. Henning, M. Silies, Motion detection: Cells, circuits and algorithms. *Neuroforum* **24**, A61–A72 (2018).
5. J. Haag, A. Arenz, E. Serbe, F. Gabbiani, A. Borst, Complementary mechanisms create direction selectivity in the fly. *Elife* **5**, e17421 (2016).
6. C. F. R. Wienecke, J. C. S. Leong, T. R. Clandinin, Linear Summation Underlies Direction Selectivity in Drosophila. *Neuron* **99**, 680-688.e4 (2018).
7. J. C. S. Leong, J. J. Esch, B. Poole, S. Ganguli, T. R. Clandinin, Direction selectivity in drosophila emerges from preferred-direction enhancement and null-direction suppression. *J. Neurosci.* **36**, 8078–8092 (2016).
8. E. Gruntman, S. Romani, M. B. Reiser, Simple integration of fast excitation and offset, delayed inhibition computes directional selectivity in Drosophila. *Nat. Neurosci.* **21**, 250–257 (2018).
9. E. Gruntman, S. Romani, M. B. Reiser, The computation of directional selectivity in the drosophila off motion pathway. *Elife* **8** (2019).
10. S. Y. Takemura, *et al.*, The comprehensive connectome of a neural substrate for 'ON' motion detection in Drosophila. *Elife* **6**, e24394 (2017).
11. K. Hausen, Motion sensitive interneurons in the optomotor system of the fly. *Biol. Cybern.* **46**, 67–79 (1982).
12. H. G. Krapp, R. Hengstenberg, Estimation of self-motion by optic flow processing in single visual interneurons. *Nature* **384**, 463–466 (1996).
13. H. G. Krapp, B. Hengstenberg, R. Hengstenberg, Dendritic structure and receptive-field organization of optic flow processing interneurons in the fly. *J. Neurophysiol.* **79**, 1902–1917 (1998).
14. R. Kern, Visual position stabilization in the hummingbird hawk moth, Macroglossum stellatarum L. II. Electrophysiological analysis of neurons sensitive to wide-field image motion. *J. Comp. Physiol. - A Sensory, Neural, Behav. Physiol.* (1998) https:/doi.org/10.1007/s003590050174.
15. J. C. Theobald, E. J. Warrant, D. C. O'Carroll, Wide-field motion tuning in nocturnal hawkmoths. *Proc. R. Soc. B Biol. Sci.* (2010) https:/doi.org/10.1098/rspb.2009.1677.
16. A. L. Stöckl, D. C. O'Carroll, E. J. Warrant, Neural summation in the hawkmoth visual system extends the limits of vision in dim light. *Curr. Biol.* (2016) https:/doi.org/10.1016/j.cub.2016.01.030.
17. J. Kien, Sensory integration in the locust optomotor system-II: Direction selective neurons in the circumoesophageal connectives and the optic lobe. *Vision Res.* (1974) https:/doi.org/10.1016/0042-6989(74)90224-7.
18. F. C. Rind, Identification of directionally selective motion-detecting neurones in the locust lobula and their synaptic connections with an identified descending neurone. *J. Exp. Biol.* (1990).
19. C. H. F. Rowell, Mechanisms of flight steering in locusts. *Experientia* (1988) https:/doi.org/10.1007/BF01940532.
20. B. J. E. Evans, D. C. O'Carroll, J. M. Fabian, S. D. Wiederman, Differential Tuning to Visual Motion Allows Robust Encoding of Optic Flow in the Dragonfly. *J. Neurosci.*

(2019) https:/doi.org/10.1523/JNEUROSCI.0143-19.2019.
21. H. G. Krapp, Estimation of self-motion for gaze and flight stabilization in flying insects. *Navig. J. Inst. Navig.* **55**, 147–158 (2008).
22. A. Borst, J. Haag, Neural networks in the cockpit of the fly. *J. Comp. Physiol. A Neuroethol. Sensory, Neural, Behav. Physiol.* **188**, 419–437 (2002).
23. M. Joesch, J. Plett, A. Borst, D. F. Reiff, Response Properties of Motion-Sensitive Visual Interneurons in the Lobula Plate of Drosophila melanogaster. *Curr. Biol.* **18**, 368–374 (2008).
24. B. Schnell, *et al.*, Processing of horizontal optic flow in three visual interneurons of the Drosophila brain. *J. Neurophysiol.* **103**, 1646–1657 (2010).
25. H. Wei, H. Y. Kyung, P. J. Kim, C. Desplan, The diversity of lobula plate tangential cells (LPTCs) in the Drosophila motion vision system. *J. Comp. Physiol. A Neuroethol. Sensory, Neural, Behav. Physiol.* **206**, 139–148 (2020).
26. V. Haikala, M. Joesch, A. Borst, A. S. Mauss, Optogenetic control of fly optomotor responses. *J. Neurosci.* **33**, 13927–13934 (2013).
27. T. Fujiwara, T. L. Cruz, J. P. Bohnslav, M. E. Chiappe, A faithful internal representation of walking movements in the Drosophila visual system. *Nat. Neurosci.* **20**, 72–81 (2017).
28. A. J. Kim, L. M. Fenk, C. Lyu, G. Maimon, Quantitative Predictions Orchestrate Visual Signaling in Drosophila. *Cell* **168**, 280–294 (2017).
29. A. S. Mauss, M. Meier, E. Serbe, A. Borst, Optogenetic and Pharmacologic Dissection of Feedforward Inhibition in Drosophila Motion Vision. *J. Neurosci.* **34**, 2254–2263 (2014).
30. A. S. Mauss, *et al.*, Neural Circuit to Integrate Opposing Motions in the Visual Field. *Cell* **162**, 351–362 (2015).
31. B. Schnell, S. V. Raghu, A. Nern, A. Borst, Columnar cells necessary for motion responses of wide-field visual interneurons in Drosophila. *J. Comp. Physiol. A Neuroethol. Sensory, Neural, Behav. Physiol.* **198**, 389–395 (2012).
32. E. L. Barnhart, I. E. Wang, H. Wei, C. Desplan, T. R. Clandinin, Sequential Nonlinear Filtering of Local Motion Cues by Global Motion Circuits. *Neuron* **100**, 229-243.e3 (2018).
33. M. Mazurek, M. Kager, S. D. Van Hooser, Robust quantification of orientation selectivity and direction selectivity. *Front. Neural Circuits* **8**, 92 (2014).
34. J. J. Koenderink, A. J. van Doorn, Facts on optic flow. *Biol. Cybern.* **56**, 247–254 (1987).
35. M. Egelhaaf, "Visual processing in free flight" in *Encyclopedia of Computational Neuroscience*, Encycloped, (2015).
36. Y. Yue, S. Ke, W. Zhou, J. Chang, In vivo imaging reveals composite coding for diagonal motion in the Drosophila visual system. *PLoS One* **11**, e0164020 (2016).
37. A. S. Mauss, A. Vlasits, A. Borst, M. Feller, Visual Circuits for Direction Selectivity. **40**, 211–230 (2017).
38. S. Y. Takemura, *et al.*, A visual motion detection circuit suggested by Drosophila connectomics. *Nature* **500**, 175–181 (2013).
39. N. Hörmann, *et al.*, A combinatorial code of transcription factors specifies subtypes of visual motion-sensing neurons in Drosophila. *Dev.* **147** (2020).
40. Y. Z. Kurmangaliyev, J. Yoo, J. Valdes-Aleman, P. Sanfilippo, S. L. Zipursky, Transcriptional Programs of Circuit Assembly in the Drosophila Visual System. *Neuron* **108**, 1045–1057 (2020).
41. Y. Z. Kurmangaliyev, J. Yoo, S. A. Locascio, S. Lawrence Zipursky, Modular transcriptional programs separately define axon and dendrite connectivity. *Elife* **8**, e50822 (2019).
42. M. N. Özel, *et al.*, Neuronal diversity and convergence in a visual system developmental atlas. *Nature* **589**, 88–95 (2020).

43. R. Petrowitz, H. Dahmen, M. Egelhaaf, H. G. Krapp, Arrangement of optical axes and spatial resolution in the compound eye of the female blowfly Calliphora. *J. Comp. Physiol. - A Sensory, Neural, Behav. Physiol.* **186**, 737–746 (2000).
44. R. Heisenberg, M. & Wolf, *Vision on Drosophila:genetics of microbehavior* (1984).
45. J. Cafaro, J. Zylberberg, G. D. Field, Global motion processing by populations of direction-selective retinal ganglion cells. *J. Neurosci.* **40**, 5807–5819 (2020).
46. M. J. Y. Zimmermann, *et al.*, Zebrafish Differentially Process Color across Visual Space to Match Natural Scenes. *Curr. Biol.* **28** (2018).
47. T. Baden, T. Euler, P. Berens, Understanding the retinal basis of vision across species. *Nat. Rev. Neurosci.* **21**, 5–20 (2020).
48. A. Bleckert, G. W. Schwartz, M. H. Turner, F. Rieke, R. O. L. Wong, Visual space is represented by nonmatching topographies of distinct mouse retinal ganglion cell types. *Curr. Biol.* **24**, 310–315 (2014).
49. M. Zhou, *et al.*, Zebrafish Retinal Ganglion Cells Asymmetrically Encode Spectral and Temporal Information across Visual Space. *Curr. Biol.* **30**, 2927-2942.e7 (2020).
50. L. Freifeld, D. A. Clark, M. J. Schnitzer, M. A. Horowitz, T. R. Clandinin, GABAergic Lateral Interactions Tune the Early Stages of Visual Processing in Drosophila. *Neuron* **78**, 1075–1089 (2013).
51. P. Kaifosh, J. D. Zaremba, N. B. Danielson, A. Losonczy, SIMA: Python software for analysis of dynamic fluorescence imaging data. *Front. Neuroinform.* **8**, 80 (2014).
52. N. Otsu, Threshold selection method from gray-level histograms. *IEEE Trans Syst Man Cybern* **9**, 62–66 (1979).
53. M. Fiorani, J. C. B. Azzi, J. G. M. Soares, R. Gattass, Automatic mapping of visual cortex receptive fields: A fast and precise algorithm. *J. Neurosci. Methods* **221**, 112–126 (2014).
54. P. Berens, CircStat : A MATLAB Toolbox for Circular Statistics. *J. Stat. Softw.* **31**, 1–21 (2009).
55. C. S. Wallace, *Statistical and Inductive Inference by Minimum Message Length* (2005).

Acknowledgments

We thank Carlotta Martelli, Yvette Fisher, Axel Methner, and members of the Silies lab for comments on the manuscript, and Christof Rickert for help with image analysis. We are grateful to Christine Gündner and Jonas Chojetzki for excellent technical assistance.
Funding: This project has received funding from the European Research Council (ERC) under the European Union's Horizon 2020 research and innovation program (grant agreement No 716512).

Author contributions:

Conceptualization: M.H and M.S
Methodology: M.H, G.R-T, B.G
Software: M.H, G.R-T, B.G
Investigation: M.H
Visualization: M.H, G.R-T
Supervision: M.S
Writing—original draft: M.H and M.S
Writing—review & editing: all authors
Funding acquisition: M.S

Competing interests: Authors declare that they have no competing interests.

Data and materials availability: All data needed to evaluate the conclusions in the paper are present in the paper and/or the Supplementary Materials. Code and data are also available on github.com/silieslab/DS_tuning_Henning.

Supplementary Materials

Science Advances
AAAS

advances.sciencemag.org/cgi/content/full/sciadv.[ms.no.]/DC1

Supplementary Materials for

Populations of local direction-selective cells encode global motion patterns generated by self-motion

Miriam Henning, Giordano Ramos-Traslosheros, Burak Gür, Marion Silies*

*Corresponding author. Email: msilies@uni-mainz.de

This PDF file includes:

Figs. S1 to S5

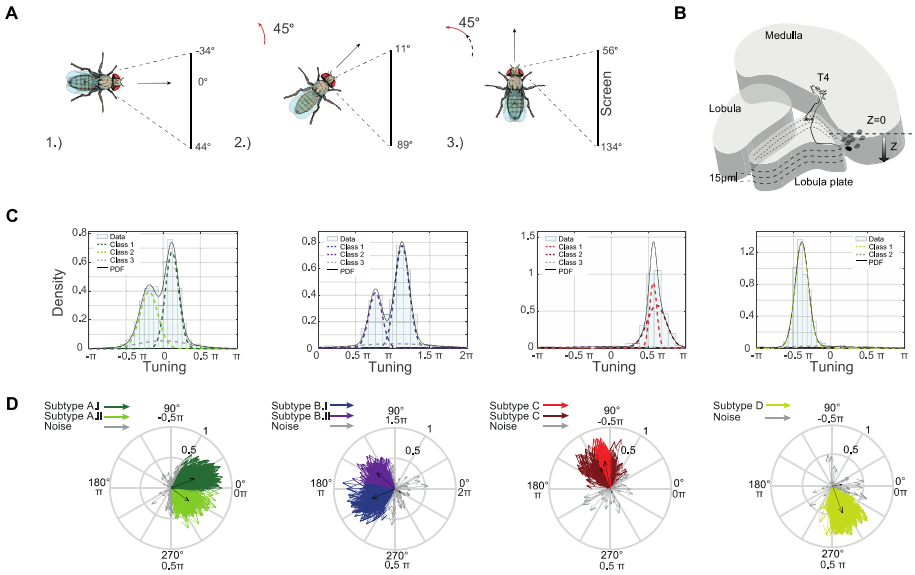

Fig. S1. Population recordings reveal that directional tuning clusters around hexagonal directions of motion. (**A**) Schematic of the experiment. The fly was positioned in three different orientations (0°, 45°, 90°) towards a screen to extend the visual field covered by one experiment, together spanning ~ 150° in azimuth. The screen covered 60° in elevation. (**B**) Illustration of the lobula plate, showing one T4 neuron. Recordings were done every 15 µm over a range of ~ 60 µm within each fly. z-depth was taken as the distance to the first expression in cell bodies that was detected while moving the objective ventrally. (**C**) Density distribution of T4/T5 tuning. Solid lines represent the fitted probability density function. Dotted lines show the underlying Gaussian distributions (classes) extracted using the finite gaussian mixture model SNOB[50]. For the neuronal population of layers A and B, this model predicted three underlying Gaussian distributions, where two of them showed a sharp peak (spread of ~0.5π, Class 1 & 2) and one had a very broad distribution with low peak densities (Class 3), which represents an underlying noise distribution. For layer C cells, three underlying Gaussian distributions were predicted as well, but the first two were highly overlapping, and the peaks were separated by less than ~0.1π. When analyzed separately for T4 and T5, only one main class of cells was found in layer C (data not shown). For layer D, only one main distribution was found. Taken together, these data suggest that layers A and B contain two subtypes of T4/T5 neurons, whereas layers C and D contain one T4/T5 subtype each. (**D**) Same as (**Fig. 1A**), but tuning of individual neurons is color coded based on subtype identity. Cells were assigned to a subtype based on the highest probability of their tuning preference falling into a class.

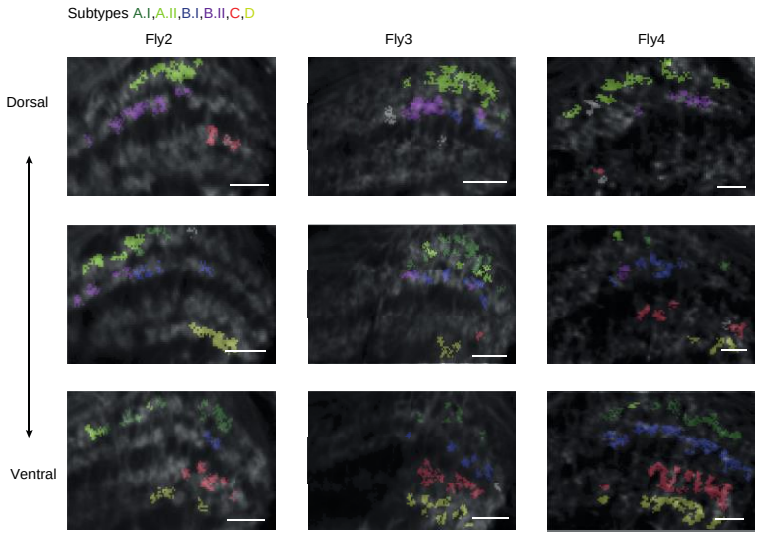

Fig. S2. Layer A and B subtypes are separated along the dorsoventral axis. 2-photon calcium images of the lobula plate at three different z-depths (Z), given in µm relative to T4/T5 cell bodies (see **fig. S1B**). ROIs are color-coded based on their subtype identity. Shown are three example flies. Individual images, corresponding to planes along the dorsoventral axis, predominantly show the two subtypes A.II and B.II, or the four subtypes A.I, B.II, C and D. Scale bar 10µm.

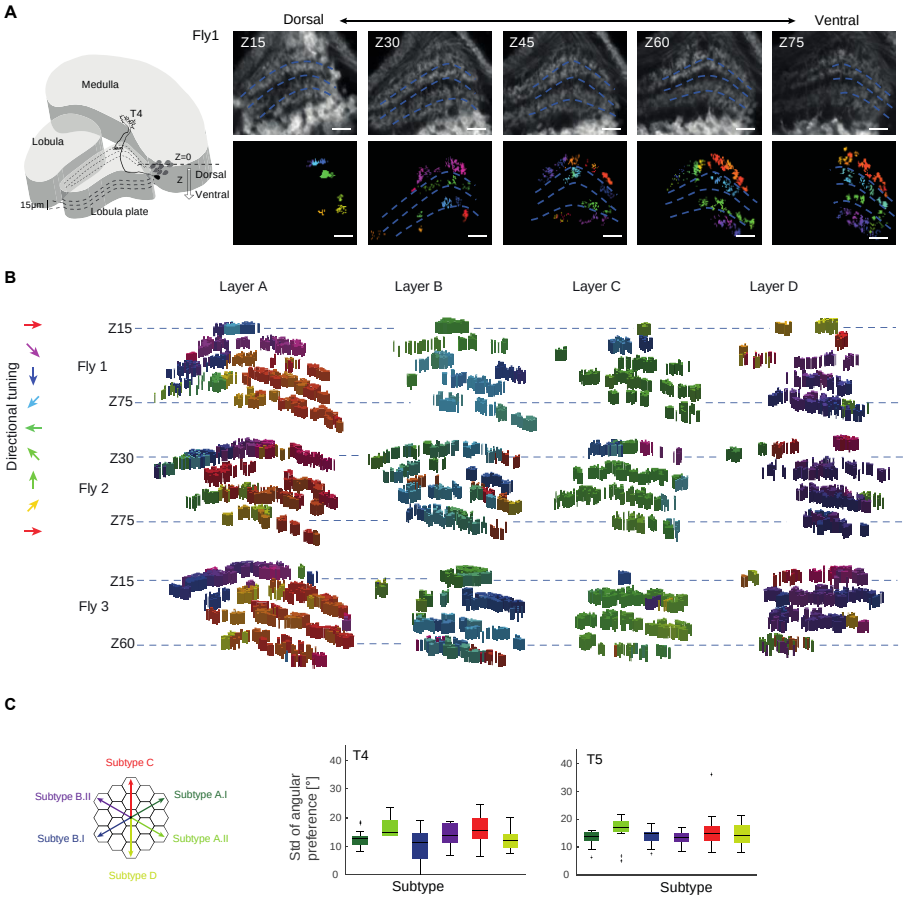

Fig. S3. Tuning within individual subtypes is topographically organized. (**A**) 3D illustration of the lobula plate. Recordings were made at different z-depths, corresponding to different locations along the dorsoventral axis. Example images from one fly recorded at different planes along the dorsoventral axis, shown as 2-photon images (upper row) or color-coded ROIs based on their tuning preference (lower row). Scale bar = 10µm. (**B**) Pseudo z-stacks of ROIs from each lobula plate layer recorded at different z-depths. Examples are shown from three different flies. Colors indicate tuning preference. The most prominent tuning difference was attributable to the two subtypes in layers A and B. Some more subtle changes in tuning were also apparent along the dorsoventral axis, but they were less prominent than along the proximodistal axis c, Variability of T4 and T5 tuning preference within one fly for each of the six subgroups shows that tuning distribution were not significantly different (Wilcoxon test, p>0.05).

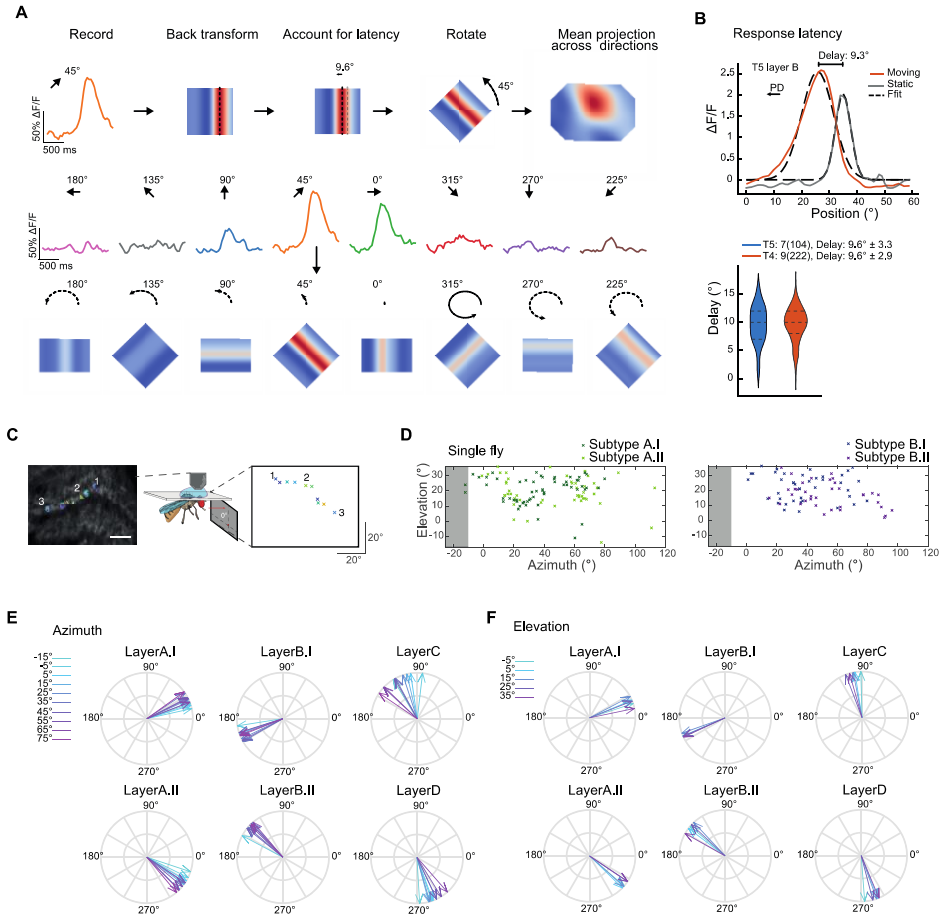

Fig. S4. Average T4/T5 tuning changes gradually along the horizontal and vertical visual axis. (**A**) Illustration of the back transformation of T4/T5 responses to edges moving into eight different directions to map receptive-field centers [48]. Response traces were transformed into two dimensional images and shifted by 9.6° to account for neuronal response latencies and calcium dynamics measured in T4/T5 cells (see (B) and methods). After rotating images according to the direction of the stimulus the mean projection across direction maps resulted in the receptive-field map. (**B**) Top: Response latency of T4/T5 neurons were measured by the spatial difference between responses to a static bar shown at different spatial locations (grey solid line) and a moving stimulus (orange solid line). Dotted lines depict the fits to the corresponding responses. Latency was 9.3° in this example. Bottom: The average delay measured for T4 and T5 neurons was 9.6°. Dotted lines represent the quartiles. (**C**) 2-photon image of the lobula plate showing example ROIs of T4/T5 axon terminals (top) and their corresponding receptive-field center positions (**D**) Receptive-field center positions plotted onto visual screen coordinates for one fly. Within one fly, the receptive field positions of the two subtypes of layer A and the two subtypes of layer B are overlapping in visual space (**E** and **F**) Mean tuning vectors across 10° wide bins

demonstrate that tuning shifts gradually along both the horizontal (E) and the vertical (F) dimension of the visual field.

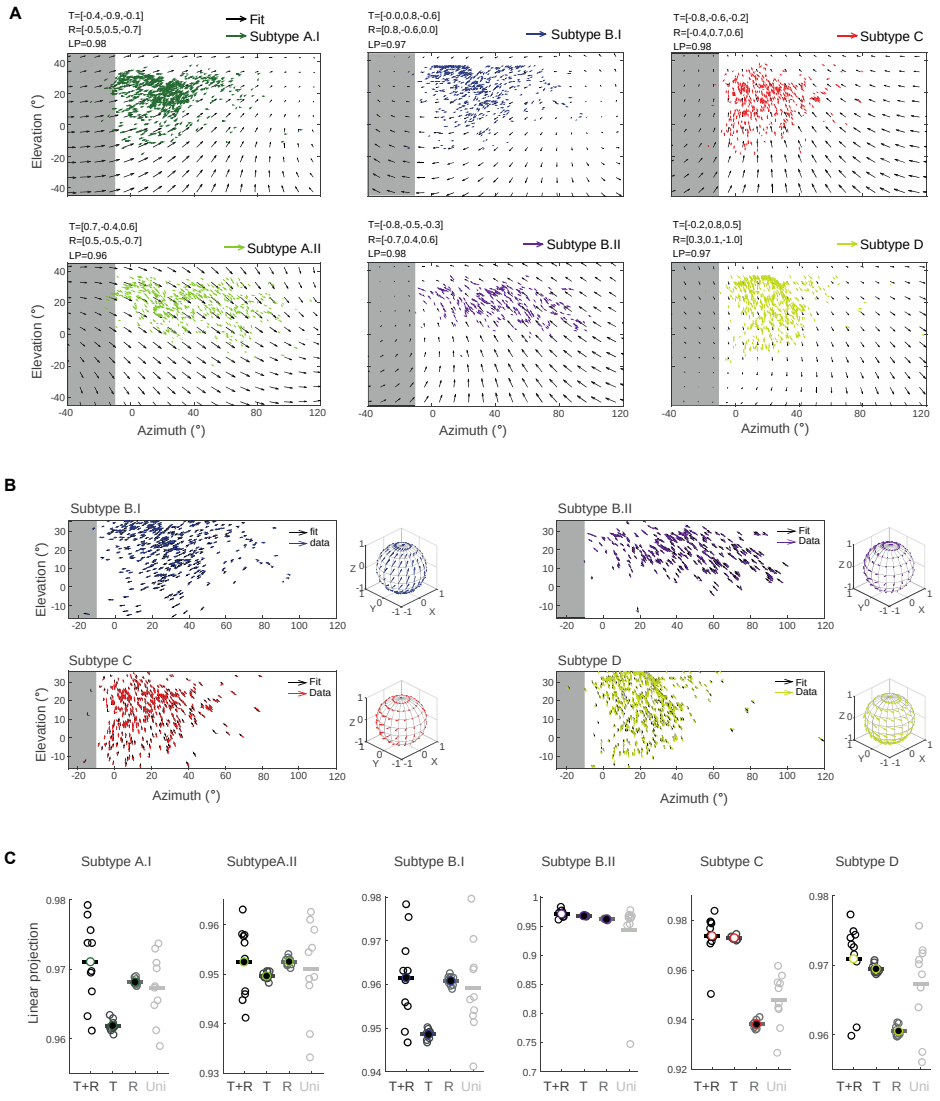

Fig. S5. Flow fields generated by self-motion are matched filters for T4/T5 population tuning (A) Flow fields of data from each subtype (colored) and the fitted normalized flow field model (black). Model vectors are shown evenly spaced across the visual field. T[x,y,z] and R[x,y,z] show the translational and rotational components producing the best matched flow fields. The goodness of the fit was calculated as the linear projection (LP) between the data and the flow field vectors, which equals +1 when all vectors fit perfectly and equals -1 when all vectors point in opposite directions. Gray shaded areas indicate the area of the visual space in the left visual hemisphere that cannot be seen by the right eye. (**B**) Flow fields of data as in (A) from four subtypes not shown in **Fig. 4C**. Model vectors are shown for each corresponding data vector. Right: Model data represented as a 3D flow field. (**C**) Quality of the fit obtained from linear projection of the model to the data, shown for four different model variations allowing to

train either all parameters for translation and rotation (T+R), only translation (T), only rotation (R) or a model with uniform direction vectors (Uni). Each circle represents the best fit of 10-fold cross-validation (see methods). Colored circles represent the average of the ten cross-validation results. Open circles indicate a significant difference to the uniform model prediction (Wilcoxon: $p<0.001$)

4 GENERAL DISCUSSION

Different types of local and global motion inform behavioral decisions. At the first processing steps of vertebrate as well as invertebrate eyes, retinotopically arranged visual units process visual information from local points in space, leading to the detection of local motion. Subsequently, this local motion information is pooled across visual space by wide-field cells that report global motion. Global optic motion patterns elicited on the eye during locomotion of animals inform the brain about the trajectory of self-movements. In this thesis, I studied both local and global motion processing. First, I investigated the tuning of the local motion detectors T4 and T5 in the visual system of the fruit fly to understand how their directional tuning is influenced locally by GABAergic circuits and revealed that the population of T4 and T5 computes global motion patterns, providing the basis for the computation of self-motion information in downstream wide-field cells.

Together with my collaborators, I found two GABAergic feedback neurons, C2 and C3, to be essential for motion-guided behaviors and direction-selectivity of local motion detectors. We show that both neurons are ON selective and heavily connect to neurons in upstream circuitry of both ON (T4) and OFF (T5) motion detectors. Blocking neuronal activity in C2 shapes responses of neurons upstream of T4 and T5 cells, for example the OFF-pathway neuron L2 as well as the ON-pathway neuron Mi1. Furthermore, blocking neuronal activity in C2 or C3 caused T4 and T5 responses to stationary and non-preferred directions of motion stimuli, leading to a substantial decrease of T4/T5 direction-selectivity. While our data suggest a specific role of C2 for ND suppression in T4, both C2 and C3 likely play another more general role in stabilizing the neuronal activity in upstream circuits of motion detection. Together this suggests a GABAergic feedback mechanism that indirectly shapes tuning of local motion detection.

To understand how global motion is computed from local T4 and T5 tuning, I used *in vivo* calcium imaging and mapped local direction tuning of the population of T4 and T5 cells across retinotopic space. My collaborators and I show that instead of four anatomically described subtypes, directional tuning preference of T4 and T5 can be grouped into six functional subtypes. Within each subtype, directional preference changes gradually across retinotopic space, forming continuous tuning maps that match optic flow fields generated during self-motion. Thus, similar to the mouse retina, one synapse before the global motion detector cells, the population of local motion detectors already encodes self-motion of the fly. In contrast to the mouse retina, where direction-selective ganglion cells encode four optic flow patterns generated during walking, the fly visual system encodes six directions of self-motion, likely reflecting the higher degrees of freedom and the more complex maneuvers encountered during flight.

In this general discussion, I will first focus on general ideas about how six subtypes of T4 and T5 cells might develop, how dendrites and axons might be organized in the visual system and how tuning differences might be shaped during development. Next, I will discuss the importance of global motion processing for understanding the function of visual systems.

Furthermore, I will discuss how much our data tell us about general principles of motion processing. In that context, I will discuss similarities of visual processing between the vertebrate and invertebrate retina. In addition, I will discuss the differences between our data and the visual processing observed in other visual species and what that might tell us about the evolutionary adaptation of visual systems to the behavioral constraints of an animal.

4.1 Development, organization and refinement of local motion tuning

During the development of the visual system, the same progenitor cells transition through two competence windows, first producing the two GABAergic C2 and C3 neurons and later T4/T5 cells (Apitz and Salecker, 2015, 2018). This argues that C2/C3 and T4/T5 are intricately linked, which is supported by the functional importance of C2 and C3 for motion detection in T4 and T5. This could indicate that functional dependence is to some extend reflected by development. Differential expression of effector genes further ensures that the local motion detectors T4 and T5 both extend their axon terminals into four distinct anatomical layers of the lobula plate of the visual system (Apitz and Salecker, 2018; Hörmann et al., 2020; Pinto-Teixeira et al., 2018). Based on these anatomical projections, T4 and T5 cells have been grouped into four subtypes (Fischbach and Dittrich, 1989). However, functionally we find six subtypes of T4 and T5 cells, with two subtypes in layers A and B each. These two subtypes in layers A and B are organized into functional subregions of the lobula plate along the dorsoventral axis, where each of these subregions seems to be retinotopically organized. However, at the level of the dendrites the organization of the six subtypes remains obscure. The visual space that is covered by each of the six subtypes is highly overlapping, arguing that dendrites of the six T4 and T5 subtypes should be distributed across the retinotopically arranged visual units of the medulla and lobula respectively. Thus, one possibility is that medulla neurons of one column, for example Mi1, synapses with each of the six, rather than four, different subtypes of T4 cells (**Figure 6A**). On the other hand, the dendrites of the different subtypes could distribute across the outputs of the retinotopic units, such that each medulla neuron may synapse onto a subset of four out of the possible six different subtypes. The same scenarios could apply to T5 dendrites, which are located in the lobula where they receive retinotopic input from transmedulla (Tm) neurons. Interestingly, EM tracing of neurons within seven neighboring medulla columns revealed more than 60 T4 cells. This is exactly the number, one would expect, if each of the seven column houses six T4 cells plus the neighboring T4 cells that extend their dendrites into the outer six columns, given that each T4 neuron extends its dendrites across three neighboring columns (Haag et al., 2017; Takemura et al., 2017). In contrast, the total number of T4 and T5 cells in the whole optic lobe was reported to be 5,300, well matching the assumption of four T4 and four T5 subtypes in each of the ~750 columns of the fly eye (Mauss et al., 2014), which supports the second scenario. However, this count is based on genetically labeling T4 and T5 cells. It thus needs to be tested if the genetic driver used in this study, labels all six subtypes of T4 and T5 cells or only four.

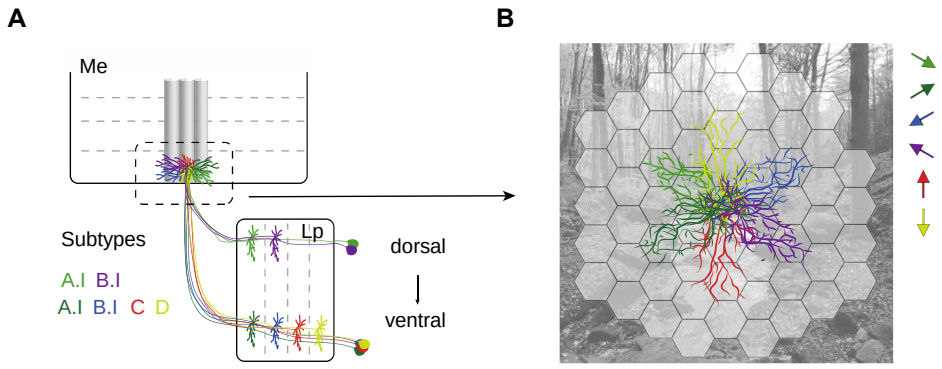

Figure 6 Organization of six T4 cells in the medulla and lobula plate. (**A**) Six T4 cells sampling from the columns in the medulla (Me) and thus the same point in visual space project to different regions of the lobula plate (Lp). (**B**) T4/T5 cells sample visual input by orienting their dendrites across the hexagonal arrangement of visual units of the fly eye. Arrows indicate the PD of the according neuron.

In both situations, we would expect a chiasm of axons along the dorsoventral axis of the visual system from retinotopically sampling T4 and T5 neurons, converging once in the dorsal and once in the ventral subregion of the lobula plate. Such a dorsoventral chiasm has not been reported. However, the one study that looked at this was mainly focused on the anteroposterior and proximodistal axis in a small region of the visual system (Shinomiya et al., 2019a). To explore a possible chiasm along the dorsoventral axis, tracing of T4 and T5 axons needs to be extended to the whole extend of the visual system. This should soon be possible with the advancement of EM tracing techniques and the availability of EM serial reconstructions of the visual system (Zheng et al., 2018). Notably, our functional data are broad along azimuth, covering ~150° of visual space, but limited along the dorsoventral size of the lobula plate, covering ~60° of visual space in elevation. This is mostly true because GCamP6f expression in T4 and T5 cells could only be detected in a range of approximately 70 µm depth of the whole volume of approximately 150-200 µm (based on immunostaining experiments and EM reconstructions, Boergens et al., 2018b). To obtain an even more comprehensive picture of T4/T5 tuning across the dorsoventral axis of the lobula plate, one might try red-shifted calcium indicator, such as RGeco1a. This could allow 2-photon activation with longer wavelength and thus deeper tissue penetration (Dana et al., 2019). Alternatively, technological advances such as 3-photon microscopy could help address this problem and obtain a more comprehensive picture of direction tuning across the full population of T4/T5 cells (Hsu et al., 2019). Taken together, it remains to be tested more specifically how the six subtypes of T4 and T5 cells are organized in the visual system and to what directions T4 and T5 cells in more ventral regions are tuned to.

To become direction tuned, each T4/T5 neuron orients their dendrites along three to four neighboring columns of the medulla or lobula (Haag et al., 2016). Given the hexagonal structure of the fly eye, the diagonal tuning preference of T4 and T5 neurons found in our study can be well explained by dendrites orienting along the three ommatidial axis (**Figure 6B**). The orientations of dendrites are formed during pupa development (Hörmann et al., 2020) and are strongly correlated with the neuron's direction preference (Takemura et al., 2013,

2017). Already manifesting during development, the dendrites of neurons from layers 3 and 4 are clearly oriented along the dorsoventral axis, matching their direction preference. In contrast, dendrite orientation of neurons from layers A and B seems to be less specific. Here dendrites seem to be rather bilobed and oriented along two diagonal axes (Hörmann et al., 2020). This perfectly matches their later directional tuning, which is also tuned to front-to-back or back-to-front on average, but indeed shows a bimodal distribution with predominant diagonal tuning directions. The size of the dendrites then reduces in a period between the late pupa stage and the adult fly. It will be interesting to see whether one of the two dendritic lobes is pruned in layer A and layer B neurons, and thus refines dendrite orientation to match adult direction tuning.

What are the processes that could shape dendrite and directional tuning? In the vertebrate retina, direction tuning is already established before eye opening (Tiriac et al., 2021; Wei et al., 2011) However, some realignment of tuning takes place after eye-opening and is based on visual experience (Bos et al., 2016; Chan and Chiao, 2013). Furthermore, unidirectional stimulation of DSGC can even reverse their directional preference in adult mice, showing that visual experience is crucial for shaping tuning preferences of local motion detectors in vertebrates (Rivlin-Etzion et al., 2012). In contrast, the local tuning properties of wide-field motion detectors, downstream of T4 and T5, in blowflies did not depend on visual experience (Karmeier et al., 2001). Although it remains to be tested if this holds true for the population of local motion tuning in T4 and T5 cells, dendrite orientation is partially already determined during pupa development. This is mainly based on genetic programs and differential gene expression, which regulate the distinct orientation of dendritic arbors and the organization of axon terminals in the lobula plate (Apitz and Salecker, 2018; Hörmann et al., 2020; Kurmangaliyev et al., 2019; Pinto-Teixeira et al., 2018; Rossi et al., 2021). In addition, spontaneous activity evoked during pupa development (Akin et al., 2019) could coordinate the refinement of presynaptic partners and thus direction tuning of T4 and T5 cells (Choi et al., 2021). Such retinal waves have just been shown to be important for tuning maps in the mouse retina (Tiriac et al., 2021).

4.2 Global processing of visual information

The tuning responses of the population of local motion detectors revealed that the T4 and T5 cells that have previously been described to be tuned to four cardinal directions of motion represent only a small subset of the entire population (Fisher et al., 2015a; Maisak et al., 2013). Only when looking at the global direction tuning, we find that the six populations of T4 and T5 cells in fact gradually change tuning across visual space to encode self-motion of the fly. This is a striking example where it is relevant to study the whole extend of visual processing across visual space, to understand what type of information the population of cells encodes. The representation of information by a population of cells is well studied in higher brain areas of vertebrates (Berens et al., 2012; Gilad and Slovin, 2015; Sanger, 2003) but also for sensory processing in insects (Campbell et al., 2013; Clemens et al., 2011).

In the visual system of the fruit fly, visual processing within each of the ~750 repetitive visual units (ommatidia), was long thought to be uniform. However, dorsoventral

differences in sensitivities of photoreceptors can already be found in the insect retina as well as the vertebrate retina (Baden et al., 2020; Wernet et al., 2015). Furthermore, it was recently found that populations of neurons show differential gene expression along the dorsoventral axis of the visual system (Kurmangaliyev et al., 2020; Özel et al., 2020). Although this dorsoventral split across the retina in terms of photosensitivity or gene expression is different from the gradually changing tuning preferences of T4/T5 cells, both examples suggests that processing of visual information varies across the visual field. Beyond differential gene expression, also different synaptic connections may explain the differential tuning of T4 and T5 cells across visual space or the recently reported variability of receptive field sizes of medulla neurons (Ramos-Traslosheros and Silies, 2021). A recent EM study tried to evaluate variations of synaptic contacts between neurons, the current data sets are limited to 7 columns and thus would not give a good estimate about variations across visual space (Takemura et al., 2015). Together this suggests that neurons within one population can greatly differ in their processing across retinotopic space. Therefore, to understand the function of visual systems it will not be enough to study only a small subset of cells in a small part of the brain, but it is necessary to extend the measures to the population of cells that process visual information across visual space.

4.3 Common design principles of visual motion processing

The theory of efficient coding predicts that neuronal circuits, which are energetically expensive, evolve to maximize the encoded information that is relevant for the different constraints of animals (Land and Nilsson, 2012; Sterling and Laughlin, 2015). To understand the principles of visual processing it is thus important to compare network functions across different species and relate them to the specific natural environments and the behavioral requirements of the animal (Baden et al., 2020). The eyes of vertebrates and invertebrates as mice and flies have evolved independently and look very different at first glance. However, these systems show several parallels in the way how visual motion information is computed (Borst and Helmstaedter, 2015). One prominent example is the retinotopic representation of visual space throughout the visual system, which is further processed in two parallel channels of motion processing, namely the ON and OFF pathways (Borst and Helmstaedter, 2015; Sanes and Zipursky, 2010).

What do the two studies proposed here tell us about common or different design principles of visual systems? In the first study we found that the visual system of *D. melanogaster* employs a GABAergic feedback mechanism implemented into upstream circuitry that is required for the computation of direction-selectivity in local motion detectors. Such GABAergic circuits are also found in the retina of different vertebrate species, including mice, humans, birds, fish, and reptiles (Baden et al., 2020; Franke and Baden, 2017). Here, GABAergic horizontal cells regulate visual processing in upstream circuitry, while for example the GABAergic starburst amacrine cells implement ND suppression to direction-selective retinal ganglion cells (Chaya et al., 2017; Diamond, 2017; Wei, 2018; Wei et al., 2011). Similarly, we found a specific role of C2 for implementing ND inhibition for the ON

motion pathway (T4). However, the underlying implementation in neural circuitry appears to be fundamentally different. Whereas C2 acts on upstream circuitry and is not direction selective, the starburst amacrine cell provides direct and direction-selective signals to retinal ganglion cells to sharpen their directional tuning. Nevertheless, in both systems the different GABAergic circuits sharpen direction-tuning and additionally inhibit neuronal activity in upstream circuitry. A balance of excitation and inhibition (E-I) in neuronal networks has been suggested to be important for reducing the energy expenses as well as maximizing the mutual information and therefore allow efficient coding (Yu et al., 2018). GABAergic interneurons are not only important for visual processing but are found in diverse neuronal networks, for example the *Drosophila* mushroom body (Pavlowsky et al., 2018), as well as the prefrontal cortex, the barrel cortex, or the hippocampus of mice (Jang et al., 2015; Saffari et al., 2019; Yu et al., 2019). Here they have been suggested to be relevant for gain control and adaptation to dynamic inputs, such that the network can efficiently respond during different behavioral states of the animal. The two GABAergic neurons C2 and C3 may thus play a similar role for stabilizing the E-I balance of the network, such that it can efficiently encode motion information across different situations.

Furthermore, the second study presented here shows that six types of global optic flow patterns containing information about the animal's self-motion are encoded by six populations of the local motion detectors in the fly eye. Downstream of the population of the local motion detectors, local motion information can simply be pooled across space, to detect global motion information. This population code for self-motion is reminiscent to the population code of direction selective retinal ganglion cells in the mouse retina (DSGC) that encode four axis of self-motion (Sabbah et al., 2017). We hypothesize, that this representation of optic flow at the level of local motion detectors facilitates the computation of diverse optic flow fields represented by downstream wide field motion cells, although in the fly eye, the mixed flow fields still need to be decomposed into its translatory and rotatory components. Furthermore, the curvature of the fly eye provides a structure that simplifies the computation of optic flow (see discussion of the manuscript), arguing that the representation of optic flow already at the level of local motion detectors might be more efficient than the representation of cardinal motion, as suggested previously. Together this suggests that our data presented in the two manuscripts represent two computational principles of visual systems that have evolved independently during evolution. However, for both examples the computations are not completely alike, but might be adapted to the visuoecological and behavioral constraints of the animal.

4.4 Behavioral constraints guide adaptation of neuronal networks

Besides common principles between the vertebrate and invertebrate visual system our data also reveal explicit differences in visual processing between the two species. Whereas in the mouse retina four populations of direction-selective ganglion cells (DSGCs) encode translational optic flow patterns generated during walking, six motion directions are encoded in the fly brain. Additionally, the six motion patterns encoded in the fly brain do not only

encode translational but additionally rotatory components of self-motion. This suggests that the fly brain may be adapted to encode the increased degrees of freedom and the more complex rotational and translational maneuvers encountered during flight (**Figure 7**).

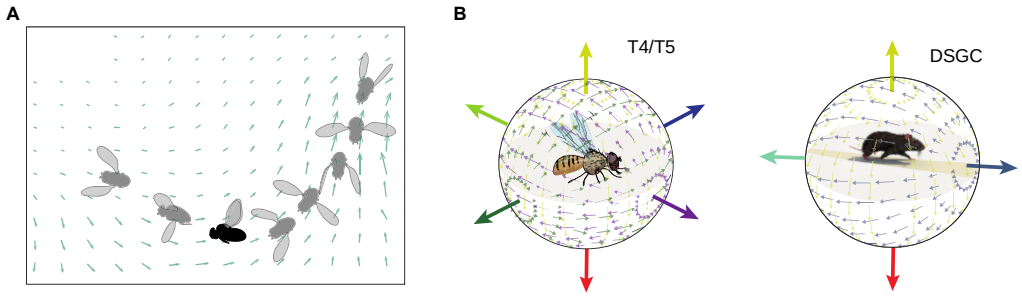

Figure 7 The fly visual system is efficiently tuned to encode self-motion during flight. (**A**) Flight trajectory of an escape maneuver of a fly induces complex optic flow fields of combined translatory and rotatory movements. (***B***) Local motion detectors in mice, the DSGC, encode four directions of self-motion, while T4 and T5 cells *in the* Drosophila *visual system* encode six.

Many examples show that the ecological constraints, as for example the light conditions of an environment or the physical distribution of contrasts given by the structure of the scene that an animal encounters shape the evolution of neural networks (Baden et al., 2020; Clark and Demb, 2016; Gonzalez-Bellido et al., 2011; Honkanen et al., 2017; Laughlin, 1981; Simoncelli and Olshausen, 2001). Also, at the level of local motion detectors T4 and T5 in the *Drosophila* visual system, it has been shown that the spatiotemporal filters and the integration of ON and OFF inputs matches the light-dark asymmetries of naturalistic stimuli (Salazar-Gatzimas et al., 2018). However, little is known about adaptations of neural networks to the behavioral constraints of an animal. In flies, wide field motion detectors (HS cells) of blow flies vs. fruit flies have been shown to be tuned to different temporal frequencies (Hausen, 1982; Schnell et al., 2010), likely reflecting the different flight speeds of the two species. To understand if the six optic flow patterns encoded by T4 and T5 really reflect an adaptation to flight or simply present a difference between the vertebrate and invertebrate visual system, we would need to know more about the encoding of self-motion in other flying versus walking species. However, only little is known about the tuning distribution of local motion detectors in other species. Notably, birds do have many more RGCs proportional to eye size as compared to non-flying species (Baden et al., 2020). For example the hummingbird, which is extremely maneuverable and can even fly upside down and backwards, contains 10 fold more RGC compared to the walking mouse (Jeon et al., 1998; Lisney et al., 2015). The Chilean eagle has ten times more RGC per eye compared to humans, although the size of the eyes are very similar (Inzunza et al., 1991). Although the type of RGCs have not been classified yet, the higher number of RGCs could be due to more cell types, including different subtypes of direction-selective ganglion cells, which could relate to the flying behavior of birds. However, this remains highly speculative, as more RGCs could also indicate more cells of the same subtypes per visual area and thus higher spatial acuity. Additionally, aquatic animals, like fish, navigate in three dimensions. In zebrafish, pretectal neurons are sensitive to global optic flow fields and mediate optomotor stabilizing behaviors (Kist and Portugues, 2019; Portugues et al., 2014). Furthermore, local DSGCs of zebrafish and goldfish could be clustered into three groups on average representing three directions of motion, but how individual tuning maps to the visual input location is so far not known

(Maximov et al., 2005; Nikolaou et al., 2012). Together this shows that we are just starting to understand how evolution shapes visual systems where the distribution of physical information depends on the animal's behavior.

4.5 OUTLOOK

To summarize, we have shown that a so far unknown GABAergic feedback circuitry, mediated by the two columnar neurons C2 and C3 is required for the computation of direction-selective responses in the local motion detectors T4 and T5. We could show that C2 shapes physiological properties of two neurons in upstream circuitry of both T4 and T5 cells, suggesting that the indirect effect on T4 and T5 neurons is mediated by interactions in upstream circuitry. To validate this hypothesis, it will be necessary to decipher the whole circuitry of interactions of both C2 and C3 with neurons in the lamina (e.g. L1 and L5) and medulla (e.g. Tm1, Tm4 and Mi9). This can be achieved by manipulating neuronal activity in C2 or C3 while measuring calcium responses of postsynaptic neurons, as shown for Mi1 and L2. Furthermore, a model analysis of the measured effects of C2 and C3 on the motion detection circuitry would be helpful to gain more insights about the mechanistic implementation and importance of the GABAergic feedback inhibition for motion detection in T4 and T5 cells. A model analysis or further manipulation experiments are also needed to understand how the inhibitory feedback mechanism might act together with previously described mechanisms for direction-selectivity. It may be important to strengthen the direction-selectivity of the local motion detectors, make the system more robust against perturbations, or be more flexible in different behavioral contexts. We also suggested a role of feedback inhibition for stabilizing network activity in upstream circuitry of motion detection. How this may be required for motion computation and how it is implemented into the circuit needs to be addressed more carefully in future studies. This could further provide a general idea about the relation of network balance for proper function of neuronal networks.

Furthermore, we showed that six T4/T5 subtypes encode six global optic flow patterns induced during flight. As discussed above, the organization of these six subtypes in the visual system could not be fully answered by our study. One possibility to address this question, could be to identify the postsynaptic partners downstream of for example Mi1 or Tm3 in the medulla. Using sparse expression of trans-Tango expression in these cells, which leads to the expression of a reporter gene (e.g. GFP) in all postsynaptic cell types could reveal if all six subtypes are postsynaptic to one medulla column (Talay et al., 2017), and reveal their projections into the lobula plate. To further understand how these six subtypes project into the lobula plate and if the proposed chiasm along the dorsoventral axis between medulla to lobula plate exist, one could trace T4 and T5 neurons in a larger region of the visual system from EM data. Such comprehensive tracing efforts of the whole visual system are currently conducted as a collaboration project between several research groups. However, this task is very time consuming. A faster approach would be to label individual neurons of the same population with different colors using a multi color flip out (MCFO) approach (Nern et al.,

2015). These can be visualized and traced by simple immunostainings and confocal imaging. In this way we could additionally analyze the distribution of dendrite orientation in the medulla and lobula to get a better understanding of how tuning relates to dendrite orientation and how the six subtypes sample across retinotopic space.

To get a better understanding of the functional importance of the six T4/T5 subtypes it will be important to have genetic access to each of the subtypes. Recently single cell RNA sequencing revealed on gene CG15537 to be specifically expressed in only a dorsal subpopulation of T4 and T5 cells from layer A and B (Kurmangaliyev et al., 2020). If this subpopulation represents the functional subpopulation revealed in our study remains to be tested. However, together with other differentially expressed genes, specific access to each subtype could be generated by genetic intersections. Specific genetic access could be further used to individually manipulate each subtype and test their functional role for motion-guided behaviors. In addition, such subtype-specific genetic access could be used to understand the mechanisms that differentiate the newly identified T4/T5 subtypes by tracing them throughout development (Apitz and Salecker, 2018; Pinto-Teixeira et al., 2018).

Finally, we proposed that the six types of self-motion encoded in the fly eye could represent an adaptation of the visual system to the complex maneuvers and enhanced degrees of freedom encountered during flight. It would thus be exciting to compare the representation of optic flow fields in other vertebrate or invertebrate visual systems that encounter different types of locomotion. Ants, for example, rely on vision during navigation (Åkesson and Wehner, 2002). Interestingly some animals of the colony, the worker ants exclusively walk, whereas the queen and the drones can fly. Thus, within the same species, different mechanisms of optic flow detection may be implemented in different animals with different behavioral tasks. Another interesting dipteran species, closely related to *D. melanogaster*, is the swift lousefly, a flightless parasite that lost its wings during evolution. On the other hand it might be interesting to compare the four self-motion directions represented in the mouse to optic flow representation in another yet flying mammalian species, the bat, which combines echo-acoustic and optic flow for navigation (Kugler et al., 2019). Such comparative studies of closely related species with different locomotion behaviors would help to better understand how different types of self-motion are represented in the visual system and how this is adapted to the behavioral constraints of the animal.

Appendix

A.I List of Abbreviations

BLM	Barlow-Levick model
Dm	Dorsal medulla
D.melanogaster	*Drosophila melanogaster*
DSGC	Direction-selective ganglion cell
DS	direction selective
EM	electron microscopy
GABA	Gamma-Aminobutyric acid
GluClα	Glutamate gated chloride channel
HRC	Hassenstein-Reichardt detector
HC	horizontal cell
HS	horizontal system
L	Lamina
Lai	Lamina intrinsic
Lat	Lamina tangential
Lawf	Lamina wide-field
LC	Lobula columnar
Lccn	Lobula-complex intrinsic
Lo	Lobula
Lp	Lobula plate
LPi	Lobula plate intrinsic
LPTC	Lobula plate tangential cell
LT	Lobula tangential
M	Medulla
MGluR	Metabotropic glutamate receptor
Mi	Medulla intrinsic
ND	Null direction (non-preferred direction)
NMDA	N-methyl-D-aspartate

PD	Preferred direction
Pm	Proximal medulla
RGC	Retinal ganglion cell
Rh	Rhodopsin
SAC	Starburst amacrine cell
Tm	Transmedulla
vGAT	vesicular GABA transporter
VPN	Visual projection neuron
VS	vertical system

A.II List of figures

Introduction Figures

Manuscript Figures 1

Manuscript Figures 2

Discussion Figures

References

Adelson, E.H., and Bergen, J.R. (1985). Spatiotemporal energy models for the perception of motion. J. Opt. Soc. Am. A *2*, 284.

Åkesson, S., and Wehner, R. (2002). Landmark navigation in desert ants.

Akin, O., Bajar, B.T., Keles, M.F., Frye, M.A., and Zipursky, S.L. (2019). Cell-type-Specific Patterned Stimulus-Independent Neuronal Activity in the Drosophila Visual System during Synapse Formation. Neuron *101*, 894-904.e5.

Ammer, G., Leonhardt, A., Bahl, A., Dickson, B.J., and Borst, A. (2015). Functional Specialization of Neural Input Elements to the Drosophila on Motion Detector. Curr. Biol. *25*, 2247–2253.

Apitz, H., and Salecker, I. (2015). A region-specific neurogenesis mode requires migratory progenitors in the Drosophila visual system. Nat. Neurosci. *18*, 46–55.

Apitz, H., and Salecker, I. (2016). Retinal determination genes coordinate neuroepithelial specification and neurogenesis modes in the *Drosophila* optic lobe. Development *143*, 2431–2442.

Apitz, H., and Salecker, I. (2018). Spatiooral relays control layer identity of direction-selective neuron subtypes in Drosophila. Nat. Commun. *9*, 1–16.

Aptekar, J.W., Shoemaker, P.A., and Frye, M.A. (2012). Figure tracking by flies is supported by parallel visual streams. Curr. Biol. *22*, 482–487.

Arenz, A., Drews, M.S., Richter, F.G., Ammer, G., and Borst, A. (2017). The Temporal Tuning of the Drosophila Motion Detectors Is Determined by the Dynamics of Their Input Elements. Curr. Biol. *27*, 929–944.

Ariel, M., and Daw, N.W. (1982). Pharmacological analysis of directionally sensitive rabbit retinal ganglion cells. J. Physiol. *324*, 161–185.

Avoli, M., Louvel, J., Drapeau, C., Pumain, R., and Kurcewicz, I. (1995). GABA(A)-mediated inhibition and in vitro epileptogenesis in the human neocortex. J. Neurophysiol. *73*, 468–484.

Baden, T., Euler, T., and Berens, P. (2020). Understanding the retinal basis of vision across species. Nat. Rev. Neurosci. *21*, 5–20.

Badwan, B.A., Creamer, M.S., Zavatone-Veth, J.A., and Clark, D.A. (2019). Dynamic nonlinearities enable direction opponency in Drosophila elementary motion detectors. Nat. Neurosci. *22*, 1318–1326.

Bahl, A., Ammer, G., Schilling, T., and Borst, A. (2013). Object tracking in motion-blind flies. Nat. Neurosci. *16*, 730–738.

Bahl, A., Serbe, E., Meier, M., Ammer, G., and Borst, A. (2015). Neural Mechanisms for Drosophila Contrast Vision. Neuron *88*, 1240–1252.

Baines, R.A., Uhler, J.P., Thompson, A., Sweeney, S.T., and Bate, M. (2001). Altered electrical properties in Drosophila neurons developing without synaptic transmission. J. Neurosci. *21*, 1523–1531.

Barlow, H.B., and Levick, W.R. (1965). The mechanism of directionally selective units in rabbit's retina. J. Physiol. *178*, 477–504.

Barnhart, E.L., Wang, I.E., Wei, H., Desplan, C., and Clandinin, T.R. (2018). Sequential Nonlinear Filtering of Local Motion Cues by Global Motion Circuits. Neuron *100*, 229-243.e3.

Bausenwein, B., and Fischbach, K.F. (1992). Activity labeling patterns in the medulla of Drosophila melanogaster caused by motion stimuli. Cell Tissue Res. *270*, 25–35.

Bausenwein, B., Dittrich, A.P.M., and Fischbach, K.-F. (1992). The optic lobe of Drosophila melanogaster - II. Sorting of retinotopic pathways in the medulla. Cell Tissue Res. *267*, 17–28.

Behnia, R., Clark, D.A., Carter, A.G., Clandinin, T.R., and Desplan, C. (2014). Processing properties of on and off pathways for Drosophila motion detection. Nature *512*, 427–430.

Berens, P., Ecker, A.S., James Cotton, R., Ma, W.J., Bethge, M., and Tolias, A.S. (2012). A fast and simple population code for orientation in primate V1. J. Neurosci. *32*, 10618–10626.

Boergens, K.M., Kapfer, C., Helmstaedter, M., Denk, W., and Borst, A. (2018). Full reconstruction of large lobula plate tangential cells in Drosophila from a 3D EM dataset. PLoS One *13*.

Bogdanik, L., Mohrmann, R., Ramaekers, A., Bockaert, J., Grau, Y., Broadie, K., and Parmentier, M.L. (2004). The Drosophila metabotropic glutamate receptor DmGluRA regulates activity-dependent synaptic facilitation and fine synaptic morphology. J. Neurosci. *24*, 9105–9116.

Borst, A. (2018). A biophysical mechanism for preferred direction enhancement in fly motion vision. PLoS Comput. Biol. *14*, e1006240.

Borst, A., and Haag, J. (2002). Neural networks in the cockpit of the fly. J. Comp. Physiol. A Neuroethol. Sensory, Neural, Behav. Physiol. *188*, 419–437.

Borst, A., and Helmstaedter, M. (2015). Common circuit design in fly and mammalian motion vision. Nat. Neurosci. *18*, 1067–1076.

Borst, A., Haag, J., and Mauss, A.S. (2020). How fly neurons compute the direction of visual motion. J. Comp. Physiol. A Neuroethol. Sensory, Neural, Behav. Physiol. *206*, 109–124.

Bos, R., Gainer, C., and Feller, M.B. (2016). Role for visual experience in the development of direction-selective circuits. Curr. Biol. *26*, 1367–1375.

Braitenberg, V. (1967). Patterns of projection in the visual system of the fly. I. Retina-lamina projections. Exp. Brain Res. *3*, 271–298.

Brotz, T.M., Gundelfinger, E.D., and Borst, A. (2001). Cholinergic and GABAergic pathways in fly motion vision. BMC Neurosci. *2*, 1.

Buchner, E., Bader, R., Buchner, S., Cox, J., Emson, P.C., Flory, E., Heizmann, C.W., Hemm, S., Hofbauer, A., and Oertel, W.H. (1988). Cell-specific immuno-probes for the brain of normal and mutant Drosophila melanogaster - I. Wildtype visual system. Cell Tissue Res. *253*, 357–370.

Campbell, R.A.A., Honegger, K.S., Qin, H., Li, W., Demir, E., and Turner, G.C. (2013). Imaging a population code for odor identity in the Drosophila mushroom body. J. Neurosci. *33*, 10568–10581.

Chan, Y.C., and Chiao, C.C. (2013). The distribution of the preferred directions of the ON–OFF direction selective ganglion cells in the rabbit retina requires refinement after eye opening. Physiol. Rep. *1*.

Chaya, T., Matsumoto, A., Sugita, Y., Watanabe, S., Kuwahara, R., Tachibana, M., and Furukawa, T. (2017). Versatile functional roles of horizontal cells in the retinal circuit. Sci. Rep. *7*, 1–15.

Chen, T.W., Wardill, T.J., Sun, Y., Pulver, S.R., Renninger, S.L., Baohan, A., Schreiter, E.R., Kerr, R.A., Orger, M.B., Jayaraman, V., et al. (2013). Ultrasensitive fluorescent proteins for imaging neuronal activity. Nature *499*, 295–300.

Choi, B.J., Chen, Y.-C.D., and Desplan, C. (2021). Building a circuit through correlated spontaneous neuronal activity in the developing vertebrate and invertebrate visual systems. Genes Dev.

Chou, W.H., Hall, K.J., Wilson, D.B., Wideman, C.L., Townson, S.M., Chadwell, L. V., and Britt, S.G. (1996). Identification of a novel Drosophila opsin reveals specific patterning of the R7 and R8 photoreceptor cells. Neuron *17*, 1101–1115.

Clark, D.A., and Demb, J.B. (2016). Parallel Computations in Insect and Mammalian Visual Motion Processing. Curr. Biol. *26*, R1062–R1072.

Clark, D.A., Bursztyn, L., Horowitz, M.A., Schnitzer, M.J., and Clandinin, T.R. (2011). Defining the Computational Structure of the Motion Detector in Drosophila. Neuron *70*, 1165–1177.

Clemens, J., Kutzki, O., Ronacher, B., Schreiber, S., and Wohlgemuth, S. (2011). Efficient transformation of an auditory population code in a small sensory system. Proc. Natl. Acad. Sci. U. S. A. *108*, 13812–13817.

Cuntz, H., Haag, J., Forstner, F., Segev, I., and Borst, A. (2007). Robust coding of flow-field parameters by axo-axonal gap junctions between fly visual interneurons. Proc. Natl. Acad. Sci. U. S. A. *104*, 10229–10233.

Dana, H., Sun, Y., Mohar, B., Hulse, B.K., Kerlin, A.M., Hasseman, J.P., Tsegaye, G., Tsang, A., Wong, A., Patel, R., et al. (2019). High-performance calcium sensors for imaging activity in neuronal populations and microcompartments. Nat. Methods.

Datum, K.H., Weiler, R., and Zettler, F. (1986). Immunocytochemical demonstration of γ-amino butyric acid and glutamic acid decarboxylase in R7 photoreceptors and C2 centrifugal fibres in the blowfly visual system. J. Comp. Physiol. A *159*, 241–249.

Davie, K., Janssens, J., Koldere, D., De Waegeneer, M., Pech, U., Kreft, Ł., Aibar, S., Makhzami, S., Christiaens, V., Bravo González-Blas, C., et al. (2018). A Single-Cell Transcriptome Atlas of the Aging Drosophila Brain. Cell.

Davis, F.P., Nern, A., Picard, S., Reiser, M.B., Rubin, G.M., Eddy, S.R., and Henry, G.L. (2020). A genetic, genomic, and computational resource for exploring neural circuit function. Elife *9*.

Diamond, J.S. (2017). Inhibitory Interneurons in the Retina: Types, Circuitry, and Function. Annu. Rev. Vis. Sci. *3*, 1–24.

Egelhaaf, M. (2013). Visual Processing in Free Flight. In Encyclopedia of Computational Neuroscience, (Springer New York), pp. 1–21.

Egelhaaf, M., Kern, R., Krapp, H.G., Kretzberg, J., Kurtz, R., and Warzecha, A.K. (2002). Neural encoding of behaviourally relevant visual-motion information in the fly. Trends

Neurosci. *25*, 96–102.

Enell, L., Hamasaka, Y., Kolodziejczyk, A., and Nässel, D.R. (2007). γ-Aminobutyric acid (GABA) signaling components in Drosophila: Immunocytochemical localization of GABAB receptors in relation to the GABAA receptor subunit RDL and a vesicular GABA transporter. J. Comp. Neurol. *505*, 18–31.

Evans, B.J.E., O'Carroll, D.C., Fabian, J.M., and Wiederman, S.D. (2019). Differential Tuning to Visual Motion Allows Robust Encoding of Optic Flow in the Dragonfly. J. Neurosci. *39*, 8051–8063.

Farrow, K., Borst, A., and Haag, J. (2005). Sharing receptive fields with your neighbors: Tuning the vertical system cells to wide field motion. J. Neurosci. *25*, 3985–3993.

Featherstone, D.E., Rushton, E.M., Hilderbrand-Chae, M., Phillips, A.M., Jackson, F.R., and Broadie, K. (2000). Presynaptic glutamic acid decarboxylase is required for induction of the postsynaptic receptor field at a glutamatergic synapse. Neuron *27*, 71–84.

Fei, H., Chow, D.M., Chen, A., Romero-Calderón, R., Ong, W.S., Ackerson, L.C., Maidment, N.T., Simpson, J.H., Frye, M.A., and Krantz, D.E. (2010). Mutation of the drosophila vesicular GABA transporter disrupts visual figure detection. J. Exp. Biol. *213*, 1717–1730.

Fendl, S., Vieira, R.M., and Borst, A. (2020). Conditional protein tagging methods reveal highly specific subcellular distribution of ion channels in motion-sensing neurons. Elife *9*, 1–48.

Fischbach, K.F., and Dittrich, A.P.M. (1989). The optic lobe of Drosophila melanogaster. I. A Golgi analysis of wild-type structure. Cell Tissue Res. *258*, 441–475.

Fisher, Y.E., Silies, M., and Clandinin, T.R. (2015a). Orientation Selectivity Sharpens Motion Detection in Drosophila. Neuron *88*, 390–402.

Fisher, Y.E., Leong, J.C.S., Sporar, K., Ketkar, M.D., Gohl, D.M., Clandinin, T.R., and Silies, M. (2015b). A Class of Visual Neurons with Wide-Field Properties Is Required for Local Motion Detection. Curr. Biol. *25*, 3178–3189.

Fisher, Y.E., Leong, J.C.S., Sporar, K., Ketkar, M.D., Gohl, D.M., Clandinin, T.R., and Silies, M. (2015c). A Class of Visual Neurons with Wide-Field Properties Is Required for Local Motion Detection. Curr. Biol. *25*, 3178–3189.

Franke, K., and Baden, T. (2017). General features of inhibition in the inner retina. J. Physiol. *595*, 5507–5515.

Freifeld, L., Clark, D.A., Schnitzer, M.J., Horowitz, M.A., and Clandinin, T.R. (2013). GABAergic Lateral Interactions Tune the Early Stages of Visual Processing in Drosophila. Neuron *78*, 1075–1089.

Fried, S.I., Münch, T.A., and Werblin, F.S. (2002). Mechanisms and circuitry underlying directional selectivity in the retina. Nature *420*, 411–414.

Fröhlich, A., and Meinertzhagen, I.A. (1982). Synaptogenesis in the first optic neuropile of the fly's visual system. J. Neurocytol. *11*, 159–180.

Gilad, A., and Slovin, H. (2015). Population responses in V1 encode different figures by response amplitude. J. Neurosci. *35*, 6335–6349.

Gisselmann, G., Plonka, J., Pusch, H., and Hatt, H. (2004). Drosophila melanogaster GRD and LCCH3 subunits form heteromultimeric GABA-gated cation channels. Br. J. Pharmacol. *142*, 409–413.

Gohl, D.M., Silies, M.A., Gao, X.J., Bhalerao, S., Luongo, F.J., Lin, C.C., Potter, C.J., and Clandinin, T.R. (2011). A versatile in vivo system for directed dissection of gene expression patterns. Nat. Methods *8*, 231–237.

Gonzalez-Bellido, P.T., Wardill, T.J., and Juusola, M. (2011). Compound eyes and retinal information processing in miniature dipteran species match their specific ecological demands. Proc. Natl. Acad. Sci. U. S. A. *108*, 4224–4229.

Götz, K.G. (1964). Optomotorische Untersuchung des visuellen systems einiger Augenmutanten der Fruchtfliege Drosophila. Kybernetik *2*, 77–92.

Gruntman, E., Romani, S., and Reiser, M.B. (2018). Simple integration of fast excitation and offset, delayed inhibition computes directional selectivity in Drosophila. Nat. Neurosci. *21*, 250–257.

Gruntman, E., Romani, S., and Reiser, M.B. (2019). The computation of directional selectivity in the drosophila off motion pathway. Elife *8*.

Haag, J., and Borst, A. (2004). Neural mechanism underlying complex receptive field properties of motion-sensitive interneurons. Nat. Neurosci. *7*, 628–634.

Haag, J., Arenz, A., Serbe, E., Gabbiani, F., and Borst, A. (2016). Complementary mechanisms create direction selectivity in the fly. Elife *5*, e17421.

Haag, J., Mishra, A., and Borst, A. (2017). A common directional tuning mechanism of Drosophila motion-sensing neurons in the ON and in the OFF pathway. Elife *6*.

Hardie, R.C. (1985). Functional Organization of the Fly Retina. pp. 1–79.

Hardie, R.C. (1987). Is histamine a neurotransmitter in insect photoreceptors? J. Comp. Physiol. A *161*, 201–213.

Hardie, R.C. (1989). A histamine-activated chloride channel involved in neurotransmission at a photoreceptor synapse. Nature *339*, 704–706.

Von Hassenstein, B., and Reichardt, W. (1956a). Systemtheoretische Analyse der Zeit-, Reihenfolgen-und Vorzeichenauswertung bei der Bewegungsperzeption des Rüsselkäfers Chlorophanus. Zeitschrift Fur Naturforsch. - Sect. B J. Chem. Sci. *11*, 513–524.

Von Hassenstein, B., and Reichardt, W. (1956b). Systemtheoretische Analyse der Zeit-, Reihenfolgen-und Vorzeichenauswertung bei der Bewegungsperzeption des Rüsselkäfers Chlorophanus. Zeitschrift Fur Naturforsch. - Sect. B J. Chem. Sci. *11*, 513–524.

Hausen, K. (1982). Motion sensitive interneurons in the optomotor system of the fly. Biol. Cybern. *46*, 67–79.

Heisenberg, M. & Wolf, R. (1984). Vision on Drosophila:genetics of microbehavior.

Heisenberg, M., and Buchner, E. (1977). The rôle of retinula cell types in visual behavior of Drosophila melanogaster. J. Comp. Physiol. ■ A *117*, 127–162.

Hengstenberg, R., Hausen, K., and Hengstenberg, B. (1982). The number and structure of giant vertical cells (VS) in the lobula plate of the blowfly Calliphora erythrocephala. J. Comp. Physiol. □ A *149*, 163–177.

Honkanen, A., Immonen, E.V., Salmela, I., Heimonen, K., and Weckström, M. (2017). Insect photoreceptor adaptations to night vision. Philos. Trans. R. Soc. B Biol. Sci. *372*.

Hörmann, N., Schilling, T., Ali, A.H., Serbe, E., Mayer, C., Borst, A., and Pujol-Martı, J. (2020). A combinatorial code of transcription factors specifies subtypes of visual motion-sensing

neurons in Drosophila. Dev. *147*.

Hsu, K.-J., Lin, Y.-Y., Chiang, A.-S., and Chu, S.-W. (2019). Optical properties of adult Drosophila brains in one-, two-, and three-photon microscopy. Biomed. Opt. Express *10*, 1627.

Inzunza, O., Bravo, H., Smith, R.L., and Angel, M. (1991). Topography and morphology of retinal ganglion cells in Falconiforms: A study on predatory and carrion-eating birds. Anat. Rec. *229*, 271–277.

Jang, H.J., Park, K., Lee, J., Kim, H., Han, K.H., and Kwag, J. (2015). GABAA receptor-mediated feedforward and feedback inhibition differentially modulate the gain and the neural code transformation in hippocampal CA1 pyramidal cells. Neuropharmacology *99*, 177–186.

Jeon, C.J., Strettoi, E., and Masland, R.H. (1998). The major cell populations of the mouse retina. J. Neurosci. *18*, 8936–8946.

Joesch, M., Plett, J., Borst, A., and Reiff, D.F. (2008). Response Properties of Motion-Sensitive Visual Interneurons in the Lobula Plate of Drosophila melanogaster. Curr. Biol. *18*, 368–374.

Joesch, M., Schnell, B., Raghu, S.V., Reiff, D.F., and Borst, A. (2010). ON and off pathways in Drosophila motion vision. Nature *468*, 300–304.

Kaifosh, P., Zaremba, J.D., Danielson, N.B., and Losonczy, A. (2014). SIMA: Python software for analysis of dynamic fluorescence imaging data. Front. Neuroinform. *8*, 80.

Karmeier, K., Tabor, R., Egelhaaf, M., and Krapp, H.G. (2001). Early visual experience and the receptive-field organization of optic flow processing interneurons in the fly motion pathway. Vis. Neurosci. *18*, 1–8.

Katz, B., and Minke, B. (2009). Drosophila photoreceptors and signaling mechanisms. Front. Cell. Neurosci. *3*, 2.

Keleş, M.F., Mongeau, J.M., and Frye, M.A. (2019). Object features and T4/T5 motion detectors modulate the dynamics of bar tracking by Drosophila. J. Exp. Biol. *222*.

Kern, R. (1998). Visual position stabilization in the hummingbird hawk moth, Macroglossum stellatarum L. II. Electrophysiological analysis of neurons sensitive to wide-field image motion. J. Comp. Physiol. - A Sensory, Neural, Behav. Physiol. *182*, 239–249.

Ketkar, M.D., Sporar, K., Gür, B., Ramos-Traslosheros, G., Seifert, M., and Silies, M. (2020). Luminance Information Is Required for the Accurate Estimation of Contrast in Rapidly Changing Visual Contexts. Curr. Biol. *30*, 657-669.e4.

Kien, J. (1974). Sensory integration in the locust optomotor system-II: Direction selective neurons in the circumoesophageal connectives and the optic lobe. Vision Res. *14*, 1255–1268.

Kirschfeld, K. (1967). Die projektion der optischen umwelt auf das raster der rhabdomere im komplexauge von Musca. Exp. Brain Res. *3*, 248–270.

Kirschfeld, K. (1973). Das neurale Superpositionsauge. Fortschr. Zool. *21*, 229–257.

Kist, A.M., and Portugues, R. (2019). Optomotor Swimming in Larval Zebrafish Is Driven by Global Whole-Field Visual Motion and Local Light-Dark Transitions. Cell Rep. *29*, 659-670.e3.

Klapoetke, N.C., Murata, Y., Kim, S.S., Pulver, S.R., Birdsey-Benson, A., Cho, Y.K., Morimoto, T.K., Chuong, A.S., Carpenter, E.J., Tian, Z., et al. (2014). Independent optical excitation of distinct neural populations. Nat. Methods *11*, 338–346.

Kolodziejczyk, A., Sun, X., Meinertzhagen, I.A., and Nässel, D.R. (2008). Glutamate, GABA and acetylcholine signaling components in the lamina of the Drosophila visual system. PLoS One *3*.

Konstantinides, N., Kapuralin, K., Fadil, C., Barboza, L., Satija, R., and Desplan, C. (2018). Phenotypic Convergence: Distinct Transcription Factors Regulate Common Terminal Features. Cell *174*, 622-635.e13.

Krapp, H.G. (2000). Neuronal matched filters for optic flow processing in flying insects. Int. Rev. Neurobiol. *44*, 93–120.

Krapp, H.G. (2008). Estimation of self-motion for gaze and flight stabilization in flying insects. Navig. J. Inst. Navig. *55*, 147–158.

Krapp, H.G., and Hengstenberg, R. (1996). Estimation of self-motion by optic flow processing in single visual interneurons. Nature *384*, 463–466.

Krapp, H.G., Hengstenberg, B., and Hengstenberg, R. (1998). Dendritic structure and receptive-field organization of optic flow processing interneurons in the fly. J. Neurophysiol. *79*, 1902–1917.

Krapp, H.G., Hengstenberg, R., and Egelhaaf, M. (2001). Binocular contributions to optic flow processing in the fly visual system. J. Neurophysiol. *85*, 724–734.

Kugler, K., Luksch, H., Peremans, H., Vanderelst, D., Wiegrebe, L., and Firzlaff, U. (2019). Optic and echo-acoustic flow interact in bats. J. Exp. Biol. *222*.

Küppers, B., Sánchez-Soriano, N., Letzkus, J., Technau, G.M., and Prokop, A. (2003). In developing Drosophila neurones the production of γ-amino butyric acid is tightly regulated downstream of glutamate decarboxylase translation and can be influenced by calcium. J. Neurochem. *84*, 939–951.

Kurmangaliyev, Y.Z., Yoo, J., Locascio, S.A., and Lawrence Zipursky, S. (2019). Modular transcriptional programs separately define axon and dendrite connectivity. Elife *8*, e50822.

Kurmangaliyev, Y.Z., Yoo, J., Valdes-Aleman, J., Sanfilippo, P., and Zipursky, S.L. (2020). Transcriptional Programs of Circuit Assembly in the Drosophila Visual System. Neuron *108*, 1045–1057.

Land, M.F., and Nilsson, D.-E. (2012). Animal eyes (Oxford University Press).

Laughlin, S. (1981). A simple coding procedure enhances a neuron's information capacity. Zeitschrift Fur Naturforsch. - Sect. C J. Biosci. *36*, 51.

Laughlin, S.B. (1989). The role of sensory adaptation in the retina. J. Exp. Biol. *146*, 39–62.

Laughlin, S.B., and Hardie, R.C. (1978). Common strategies for light adaptation in the peripheral visual systems of fly and dragonfly. J. Comp. Physiol. □ A *128*, 319–340.

Leong, J.C.S., Esch, J.J., Poole, B., Ganguli, S., and Clandinin, T.R. (2016). Direction selectivity in drosophila emerges from preferred-direction enhancement and null-direction suppression. J. Neurosci. *36*, 8078–8092.

Leuckart, R. (1876). Organologie des Auges: vergleichende Anatomie.

Liang, P., Kern, R., Egelhaaf, M., Heitwerth, J., Kern, R., Kurtz, R., Egelhaaf, M., Lindemann,

J.P., Kern, R., Michaelis, C., et al. (1989). ll . Optics of the Compound Eye System of Musca : Studies on Optics , Structure and Function. J. Exp. Biol. *6*, 116–127.

Lisney, T.J., Wylie, D.R., Kolominsky, J., and Iwaniuk, A.N. (2015). Eye Morphology and Retinal Topography in Hummingbirds (Trochilidae: Aves). Brain. Behav. Evol. *86*, 176–190.

Liu, W.W., and Wilson, R.I. (2013). Glutamate is an inhibitory neurotransmitter in the Drosophila olfactory system. Proc. Natl. Acad. Sci. U. S. A. *110*, 10294–10299.

Maisak, M.S., Haag, J., Ammer, G., Serbe, E., Meier, M., Leonhardt, A., Schilling, T., Bahl, A., Rubin, G.M., Nern, A., et al. (2013). A directional tuning map of Drosophila elementary motion detectors. Nature *500*, 212–216.

Mann, E.O., Kohl, M.M., and Paulsen, O. (2009). Distinct roles of GABAA and GABAB receptors in balancing and terminating persistent cortical activity. J. Neurosci. *29*, 7513–7518.

Mattis, J., Tye, K.M., Ferenczi, E.A., Ramakrishnan, C., O'Shea, D.J., Prakash, R., Gunaydin, L.A., Hyun, M., Fenno, L.E., Gradinaru, V., et al. (2012). Principles for applying optogenetic tools derived from direct comparative analysis of microbial opsins. Nat. Methods *9*, 159–172.

Mauss, A.S., Meier, M., Serbe, E., and Borst, A. (2014). Optogenetic and pharmacologic dissection of feedforward inhibition in Drosophila motion vision. J. Neurosci. *34*, 2254–2263.

Mauss, A.S., Pankova, K., Arenz, A., Nern, A., Rubin, G.M., and Borst, A. (2015). Neural Circuit to Integrate Opposing Motions in the Visual Field. Cell *162*, 351–362.

Mauss, A.S., Vlasits, A., Borst, A., and Feller, M. (2017). Visual Circuits for Direction Selectivity. *40*, 211–230.

Maximov, V., Maximova, E., and Maximov, P. (2005). Direction selectivity in the goldfish tectum revisited. In Annals of the New York Academy of Sciences, (New York Academy of Sciences), pp. 198–205.

Mazurek, M., Kager, M., and Van Hooser, S.D. (2014). Robust quantification of orientation selectivity and direction selectivity. Front. Neural Circuits *8*, 92.

Meier, M., and Borst, A. (2019). Extreme Compartmentalization in a Drosophila Amacrine Cell. Curr. Biol. *29*, 1545-1550.e2.

Meier, M., Serbe, E., Maisak, M.S., Haag, J., Dickson, B.J., and Borst, A. (2014). Neural circuit components of the drosophila off motion vision pathway. Curr. Biol. *24*, 385–392.

Meinertzhagen, I.A., and O'Neil, S.D. (1991). Synaptic organization of columnar elements in the lamina of the wild type in Drosophila melanogaster. J. Comp. Neurol. *305*, 232–263.

Meyer, E.P., Matute, C., Streit, P., and Nässel, D.R. (1986). Insect optic lobe neurons identifiable with monoclonal antibodies to GABA. Histochemistry *84*, 207–216.

Molina-Obando, S., Vargas-Fique, J.F., Henning, M., Gür, B., Schlad, T.M., Akhtar, J., Berger, T.K., and Silies, M. (2019). On selectivity in the drosophila visual system is a multisynaptic process involving both glutamatergic and GABAergic inhibition. Elife *8*.

Mu, L., Ito, K., Bacon, J.P., and Strausfeld, N.J. (2012). Optic glomeruli and their inputs in Drosophila share an organizational ground pattern with the antennal lobes. J. Neurosci. *32*, 6061–6071.

Nern, A., Pfeiffer, B.D., and Rubin, G.M. (2015). Optimized tools for multicolor stochastic labeling reveal diverse stereotyped cell arrangements in the fly visual system. Proc. Natl. Acad. Sci. *112*, E2967–E2976.

Nikolaou, N., Lowe, A.S., Walker, A.S., Abbas, F., Hunter, P.R., Thompson, I.D., and Meyer, M.P. (2012). Parametric Functional Maps of Visual Inputs to the Tectum. Neuron *76*, 317–324.

Nilsson D. E. (1989). Vision Optics and Evolution. Bioscience *39*, 298–307.

Otsu, N. (1979). Threshold selection method from gray-level histograms. IEEE Trans Syst Man Cybern *9*, 62–66.

Özel, M.N., Simon, F., Jafari, S., Holguera, I., Chen, Y.C., Benhra, N., El-Danaf, R.N., Kapuralin, K., Malin, J.A., Konstantinides, N., et al. (2020). Neuronal diversity and convergence in a visual system developmental atlas. Nature *589*, 88–95.

Pankova, K., and Borst, A. (2017). Transgenic line for the identification of cholinergic release sites in Drosophila melanogaster. J. Exp. Biol. *220*, 1405–1410.

Pavlowsky, A., Schor, J., Plaçais, P.Y., and Preat, T. (2018). A GABAergic Feedback Shapes Dopaminergic Input on the Drosophila Mushroom Body to Promote Appetitive Long-Term Memory. Curr. Biol. *28*, 1783-1793.e4.

Pei, Z., Chen, Q., Koren, D., Giammarinaro, B., Ledesma, H.A., and Wei, W. (2015). Conditional knock-out of vesicular GABA transporter gene from starburst amacrine cells reveals the contributions of multiple synaptic mechanisms underlying direction selectivity in the retina. J. Neurosci. *35*, 13219–13232.

Petrowitz, R., Dahmen, H., Egelhaaf, M., and Krapp, H.G. (2000). Arrangement of optical axes and spatial resolution in the compound eye of the female blowfly Calliphora. J. Comp. Physiol. - A Sensory, Neural, Behav. Physiol. *186*, 737–746.

Pinto-Teixeira, F., Koo, C., Rossi, A.M., Neriec, N., Bertet, C., Li, X., Del-Valle-Rodriguez, A., and Desplan, C. (2018). Development of Concurrent Retinotopic Maps in the Fly Motion Detection Circuit. Cell *173*, 485-498.e11.

Poggio, T., and Reichardt, W. (1976). Visual control of orientation behaviour in the fly-Part II. Towards the underlying neural interactions. Q. Rev. Biophys. *9*, 377–438.

Poleg-Polsky, A., and Diamond, J.S. (2011). Imperfect Space Clamp Permits Electrotonic Interactions between Inhibitory and Excitatory Synaptic Conductances, Distorting Voltage Clamp Recordings. PLoS One *6*, e19463.

Portugues, R., Feierstein, C.E., Engert, F., and Orger, M.B. (2014). Whole-brain activity maps reveal stereotyped, distributed networks for visuomotor behavior. Neuron *81*, 1328–1343.

Raghu, S.V., and Borst, A. (2011). Candidate glutamatergic neurons in the visual system of drosophila. PLoS One *6*, e19472.

Raghu, S.V., Reiff, D.F., and Borst, A. (2011). Neurons with cholinergic phenotype in the visual system of Drosophila. J. Comp. Neurol. *519*, 162–176.

Raghu, S.V., Claussen, J., and Borst, A. (2013). Neurons with GABAergic phenotype in the visual system of Drosophila. J. Comp. Neurol. *521*, 252–265.

Ramos-Traslosheros, G., and Silies, M. (2021). The physiological basis for the computation of direction selectivity in the Drosophila OFF pathway. BioRxiv 2021.04.17.440268.

Ramos-Traslosheros, G., Henning, M., and Silies, M. (2018). Motion detection: Cells, circuits and algorithms. Neuroforum *24*, A61–A72.

Rind, F.C. (1990). Identification of directionally selective motion-detecting neurones in the locust lobula and their synaptic connections with an identified descending neurone. J. Exp. Biol. *149*.

Rister, J., Pauls, D., Schnell, B., Ting, C.Y., Lee, C.H., Sinakevitch, I., Morante, J., Strausfeld, N.J., Ito, K., and Heisenberg, M. (2007). Dissection of the Peripheral Motion Channel in the Visual System of Drosophila melanogaster. Neuron *56*, 155–170.

Rivera-Alba, M., Vitaladevuni, S.N., Mischenko, Y., Lu, Z., Takemura, S.Y., Scheffer, L., Meinertzhagen, I.A., Chklovskii, D.B., and De Polavieja, G.G. (2011). Wiring economy and volume exclusion determine neuronal placement in the Drosophila brain. Curr. Biol. *21*, 2000–2005.

Rivlin-Etzion, M., Wei, W., and Feller, M.B. (2012). Visual Stimulation Reverses the Directional Preference of Direction-Selective Retinal Ganglion Cells. Neuron *76*, 518–525.

Rossi, A.M., Jafari, S., and Desplan, C. (2021). Integrated Patterning Programs During Drosophila Development Generate the Diversity of Neurons and Control Their Mature Properties . Annu. Rev. Neurosci. *44*.

Rowell, C.H.F. (1988). Mechanisms of flight steering in locusts. Experientia *44*, 389–395.

Sabbah, S., Gemmer, J.A., Bhatia-Lin, A., Manoff, G., Castro, G., Siegel, J.K., Jeffery, N., and Berson, D.M. (2017). A retinal code for motion along the gravitational and body axes. Nature *546*, 492–497.

Saffari, R., Grotefeld, K., Kravchenko, M., Zhang, M., and Zhang, W. (2019). Calretinin+-neurons-mediated GABAergic inhibition in mouse prefrontal cortex. Prog. Neuro-Psychopharmacology Biol. Psychiatry *94*.

Salazar-Gatzimas, E., Chen, J., Creamer, M.S., Mano, O., Mandel, H.B., Matulis, C.A., Pottackal, J., and Clark, D.A. (2016). Direct Measurement of Correlation Responses in Drosophila Elementary Motion Detectors Reveals Fast Timescale Tuning. Neuron *92*, 227–239.

Salazar-Gatzimas, E., Agrochao, M., Fitzgerald, J.E., and Clark, D.A. (2018). The Neuronal Basis of an Illusory Motion Percept Is Explained by Decorrelation of Parallel Motion Pathways. Curr. Biol. *28*, 3748-3762.e8.

Salcedo, E., Huber, A., Henrich, S., Chadwell, L. V., Chou, W.H., Paulsen, R., and Britt, S.G. (1999). Blue- and green-absorbing visual pigments of Drosophila: Ectopic expression and physiological characterization of the R8 photoreceptor cell- specific Rh5 and Rh6 rhodopsins. J. Neurosci. *19*, 10716–10726.

Sanes, J.R., and Zipursky, S.L. (2010). Design Principles of Insect and Vertebrate Visual Systems. Neuron *66*, 15–36.

Sanger, T.D. (2003). Neural population codes. Curr. Opin. Neurobiol. *13*, 238–249.

Schnell, B., Joesch, M., Forstner, F., Raghu, S. V., Otsuna, H., Ito, K., Borst, A., and Reiff, D.F. (2010). Processing of horizontal optic flow in three visual interneurons of the Drosophila brain. J. Neurophysiol. *103*, 1646–1657.

Schnell, B., Raghu, S.V., Nern, A., and Borst, A. (2012). Columnar cells necessary for motion responses of wide-field visual interneurons in Drosophila. J. Comp. Physiol. A Neuroethol.

Sensory, Neural, Behav. Physiol. *198*, 389–395.

Schousboe, A. (2000). Pharmacological and Functional Characterization of Astrocytic GABa Transport: A Short Review. Neurochem. Res. *25*, 1241–1244.

Scott, E.K., Raabe, T., and Luo, L. (2002). Structure of the vertical and horizontal system neurons of the lobula plate in Drosophila. J. Comp. Neurol. *454*, 470–481.

Serbe, E., Meier, M., Leonhardt, A., and Borst, A. (2016). Comprehensive Characterization of the Major Presynaptic Elements to the Drosophila OFF Motion Detector. Neuron *89*, 829–841.

Shelley, J., Dedek, K., Schubert, T., Feigenspan, A., Schultz, K., Hombach, S., Willecke, K., and Weiler, R. (2006). Horizontal cell receptive fields are reduced in connexin57-deficient mice. Eur. J. Neurosci. *23*, 3176–3186.

Shinomiya, K., Karuppudurai, T., Lin, T.Y., Lu, Z., Lee, C.H., and Meinertzhagen, I.A. (2014). Candidate neural substrates for off-edge motion detection in drosophila. Curr. Biol. *24*, 1062–1070.

Shinomiya, K., Horne, J.A., McLin, S., Wiederman, M., Nern, A., Plaza, S.M., and Meinertzhagen, I.A. (2019a). The Organization of the Second Optic Chiasm of the Drosophila Optic Lobe. Front. Neural Circuits *13*, 65.

Shinomiya, K., Huang, G., Lu, Z., Parag, T., Xu, C.S., Aniceto, R., Ansari, N., Cheatham, N., Lauchie, S., Neace, E., et al. (2019b). Comparisons between the ON- and OFF-edge motion pathways in the Drosophila brain. Elife *8*.

Silies, M., Gohl, D.M., Fisher, Y.E., Freifeld, L., Clark, D.A., and Clandinin, T.R. (2013). Modular Use of Peripheral Input Channels Tunes Motion-Detecting Circuitry. Neuron *79*, 111–127.

Silies, M., Gohl, D.M., and Clandinin, T.R. (2014). Motion-Detecting Circuits in Flies: Coming into View. Annu. Rev. Neurosci. *37*, 307–327.

Simoncelli, E.P., and Olshausen, B.A. (2001). Natural image statistics and neural representation. Annu. Rev. Neurosci. *24*, 1193–1216.

Simpson, J.H. (2009). Chapter 3 Mapping and Manipulating Neural Circuits in the Fly Brain. Adv. Genet. *65*, 79–143.

Sinakevitch, I., Douglass, J.K., Scholtz, G., Loesel, R., and Strausfeld, N.J. (2003). Conserved and Convergent Organization in the Optic Lobes of Insects and Isopods, with Reference to Other Crustacean Taxa. J. Comp. Neurol. *467*, 150–172.

Sterling, P., and Laughlin, S. (2015). Principles of neural design (MIT Press).

Stöckl, A.L., O'Carroll, D.C., and Warrant, E.J. (2016). Neural summation in the hawkmoth visual system extends the limits of vision in dim light. Curr. Biol. *26*, 821–826.

Strother, J.A., Wu, S.T., Wong, A.M., Nern, A., Rogers, E.M., Le, J.Q., Rubin, G.M., and Reiser, M.B. (2017). The Emergence of Directional Selectivity in the Visual Motion Pathway of Drosophila. Neuron *94*, 168-182.e10.

Strother, J.A., Wu, S.T., Rogers, E.M., Eliason, J.L.M., Wong, A.M., Nern, A., and Reiser, M.B. (2018). Behavioral state modulates the on visual motion pathway of drosophila. Proc. Natl. Acad. Sci. U. S. A. *115*, E102–E111.

Suver, M.P., Huda, A., Iwasaki, N., Safarik, S., and Dickinson, M.H. (2016). An array of

descending visual interneurons encoding self-motion in Drosophila. J. Neurosci. *36*, 11768–11780.

Tabone, C.J., and Ramaswami, M. (2012). Is NMDA Receptor-Coincidence Detection Required for Learning and Memory? Neuron *74*, 767–769.

Takemura, S.Y., Lu, Z., and Meinertzhagen, I.A. (2008). Synaptic circuits of the Drosophila optic lobe: The input terminals to the medulla. J. Comp. Neurol. *509*, 493–513.

Takemura, S.Y., Bharioke, A., Lu, Z., Nern, A., Vitaladevuni, S., Rivlin, P.K., Katz, W.T., Olbris, D.J., Plaza, S.M., Winston, P., et al. (2013). A visual motion detection circuit suggested by Drosophila connectomics. Nature *500*, 175–181.

Takemura, S.Y., Xu, C.S., Lu, Z., Rivlin, P.K., Parag, T., Olbris, D.J., Plaza, S., Zhao, T., Katz, W.T., Umayam, L., et al. (2015). Synaptic circuits and their variations within different columns in the visual system of Drosophila. Proc. Natl. Acad. Sci. U. S. A. *112*, 13711–13716.

Takemura, S.Y., Nern, A., Chklovskii, D.B., Scheffer, L.K., Rubin, G.M., and Meinertzhagen, I.A. (2017). The comprehensive connectome of a neural substrate for 'ON' motion detection in Drosophila. Elife *6*, e24394.

Talay, M., Richman, E.B., Snell, N.J., Hartmann, G.G., Fisher, J.D., Sorkaç, A., Santoyo, J.F., Chou-Freed, C., Nair, N., Johnson, M., et al. (2017). Transsynaptic Mapping of Second-Order Taste Neurons in Flies by trans-Tango. Neuron *96*, 783-795.e4.

Tatsukawa, T., Hirasawa, H., Kaneko, A., and Kaneda, M. (2005). GABA-mediated component in the feedback response of turtle retinal cones. Vis. Neurosci. *22*, 317–324.

Theobald, J.C., Warrant, E.J., and O'Carroll, D.C. (2010). Wide-field motion tuning in nocturnal hawkmoths. Proc. R. Soc. B Biol. Sci. *277*, 853–860.

Thoreson, W.B., and Mangel, S.C. (2012). Lateral interactions in the outer retina. Prog. Retin. Eye Res. *31*, 407–441.

Tiriac, A., Bistrong, K., and Feller, M.B. (2021). Retinal waves but not visual experience are required for development of retinal direction selectivity maps. BioRxiv 2021.03.25.437067.

Tononi, G., Sporns, O., and Edelman, G.M. (1999). Measures of degeneracy and redundancy in biological networks. Proc. Natl. Acad. Sci. U. S. A. *96*, 3257–3262.

Triphan, T., Nern, A., Roberts, S.F., Korff, W., Naiman, D.Q., and Strauss, R. (2016). A screen for constituents of motor control and decision making in Drosophila reveals visual distance-estimation neurons. Sci. Rep. *6*, 1–12.

Tsodyks, M. V., Skaggs, W.E., Sejnowski, T.J., and McNaughton, B.L. (1997). Paradoxical effects of external modulation of inhibitory interneurons. J. Neurosci. *17*, 4382–4388.

Tuthill, J., Nern, A., Holtz, S., Rubin, G., and Reiser, M.B. (2013). Contributions of the 12 Neuron Classes in the Fly Lamina to Motion Vision. Neuron *79*, 128–140.

de Vries, S.E.J., Baccus, S.A., and Meister, M. (2011). The projective field of a retinal amacrine cell. J. Neurosci. *31*, 8595–8604.

Wei, W. (2018). Neural mechanisms of motion processing in the mammalian retina. Annu. Rev. Vis. Sci. *4*, 165–192.

Wei, H., Kyung, H.Y., Kim, P.J., and Desplan, C. (2020). The diversity of lobula plate tangential cells (LPTCs) in the Drosophila motion vision system. J. Comp. Physiol. A Neuroethol. Sensory, Neural, Behav. Physiol. *206*, 139–148.

Wei, W., Hamby, A.M., Zhou, K., and Feller, M.B. (2011). Development of asymmetric inhibition underlying direction selectivity in the retina. Nature *469*, 402–406.

Werner, R. (2013). Autocorrelation, a Principle for the Evaluation of Sensory Information by the Central Nervous System. In Sensory Communication, pp. 302–317.

Wernet, M.F., Perry, M.W., and Desplan, C. (2015). The evolutionary diversity of insect retinal mosaics: Common design principles and emerging molecular logic. Trends Genet. *31*, 316–328.

Wienecke, C.F.R., Leong, J.C.S., and Clandinin, T.R. (2018). Linear Summation Underlies Direction Selectivity in Drosophila. Neuron *99*, 680-688.e4.

Wilson, R.I., and Laurent, G. (2005). Role of GABAergic inhibition in shaping odor-evoked spatiotemporal patterns in the Drosophila antennal lobe. J. Neurosci. *25*, 9069–9079.

Wong, A.M., Wang, J.W., and Axel, R. (2002). Spatial representation of the glomerular map in the Drosophila protocerebrum. Cell *109*, 229–241.

Wu, S.M. (1992). Feedback connections and operation of the outer plexiform layer of the retina. Curr. Opin. Neurobiol. *2*, 462–468.

Wu, M., Nern, A., Ryan Williamson, W., Morimoto, M.M., Reiser, M.B., Card, G.M., and Rubin, G.M. (2016). Visual projection neurons in the Drosophila lobula link feature detection to distinct behavioral programs. Elife *5*.

Xia, S., and Chiang, A.S. (2008). NMDA receptors in Drosophila. In Biology of the NMDA Receptor, p.

Yamaguchi, S., Wolf, R., Desplan, C., and Heisenberg, M. (2008). Motion vision is independent of color in Drosophila. Proc. Natl. Acad. Sci. U. S. A. *105*, 4910–4915.

Yang, H.H., and Clandinin, T.R. (2018). Elementary motion detection in drosophila: Algorithms and mechanisms. Annu. Rev. Vis. Sci. *4*, 143–163.

Yang, H.H.H., St-Pierre, F., Sun, X., Ding, X., Lin, M.Z.Z., and Clandinin, T.R.R. (2016). Subcellular Imaging of Voltage and Calcium Signals Reveals Neural Processing In Vivo. Cell *166*, 245–257.

Yoshida, K., Watanabe, D., Ishikane, H., Tachibana, M., Pastan, I., and Nakanishi, S. (2001). A key role of starburst amacrine cells in originating retinal directional selectivity and optokinetic eye movement. Neuron *30*, 771–780.

Yu, J., Hu, H., Agmon, A., and Svoboda, K. (2019). Recruitment of GABAergic Interneurons in the Barrel Cortex during Active Tactile Behavior. Neuron *104*, 412-427.e4.

Yu, L., Shen, Z., Wang, C., and Yu, Y. (2018). Efficient coding and energy efficiency are promoted by balanced excitatory and inhibitory synaptic currents in neuronal network. Front. Cell. Neurosci. *12*.

Zavatone-Veth, J.A., Badwan, B.A., and Clark, D.A. (2020). A minimal synaptic model for direction selective neurons in Drosophila. J. Vis. *20*, 1–22.

Zhang, H.G., Lee, H.J., Rocheleau, T., Ffrench-Constant, R.H., and Jackson, M.B. (1995). Subunit composition determines picrotoxin and bicuculline sensitivity of Drosophila γ-aminobutyric acid receptors. Mol. Pharmacol. *48*, 835–840.

Zheng, L., De Polavieja, G.G., Wolfram, V., Asyali, M.H., Hardie, R.C., and Juusola, M. (2006). Feedback network controls photoreceptor output at the layer of first visual synapses in

Drosophila. J. Gen. Physiol. *127*, 495–510.

Zheng, Z., Lauritzen, J.S., Perlman, E., Robinson, C.G., Nichols, M., Milkie, D., Torrens, O., Price, J., Fisher, C.B., Sharifi, N., et al. (2018). A Complete Electron Microscopy Volume of the Brain of Adult Drosophila melanogaster. Cell *174*, 730-743.e22.

Acknowledgements

At this point, I want to thank all the people that made this work possible, the people that supported and accompanied me throughout the last four years of this thesis and that made this to a wonderful time of my life. My honest thank goes to:

Marion Silies for her loving care, outstanding support and guidance. Marion, thank you for your continuous and contagious excitement and the positive but also critical feedback about my work. This has pushed me forwards so many times. Thank you for taking so much of your time and sharing your knowledge about genetics, neuroscience and anything else. Furthermore, my success in winning talk awards goes back to you. I have learned so much from you about presenting my data in a scientific and additionally exciting way. Moreover, I want to thank you for giving me the chance to visit so many conferences and courses where I could not only learn a lot but also meet the scientific community. Taken together, thanks for being my supervisor, mentor and teacher. I couldn't have asked for a better one!

Andreas Stumpner and **Hansjörg Scherberger** for being part of my thesis committee and for reviewing my work. Thank you a lot for all your fruitful discussions and valuable comments in our committee meetings and for guiding me through this PhD thesis.

Tim Gollisch, **Jan Clemens** and **Siegrid Löwel** for being my extended thesis board members. Thank you for taking your time to evaluate my work.

All members of the **Silies lab** and **Martelli lab** for being such a wonderful group of open minded and loving people. You are all not only great colleagues but also good friends. Without you the last years would have been pretty bleak. I want to especially thank **Luis** and **Burak** for contributing to my work and the manuscript. Thank you so much for your expertise in modeling and data analysis which greatly advanced the data in the manuscript. Also, thank you for the long-lasting discussions about the data. Burak, thank you additionally for proofreading parts of my thesis. Furthermore, I want to thank **Katja** for the nice office atmosphere in Göttingen, your help when starting into my PhD, for answering all my questions and for teaching me two photon microscopy. In that sense, I want to also thank **Madhura**, **Sebastian**, and **Juan** for all your scientific feedback about my project. I really appreciate that everyone in the lab is always open and happy to discuss scientific but also personal matters. Thanks for all the social and fun activities in times where social distancing was not yet controlling our lives. **Freya,** thank you also for teaching me so much about my new home Mainz. My sincere thanks also goes to our lab technicians **Christine**, **Jonas** and **Simone**, for taking care of flies, helping out with PRCs or immunostainings and for taking care of so many more things in the lab that I am not even aware of.

Margot Elmaleh thank you for being the best roommate I could have wished for during the 6 weeks of Cajal course and for making this a wonderful experience. As Joe used to say, the most valuable thing from this course is the friends you will make. And most importantly, thank you for proofreading this thesis.

My family for your never-ending love and support. I wouldn't be where I am without you.

Jonas for his love and support, especially in the last month of this thesis. Thank you for putting up with my whims, always having an open ear when I didn't feel good, and your wonderful moral support.